Wireless Electrochemistry: 3D Bipolar Electrode Systems towards Spatially Controlled Bioelectronic Function



Author

Oisín Foley Doyle BSc.

A thesis submitted to Dublin City University for the degree of Doctor of Philosophy

School of Chemical Sciences

Supervisor

Prof. Robert Forster

August 2026

DELCARATION

I hereby certify that this material, which I now submit for assessment on the programme of study leading to the award of Doctor of Philosophy is entirely my own work, and that I have exercised reasonable care to ensure that the work is original and have conformed to the regulations on the use and declaration of Generative AI, and does not to the best of my knowledge breach any law of copyright, and has not been taken from the work of others save and to the extent that such work has been cited and acknowledged within the text of my work. I hereby certify that no Generative Artificial Intelligence (Gen AI) tools have been used in the creation of the thesis.

Signed Oisín Foley Doyle

ID No 23271697

Date 21st August 2026

DEDICATION

To my family, for their constant support and encouragement throughout this journey.

Most especially, to my mother. Throughout this PhD, you faced one of life's hardest battles with extraordinary courage, resilience, and determination. Even during the most difficult and uncertain of times, your strength never wavered, and your ability to keep going with such grace and positivity was nothing short of inspirational.

Watching you persevere through so much while continuing to support and encourage everyone around you changed my perspective on true strength and what truly matters in life. Your courage carried our family through moments that at times felt impossible, and in your example gave me the motivation to keep going throughout this work. This thesis is as much a reflection of your strength as it is of my work.

This thesis is dedicated to you Sinead, with all my love, admiration, and gratitude.

'Education is not the filling of a pail, but the lighting of a fire'.

-W.B. Yeats

ACKNOWLEDGEMENTS

I would first like to thank the entire Forster Research Team for creating an environment that made this PhD such a rewarding experience, both scientifically and personally. To Indher, Michal, Francesca, Luigi, Ewa, Francesco and Sam, thank you for your friendship, encouragement, and constant support throughout the years. The open discussions, willingness to help one another, and shared enthusiasm for each other's work made even the most challenging days enjoyable. Whether through problem solving in the lab, exchanging ideas, or simply keeping morale high, each of you contributed enormously to both this thesis and my overall experience during the PhD. I feel very fortunate to have been part of such a supportive and close-knit team.

A very special thank you goes to Áine. From the very beginning, when the group was only a small team of three, we have seen it grow together into what it is today. Throughout all of it, you have been one of the strongest sources of support. From countless coffees and walks spent discussing science, life, frustrations, and ideas, to the consistent encouragement and honesty you always provided, your friendship has meant more to me than I could ever properly put into words. We have truly become thick as thieves over the years, and I consider you far more like family than anything else. I am incredibly grateful for your support, loyalty, and friendship throughout this journey.

Finally, I would like to express my deepest gratitude to my supervisor, Robert. I feel extremely fortunate to have first been given the opportunity to collaborate with Robert during my final year undergraduate project, and then he was stuck with me to continue that work through a PhD programme. His passion for science, creativity, and dedication to research are truly nothing short of inspirational, and if I can aspire to achieve even a fraction of what he has accomplished to date, I will consider that a success. Beyond his scientific guidance, Robert has always been there whenever needed, no problem was ever too small, no discussion ever too much trouble. He consistently treated me with respect, trust, and encouragement, while also giving me the autonomy to develop confidence in my own ideas and direction as a researcher. For all of this, and for the opportunities he has given me over the years, I will always be indebted and deeply grateful.

TABLE OF CONTENTS

Declaration……

Dedication……

Acknowledgments……

Thesis Abstract…… 6

Chapter 1 : Thesis Introduction…… 7

Chapter 2 : Wirefree Electrochemistry for Enhanced Detection and Treatment of disease…… 20

Chapter 3 : Advancing Bipolar Electrochemistry for Targeted Deposition of Biocompatible Polymers in Electrolyte-Free Solutions *via* Finite Element Modeling…… 46

Chapter 4 : Directing the glow: 3D feeder geometries to enhance planar bipolar electrochemiluminescence…… 76

Chapter 5 : Spatially Controlled Wireless Electrochemistry *via* 3D Bipolar Electrodes…. 91

Thesis Conclusion…… 98

Future Work…… 109

Declaration of Authorship…… 117

Abstract

Wireless Electrochemistry: 3D Bipolar Electrode Systems towards Spatially Controlled Bioelectronic Function - Oisín Foley Doyle

Bipolar electrochemistry represents a fundamentally different approach to electrochemical control, enabling spatially resolved redox processes on electrically isolated electrodes through externally imposed electric fields rather than direct electrical connection. This wire-free paradigm offers significant potential for emerging applications including distributed sensing, bioelectronic interfaces, adaptive materials, and electrochemical manufacturing. However, despite extensive development of bipolar systems, the relationship between electrode architecture, electrolyte properties, local potential distribution, and the resulting electrochemical response remains only partially understood, limiting the ability to rationally design bipolar platforms.

This thesis investigates the fundamental principles governing spatially controlled electrochemical activity in bipolar systems, with particular emphasis on the use of electrochemical reactions as probes of local potential landscapes. PEDOT electropolymerisation was employed as a spatial reporter of anodic polarisation, enabling investigation of bipolar systems under conditions extending beyond conventional high conductivity electrolyte environments. Through combined experimental analysis, electrochemical characterisation, finite element modelling, and mass transport considerations, this work demonstrates that polymer deposition patterns in low conductivity media cannot be fully described by traditional linear potential models, revealing the importance of local electron-transfer processes, solution resistance, and interfacial effects.

Building upon this understanding, the role of feeder electrode geometry in controlling bipolar polarisation was systematically investigated. Three-dimensional feeder architectures were shown to modify ionic current pathways and reshape local potential distributions, enhancing the spatial resolution and intensity of BP-ECL. These findings establish feeder design as a powerful tool for directing wireless electrochemical activation.

Finally, bipolar electrode topology itself was explored as an active parameter for programmable material synthesis. By engineering 2D and 3D electrode architectures, localised PEDOT growth was achieved without lithographic patterning or direct electrode addressing, demonstrating that electrode geometry itself can be used to encode electrochemical function.

Overall, this thesis establishes design principles for controlling bipolar electrochemical systems and advances BPEs from passive electrically polarised elements towards programmable platforms for spatially defined electrochemical materials and devices.

Chapter 1

Thesis Introduction

Introduction

Electrochemistry sits at a unique intersection of physics, chemistry, materials science, and biology as it directly couples electronic and ionic charge transport.(1) This duality makes electrochemical processes fundamentally suited to biological environments, where signalling is inherently electrochemical rather than strictly chemical or electrical. In living systems, ionic gradients regulate cellular excitability, membrane potentials govern communication, and endogenous electric fields influence processes ranging from embryonic development and tissue regeneration to wound healing and disease progression.(2–5) Therefore, electrochemical principles are increasingly embedded in technologies designed not only to interrogate biological systems, but also to actively modulate, and even mimic, them.

This convergence has driven the emergence of electroceuticals, therapies that use electrical or electrochemical stimulation to regulate physiological function.(6) Clinically established examples include deep brain stimulation (DBS) for movement disorders, cochlear implants for hearing restoration, and cardiac pacing systems.(6–9) Beyond these applications, electrochemical modulation is being explored for neural interfacing, cancer therapy, wound repair, immune regulation, and bioelectronic medicine more broadly.(2,6,10–12) In parallel , electrochemical sensing has become central to modern diagnostics, enabling ultrasensitive biomarker detection and multiplexed analysis of complex disease states.(13–16) Together, these advances illustrate the growing importance of electrochemical technologies capable of operating within biologically complex environments.

Despite this progress, the translation of electrochemical systems into biological settings remains fundamentally constrained by architecture.(17–19) Conventional electrochemical devices rely on direct electrical connections between electrodes and external power sources. While this provides precise electrical control under laboratory conditions, it imposes major limitations *in vivo,* where implanted systems require physical leads, power delivery circuitry, and associated hardware. In DBS, for example, intracranial electrodes are connected via insulated leads to a pulse generator implanted in the chest cavity, necessitating additional invasive procedures while introducing multiple points of mechanical failure, infection risk, and long-term tissue damage. Similar challenges arise across implantable electrochemical technologies, where increasing device complexity often scales directly with the number of independently addressable electrodes.

More fundamentally, wired architectures restrict spatial programmability. Each electrochemical element must be individually connected and electronically addressed, limiting scalability, miniaturisation, and spatial flexibility. These constraints become particularly significant in biological systems such as neural tissue, where function emerges from highly distributed and spatially heterogenous networks. Future bioelectronic technologies will therefore require strategies capable of delivering localised sensing, stimulation, and electrochemical communication without relying on increasingly complex wiring. (20)

These limitations motivate bipolar (BP) electrochemistry, a field-driven electrochemical framework in which electrically floating, polarisable conductors are placed within a solution potential gradient generated by an externally applied field. This potential difference across the electrolyte induced a corresponding interfacial potential difference along the length of the conductive object i.e. BPE, leading to spontaneous anodic and cathodic polarisation at opposing ends. In bipolar systems, electrochemical reactions are therefore induced without direct electrical connection to the electrode itself.(21–23) Instead, oxidation and reduction processes arise from field-driven polarisation governed by the local solution potential distribution rather than physical wiring or externally imposed electrode potentials.

This decoupling of electrochemical function from direct electrical connectivity creates opportunities for inherently wireless electrochemical systems. Multiple BPEs can be activated simultaneously using a single externally applied field, enabling parallel operation without the need for individual wiring. However, realising and predicting such behaviour is non-trivial, as the local electric field strength and potential distribution within the electrolyte are strongly dependent on cell geometry, boundary conditions, and solution conductivity, and are not always directly accessible without modelling or indirect visualisation approaches.

Importantly, electrochemical behaviour in such systems is heavily reliant on the relationship between electrode geometry, orientation, material properties, and the resulting local field distribution. Consequently, bipolar electrochemistry offers more than a wireless analogue of conventional electrochemistry, it introduces the possibility that electrochemical function itself may be spatially directed through manipulation and engineering of the electric field.

Conducting polymers such as poly(3,4-ethylenedioxythiophene), PEDOT, are especially relevant within this context because they combine electronic conductivity, ionic transport capability, electrochemical activity, and biocompatibility. These materials can be electrochemically deposited directly onto electrode surfaces while simultaneously supporting ion-electron transduction at biological interfaces. As a result, conducting polymers have become increasingly important in bioelectronic devices, neural interfaces, electrochemical sensors, and electroactive biomaterials.

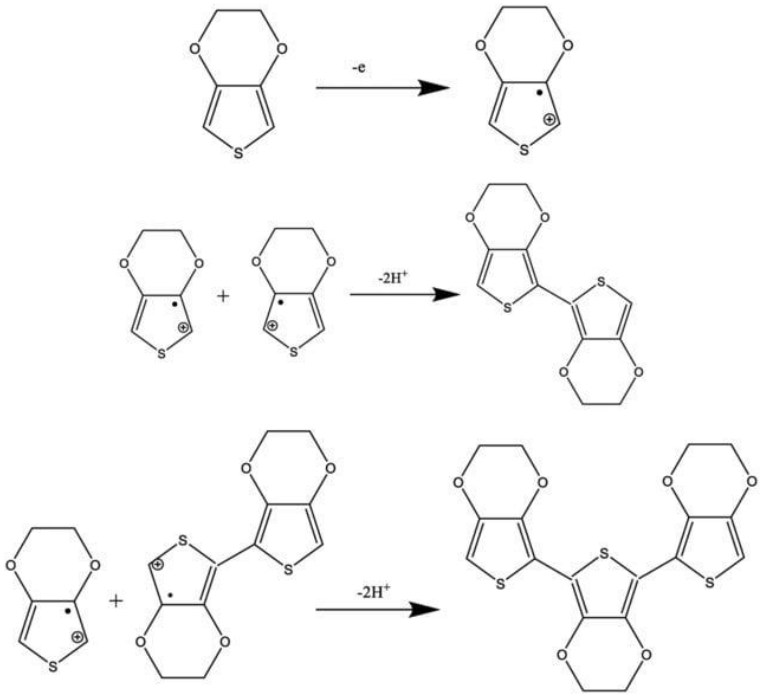


Figure 1 – Schematic illustration of the oxidative electropolymerisation mechanism of neutral EDOT monomers. Oxidation via heterogeneous electron transfer at the polarised electrode surface generates EDOT radical cations, which undergo homogeneous radical-radical coupling followed by deprotonation to produce dimers, trimers, higher oligomers, and ultimately repeating PEDOT polymer chains.

More recently, their compatibility with bipolar electrochemical methods has begun to be explored, suggesting potential routes towards spatially controlled formation of functional

electroactive interfaces under wireless conditions, although the number of demonstrated systems remains limited and the approach is still largely at a proof-of-concept stage.

Despite the considerable appeal of bipolar electrochemistry, the field remains dominated by function-oriented demonstrations, e.g., electroanalysis, in which emphasis is often placed on the final electrochemical output rather than on developing a detailed mechanistic understanding of how electric fields, ionic currents, and interfacial polarisation evolve throughout bipolar systems. Bipolar platforms are frequently evaluated according to observable responses, such as material deposition,(24–27) electrochemiluminescence generation,(28–31) sensing performance,(23,32) or biological stimulation,(33–35) while comparatively less attention has been devoted to understanding the spatial electrochemical processes that fundamentally govern why these systems behave as they do.

Consequently, bipolar electrochemistry is still commonly interpreted using simplified descriptions that assume planar electrode geometries, uniform solution conductivity, and approximately linear potential decay between feeder electrodes. While these approximations may adequately describe idealised systems operating in highly conductive electrolytes, they become increasingly insufficient in low-conductivity or spatially heterogenous environments. Under such conditions, electric field distributions because highly non-uniform, local ohmic drop becomes significant, and electrochemical behaviour becomes strongly dependent on geometry, confinement, ionic transport, and interfacial kinetics. These effects are particularly important in biologically relevant systems, where conductivity is spatially diverse and electrochemical interfaces frequently exist within confined or structurally complex environments.

A central objective of this thesis is therefore to transition bipolar electrochemistry from a predominantly phenomenological technique towards a predictive, geometry-driven electrochemical farmwork. Rather than treating bipolar electrodes as conductors responding to uniformly to externally imposed fields, this work investigates how electrode architecture itself influences local field distributions, redistributes ionic current pathways, and determines where electrochemical activity can occur. In doing so, the thesis explores how electrochemical functionality may be spatially programmed through deliberate manipulation of geometry, confinement, orientation, and topological coupling.

This work situates bipolar electrochemistry within the broader context of electroceuticals and bioelectronic systems, where the limitations of conventional wired architectures motivate the development of field-driven alternatives. This establishes the conceptual basis for viewing BP-electrochemistry not simply as a wireless experimental configuration, but as a fundamentally different mode of electrochemical control in which spatial activity emerges through externally imposed electric fields. For example, whereas induced potential in conventional planar bipolar systems is largely governed by electrode length and orientation within a uniform field, extending into three-dimensional architectures may permit more complex field distributions, enabling spatially differentiated electrochemical activity within discrete regions of a single structure.

From this perspective, an important mechanistic question emerges, how electric fields generate within bipolar systems once the assumptions underpinning classical one-dimensional descriptions begin to break down. This question becomes especially relevant in low-conductivity environments, where ionic transport limitations and spatial confinement are expected to strongly influence local polarisation behaviour. To investigate these effects, this thesis examines conducting polymer deposition in electrolyte-free bipolar systems through the electropolymerisation of PEDOT in ultrapure water. Combining finite element modelling (FEM) with experimental electrochemical characterisation revealed that electrochemical activity under these conditions cannot be adequately described using conventional linear potential approximations. Instead, strong local electric field redistribution, interfacial resistance, and geometry-dependent polarisation effects were found to produce highly non-uniform electrochemical behaviour, including spatially confined deposition and asymmetric activation across planar bipolar structures.

Once it becomes apparent that bipolar electrochemical behaviour is governed not solely by applied voltage, but by the spatial redistribution of electric fields within the system, a further question arises, can electrochemical activity itself be deliberately localised or amplified through geometric manipulation of the field environment? This question is particularly important because one of the major limitations associated with the miniaturisation of bipolar systems is the progressively larger electric fields required to maintain sufficient polarisation as electrode dimensions decrease. Developing alternative approaches capable of enhancing

local electrochemical responses without relying exclusively on voltage escalations therefore represents an important challenge for the future development of scalable bipolar technologies.

In conventional BP-electrochemistry, feeder electrodes are generally treated as passive components whole sole function is to establish the external electric field required for bipolar polarisation. Relatively little attention has been directed towards understanding how feeder geometry itself influences field distribution and therefore controls the localisation, intensity, and efficiency of electrochemical activation. This issue is especially significant for wireless bioelectronic systems, where localised stimulation or sensing may be required within highly confined environments while simultaneously minimising device footprint and architectural complexity. (32,36)

Bipolar electrochemiluminescence (BP-ECL) provides a particularly powerful system for investigating these effects because light emission directly visualises regions of local electrochemical activation. By examining how three-dimensional feeder architectures influence BP-ECL behaviour, it becomes possible to probe whether field distributions can be deliberately manipulated to spatially concentrate or redistribute electrochemical activity. More broadly, this provides a means of determining whether electrode geometry itself can function as a programmable parameter for wireless electrochemical activation.

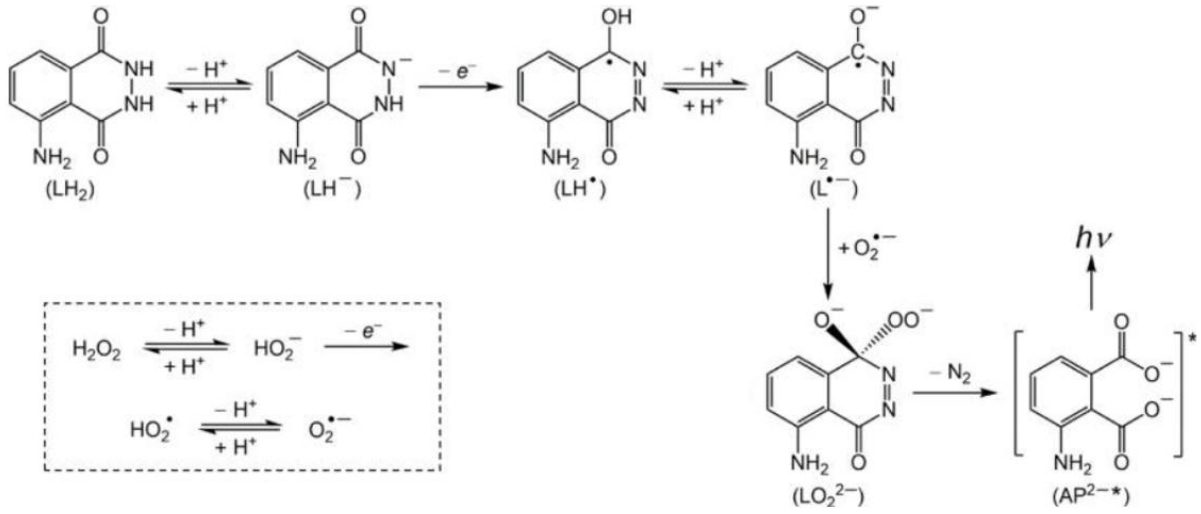


Figure 2 – Schematic representation of the luminol-hydrogen peroxide electrochemiluminescence (ECL) mechanism under alkaline conditions. Luminol is first deprotonated in NaOH to form the electroactive luminol dianion, which undergoes heterogeneous electron transfer at the anodic pole to generate a luminol radical. Simultaneously, hydrogen peroxide is reduced at the cathodic pole to produce reactive oxygen species, predominantly superoxides. Subsequent homogenous chemical reactions between these intermediates form an unstable endoperoxide, which decomposes to generate electronically excited 3-aminopthalate. Relaxation of the excited 3-aminopthalate ion to its ground state results in the emission of blue light (~ 425 nm), producing the observed wireless electrochemiluminescence signal.

While feeder geometry influences how electric fields are delivered throughout bipolar systems, this leads to a wider consideration as to whether architecture of BPEs themselves can actively reshape local electrochemical behaviour. Conventional BP-electrochemistry is predominantly described using planar or quasi-one-dimensional configurations in which electrochemical activity is assumed to scale predictably along a single conductor. Such descriptions, however, overlook the possibility that three-dimensional electrode architectures may fundamentally perturb local field distributions and ionic current pathways in ways that cannot be captured using classical approximations.

Understanding these effects is particularly important for the development of advanced electroactive materials, wireless bio interfaces, and spatially programmable electrochemical systems. If electrode topology can be used to direct local polarisation behaviour in a predictable manner, BP-electrochemistry could provide a route towards electrochemical platforms in which functionality is encoded geometrically rather than electronically. Such an approach would create opportunities for targeted and region-specific electrosynthesis, asymmetric catalytic interfaces, distributed sensing architectures, and spatially selective bioelectronic stimulation. (6,21,35,37,38*)*

Three-dimensional BPE architectures provides a means of exploring this possibility because they introduce geometric heterogeneity, confinement effects, and field interactions that are absent in planar systems. Vertical structures, coupled bipolar elements, and non-planar

geometries e.g. L-shaped BPEs are expected to alter local field distributions, potentially enabling field focusing, confinement-driven amplification, and cooperative electrochemical behaviour between neighbouring conductive structures. Establishing how such architectures influence electrochemical activity is therefore paramount for developing general design principles capable of linking electrode geometry to spatial electrochemical function.

Collectively, the studies presented throughout this thesis investigate how geometry, confinement, and topology govern electrochemical behaviour within open bipolar cells. By integrating concepts from electrochemistry, electric field theory, materials science, and bioelectronics, this work aims to establish BP-electrochemistry not simply as a wireless alternative to conventional electrochemistry, but as a framework for architecturally programmable electrochemical systems in which spatial functionality can be encoded through deliberate manipulation of electric fields.

References

1. Tarabella, G.; Mohammadi, F. M.; Coppedè, N.; Barbero, F.; Iannotta, S.; Santato, C.; et al. New opportunities for organic electronics and bioelectronics: ions in action. *Chemical Science* **2013**, *4*(4), 1395–1409. doi:10.1039/C2SC21740F.

2. Zhao, M.; Song, B.; Pu, J.; Wada, T.; Reid, B.; Tai, G.; et al. Electrical signals control wound healing through phosphatidylinositol-3-OH kinase-γ and PTEN. *Nature* **2006**, *442*(7101), 457–460. doi:10.1038/nature04925.

3. Nuccitelli, R. Endogenous electric fields in embryos during development, regeneration and wound healing. *Radiation Protection Dosimetry* **2003**, *106*(4), 375–383. doi:10.1093/oxfordjournals.rpd.a006375.

4. *Molecular bioelectricity: how endogenous voltage potentials control cell behavior and instruct pattern regulation in vivo | Molecular Biology of the Cell*. <https://www.molbiolcell.org/doi/10.1091/mbc.e13-12-0708?utm_source=chatgpt.com> Accessed 26.05.25.

5. Forster, R. J. Wirefree electroceuticals: 3D electrical and electrochemical stimulation of biological systems. *Current Opinion in Electrochemistry* **2023**, *39*, 101297. doi:10.1016/j.coelec.2023.101297.

6. Sanjuan-Alberte, P.; Alexander, M. R.; Hague, R. J. M.; Rawson, F. J. Electrochemically stimulating developments in bioelectronic medicine. *Bioelectronic Medicine* **2018**, *4*(1), 1. doi:10.1186/s42234-018-0001-z.

7. Segovia-Martinez, M.; Vanpoucke, F.; Landsberger, D.; Molaee-Ardekani, B. Cochlear Implant Development: From Early Concepts to Future Directions. In *Advancing Cochlear Implants: Current and Emerging Methods and Technologies*. Molaee-Ardekani, B., Segovia-Martinez, M., Eds.; Springer Nature Switzerland: Cham, 2026; pp 3–31. doi:10.1007/978-3-032-15719-5_1.

8. Lozano, A. M.; Lipsman, N.; Bergman, H.; Brown, P.; Chabardes, S.; Chang, J. W.; et al. Deep brain stimulation: current challenges and future directions. *Nature Reviews Neurology* **2019**, *15*(3), 148–160. doi:10.1038/s41582-018-0128-2.

9. Doyle, O. F.; Forster, R. J. Wirefree Electrochemistry for Enhanced Detection and Treatment of Disease. *Electrochemistry Communications* **2024**, *169*, 107832. doi:10.1016/j.elecom.2024.107832.

10. Das, R.; Langou, S.; Le, T. T.; Prasad, P.; Lin, F.; Nguyen, T. D. Electrical Stimulation for Immune Modulation in Cancer Treatments. *Frontiers in Bioengineering and Biotechnology* **2022**, *9*. doi:10.3389/fbioe.2021.795300.

11. Yuk, H.; Lu, B.; Zhao, X. Hydrogel bioelectronics. *Chemical Society Reviews* **2019**, *48*(6), 1642–1667. doi:10.1039/C8CS00595H.

12. Yu, R.; Zhang, H.; Guo, B. Conductive Biomaterials as Bioactive Wound Dressing for Wound Healing and Skin Tissue Engineering. *Nano-Micro Letters* **2021**, *14*(1), 1. doi:10.1007/s40820-021-00751-y.

13. Electrochemical Biosensing of Bacteria and Biofilms. **2023**, 800–813. doi:10.1016/B978-0-12-822548-6.00117-5.

14. Popov, A.; Brasiunas, B.; Blazevic, K.; Kausaite-Minkstimiene, A.; Ramanaviciene, A. Ultra-sensitive electrochemical immunosensors for clinically important biomarker detection: Prospects, opportunities, and global trends. *Current Opinion in Electrochemistry* **2024**, *46*, 101524. doi:10.1016/j.coelec.2024.101524.

15. Wu, J.; Liu, H.; Chen, W.; Ma, B.; Ju, H. Device integration of electrochemical biosensors. *Nature Reviews Bioengineering* **2023**, *1*(5), 346–360. doi:10.1038/s44222-023-00032-w.
16. Sharafeldin, M.; Rusling, J. F. Multiplexed electrochemical assays for clinical applications. *Current Opinion in Electrochemistry* **2023**, *39*, 101256. doi:10.1016/j.coelec.2023.101256.
17. Polyravas, A. G.; Proctor, C. M.; Curto, V. F.; Carnicer-Lombarte, A.; Malliaras, G. G.; Barone, D. G. Organic Bioelectronics. In *Handbook of Neuroengineering*; Springer, Singapore, 2023; pp 441–466. doi:10.1007/978-981-16-5540-1_106.
18. Rivnay, J.; Inal, S.; Salleo, A.; Owens, R. M.; Berggren, M.; Malliaras, G. G. Organic electrochemical transistors. *Nature Reviews Materials* **2018**, *3*(2), 17086. doi:10.1038/natrevmats.2017.86.
19. Rivnay, J.; Owens, R. M.; Malliaras, G. G. The Rise of Organic Bioelectronics. *Chemistry of Materials* **2014**, *26*(1), 679–685. doi:10.1021/cm4022003.
20. Famm, K.; Litt, B.; Tracey, K. J.; Boyden, E. S.; Slaoui, M. A jump-start for electroceuticals. *Nature* **2013**, *496*(7444), 159–161. doi:10.1038/496159a.
21. Shida, N.; Zhou, Y.; Inagi, S. Bipolar Electrochemistry: A Powerful Tool for Electrifying Functional Material Synthesis. *Accounts of Chemical Research* **2019**, *52*(9), 2598–2608. doi:10.1021/acs.accounts.9b00337.
22. Loget, G.; Zigah, D.; Bouffier, L.; Sojic, N.; Kuhn, A. Bipolar Electrochemistry: From Materials Science to Motion and Beyond. *Accounts of Chemical Research* **2013**, *46*(11), 2513–2523. doi:10.1021/ar400039k.
23. Mavré, F.; Anand, R. K.; Laws, D. R.; Chow, K.-F.; Chang, B.-Y.; Crooks, J. A.; et al. Bipolar Electrodes: A Useful Tool for Concentration, Separation, and Detection of Analytes in Microelectrochemical Systems. *Analytical Chemistry* **2010**, *82*(21), 8766–8774. doi:10.1021/ac101262v.
24. Brady, Á.; Wagner, M.; Forster, R. J. Regio selective deposition of conducting polymers using wireless electropolymerisation. *Chemical Communications* **2024**, *60*(89), 13000–13003. doi:10.1039/D4CC03996C.
25. Koizumi, Y.; Shida, N.; Ohira, M.; Nishiyama, H.; Tomita, I.; Inagi, S. Electropolymerization on wireless electrodes towards conducting polymer microfibre networks. *Nature Communications* **2016**, *7*(1), 10404. doi:10.1038/ncomms10404.
26. Wagner, M.; Brady, Á.; Doyle, O. F.; Forster, R. J. Advancing Bipolar Electrochemistry for Targeted Deposition of Biocompatible Polymers in Electrolyte-Free Solutions via Finite Element Modeling. *ChemElectroChem* **2025**, *12*(6), e202400506. doi:10.1002/celc.202400506.
27. Brady, Á.; Forster, R. J. Electric Field Distribution in Bipolar Electrochemical Cells: Effects on the Wirefree Electrodeposition of Conducting Polymer Films. *Analytical Chemistry* **2025**, *97*(1), 410–418. doi:10.1021/acs.analchem.4c04454.
28. Villani, E.; Zhang, Y.; Chen, Z.; Zhou, Y.; Konishi, M.; Tomita, I.; et al. AC-Bipolar Electrosynthesis and Luminol Electrochemiluminescence Imaging of Poly(3,4-ethylenedioxythiophene) and Its Composite Films. *ACS Applied Polymer Materials* **2023**, *5*(8), 6186–6198. doi:10.1021/acsapm.3c00838.
29. Villani, E.; Ino, K.; Inagi, S.; Shiku, H. Bipolar Electrochemiluminescence Imaging for Electroanalysis. In *Electrogenerated Chemiluminescence Microscopy and Imaging: Theory, Instruments, and Applications*. Paolucci, F., Fiorani, A., Valenti, G., Marcaccio, M.,

Eds.; Springer Nature Switzerland: Cham, 2026; pp 313–332. doi:10.1007/978-3-032-14602-1_11.
30. Cumba, L.; Pellegrin, Y.; Melinato, F.; Forster, R. J. Enhanced Electrochemiluminescence from 3D Nanocavity Electrode Arrays. *Sensors and Actuators Reports* **2022**, *4*, 100082. doi:10.1016/j.snr.2022.100082.
31. Li, C.; Feng, M.; Stanković, D.; Bouffier, L.; Zhang, F.; Wang, Z.; et al. Wireless rotating bipolar electrochemiluminescence for enzymatic detection. *Analyst* **2024**, *149*(9), 2756–2761. doi:10.1039/D4AN00365A.
32. Wang, Y.-L.; Cao, J.-T.; Liu, Y.-M. Bipolar Electrochemistry – A Powerful Tool for Micro/Nano-Electrochemistry. *ChemistryOpen* **2022**, *11*(12), e202200163. doi:10.1002/open.202200163.
33. Rajnicek, A. M. Bioelectricity Buzz. *Bioelectricity* **2022**, *4*(2), 126–132. doi:10.1089/bioe.2022.0018.
34. Qin, C.; Yue, Z.; Chao, Y.; Forster, R. J.; Maolmhuaidh, F. Ó.; Huang, X.-F.; et al. Bipolar electroactive conducting polymers for wireless cell stimulation. *Applied Materials Today* **2020**, *21*, 100804. doi:10.1016/j.apmt.2020.100804.
35. *Bipolar Electrochemical Stimulation Using Conducting Polymers for Wireless Electroceuticals and Future Directions | ACS Applied Bio Materials*. <https://pubs.acs.org/doi/10.1021/acsabm.2c00679> Accessed 26.05.25.
36. Foley Doyle, O.; G. Wallace, G.; Yue, Z.; Chen, J.; Beirne, S.; J. Forster, R. Directing the glow: 3D feeder geometries to enhance planar bipolar electrochemiluminescence. *Chemical Communications* **2025**, *61*(97), 19221–19224. doi:10.1039/D5CC04706D.
37. Ab Mutalib, N. A.; Suzuki, H. Evolution in the development of next generation electrochemical microdevices via bipolar electrochemistry. *Current Opinion in Electrochemistry* **2024**, *43*, 101424. doi:10.1016/j.coelec.2023.101424.
38. Koefoed, L.; Pedersen, S. U.; Daasbjerg, K. Bipolar electrochemistry—A wireless approach for electrode reactions. *Current Opinion in Electrochemistry* **2017**, *2*(1), 13–17. doi:10.1016/j.coelec.2017.02.001.

Bipolar electrochemistry has evolved from a niche electrochemical phenomenon into a versatile platform capable of supporting applications across sensing, materials science, bioelectronics and electroceutical technologies. The wireless nature of bipolar systems offers significant advantages over conventional electrochemical approaches, including simplified device architectures, parallelisation of electrochemical processes and opportunities for remote control of electrochemical activity. However, despite rapid growth in both fundamental and application driven research, several critical scientific and engineering challenges remain unresolved. Many existing bipolar electrochemical systems have been developed empirically, with comparatively limited understanding of how electric field affects can be deliberately manipulated to predict and control electrochemical behaviour.

Electric fields within bipolar electrochemical systems remains incompletely understood or in many cases assumed to be uniformly distributed between the feeder couple, despite electric field distributions ultimately governing the magnitude, location, and selectivity of electrochemical reactions. Furthermore, advances in biosensing, conducting polymer synthesis, controlled drug delivery and wireless cellular stimulation have increasingly highlighted the importance of understanding how electrochemical activity can be spatially controlled and manipulated within these systems. This forms the central hypothesis of the present thesis: that rational engineering of electric field distributions, through deliberate control of system geometry and architecture, can provide a powerful strategy for directing and enhancing wireless electrochemical function. This chapter provides a critical review of contemporary developments in bipolar electrochemistry, with particular emphasis placed on biomedical applications and emerging wirefree electrochemical technologies.

Rather than serving solely as a summary of existing knowledge, this review establishes the conceptual framework underpinning the research presented throughout this thesis by identifying the principal scientific barriers limiting wider implementation of bipolar electrochemistry. Importantly, this review frames the scientific context for the research presented throughout the remainder of this thesis and identifies electric field distribution and spatial control of electrochemical activity as central unresolved challenges that motivate the experimental investigations described in the subsequent chapters.

Chapter 2

Wirefree Electrochemistry for Enhanced Detection and Treatment of Disease

Electrochemistry Communications 169 (2024) 107832 *doi.org/10.1016/j.elecom.2024.10782*

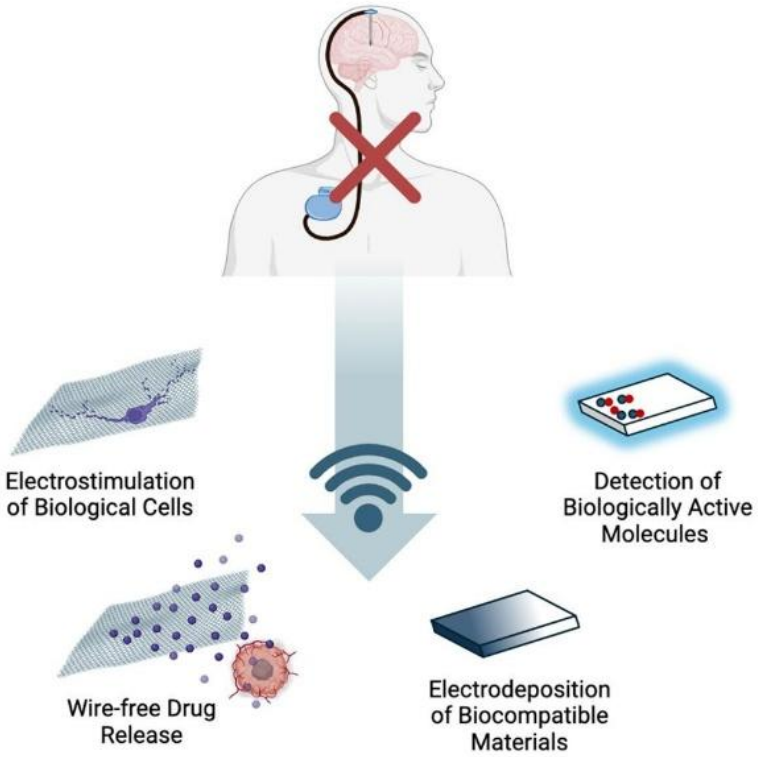
Wirefree Electrochemistry for Enhanced Detection and Treatment of Disease

Oisín Foley Doyle [a], Robert J. Forster [ab*]

a. School of Chemical Sciences, Dublin City University, Glasnevin, Ireland

b. FutureNeuro, SFI Research Centre for Chronic and Rare Neurological Diseases, Dublin City University, Dublin 9, Ireland

Graphical Abstract



Abstract

Wirefree, or bipolar electrochemistry, BPE, has the potential to transform patient outcomes through early diagnosis using ultrasensitive sensors for multiple biomarkers and personalised treatments such as enhanced cell growth, differentiation and destruction as well as local delivery of therapeutics . We highlight the emerging field of wirefree electroceuticals and show how BPE could enable precise modulation of neural circuits, non- pharmaceutical therapies for conditions like Parkinson's Disease and chronic pain management , as well as on-demand drug delivery with high spatial and temporal precision. Moreover, it explores the integration of advanced nanomaterials illustrating their pivotal role in enhancing electrode performance and biocompatibility, thereby maximising their potential diagnostic and therapeutic efficacy especially *in vivo.*

1. Introduction

Electrochemistry enables many aspects that are central to contemporary, personalised, healthcare from the detection of disease biomarkers at ultralow concentrations (sub-pM) [1], to the electrical stimulation of biological cells to block Parkinson's Tremor as well as enhancing cell proliferation, differentiation, interconnection and selective destruction [1–6]. For certain diseases and conditions, e.g., the control of epileptic seizures, Parkinson's tremor, incontinence, chronic pain, cancer, hypertension, cerebrovascular and pulmonary diseases, electroceuticals represent a powerful alternative to the challenges and costs (≈€10bn) of developing a new active pharmaceutical ingredient (API) and bringing it successfully through clinical trials. However, traditional electrochemical approaches typically use physical wires to connect a working electrode or sensor to a potentiostat or power supply. This "wired" approach can make it challenging to create wearable or implantable devices, e.g., the highly successful deep brain stimulation electrodes used for Parkinson's tremor require wires from the brain to a power pack and waveform generator implanted in the chest, a significant invasive, *additional*, procedure which can cause persistent complications.

The incidence of either hardware or bio-related *in-vivo* complications occurring post-therapy can be as high as 30–40 % [7]. Common hardware-related complications include migration, fracture and failure of wired components which can damage the surrounding tissues and cellular microenvironment. Moreover, the number of electrodes (stimulation locations) is limited in part due to the challenge of wiring large numbers of electrodes. These issues could be reduced using bipolar electrochemistry since the *implanted* physical infrastructure, wiring, batteries, charging system etc., is substantially reduced or removed entirely. From a disease detection and diagnosis perspective, it is increasingly clear that for most conditions, *multiple* analytes must be quantified simultaneously to achieve the required clinical sensitivity (true positive rate, probability of a positive test result for a positive individual) and specificity (true negative rate, probability of a negative test result for an individual who is actually negative). However, this can be very challenging when each sensor must be individually wired to an independently controllable potentiostat/ power supply. In contrast, BPE allows the potential of individual elements within an array of electrodes to be controlled independently, e.g., by changing their length, in a manner that is scalable in terms of the number of electrodes.

Poor patient health outcomes and low quality of life continue to challenge people with neurological issues such as Alzheimer's disease, Parkinson's disease and Amyotrophic lateral sclerosis (ALS) including cognitive decline, premature death and high rates of institutionalised care [8]. The primary factors which contribute to poor patient prognosis in neurological disorders include the complexity of the central nervous system (CNS) and brain neural network, the degenerative nature of the disease, lack of distinctive biomarkers and effective diagnostic techniques and an incomplete understanding of disease mechanisms at the cellular level [9–13]. As a result, many approaches are currently focused on treating symptoms treatments rather than the underlying pathophysiology [14]. The burgeoning field of *wired* electroceuticals has significantly improved the quality of life for patients suffering from chronic pain, muscle damage and combating involuntary movement disorders such as tardive dyskinesia, akinesia and dystonia [15]. Electroceuticals use electrical/electrochemical impulses to stimulate cells locally and can be applied to neuronal/nerve cells as well as cardiac, smooth muscle, and mitotic cells. Recent work suggests that all cells may respond to electrical/electrochemical stimuli most likely linked to their resting membrane potential. Therefore, there may be broad scope to use electroceuticals for cell manipulation, e.g., stimulated growth and differentiation, and stimulation through electrical, electrochemical and active pharmaceutical ingredients delivered using electrically driven drug delivery systems [16].

2. Mechanism of Wirefree Electrical and Electrochemical Stimulation

As illustrated in Fig. 1, in wirefree or bipolar electrochemistry, a voltage difference is applied to two or more feeder or drive electrodes by connecting them to an external DC or AC power source to generate an electric field within a (biological) sample, an array of biological cells or tissue. The simplest configuration involves a pair of feeder electrodes placed perpendicularly a short distance from either end of a horizontal bipolar electrode. Under ideal conditions, the electric field through the solution would decay approximately linearly causing a linear change in the potential induced in the bipolar electrode along its length [17]. The magnitude of the voltage induced within the bipolar electrode is determined by the local electric field strength (controlled by the voltage difference applied to the pair of drive electrodes), the separation between the feeders, the physical size of the bipolar electrode and the concentration of the

supporting electrolyte. The bipolar electrode acts as a complete electrochemical cell and, if the induced potentials are sufficient, oxidation can occur at one end, or pole, of the bipolar electrode and reduction at the other with the electrons transferred being balanced [18].

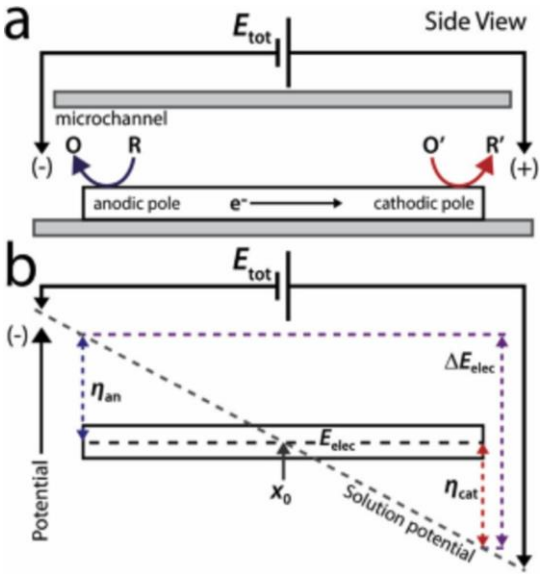


Fig. 1. a) Side-view schematic representation of bipolar inherent dual redox capabilities. A planar BPE placed between two feeder electrodes with specific voltage potentials leads to distinct redox reactions occurring at the poles of the BPE structure. Oxidation of the solution species occurs at the anodic pole whereas simultaneous reduction of the solution species is experienced at the cathodic pole. b) Schematic illustration of the electric field-induced gradient overpotential across the BPE surface. The highest potentials are observed at the poles i.e. site of redox reactions. A depletion zone of which no overpotential is observed is depicted at the midpoint of the BPE however the nature of the faradaic reactions impacts the exact location of this zero potential boundary for each BPE. Reproduced from Crooks, R. M. Principles of Bipolar Electrochemistry. ChemElectroChem 2016, 3 (3), 357–359. Doi:10.1002/celc.201500549.

One challenge of this electrode configuration is that the current cannot be easily measured directly, but this issue can be solved by more sophisticated configurations. For example, a pair of split BPEs linked by an ammeter or linking the current flow to electrochemiluminescence.

As shown in Fig. 2, the potential distribution through the solution is rarely truly linear,[2] e.g., when an electrolyte is present (almost inevitable for biological samples) the electric field strength will decrease essentially exponentially close to the feeder electrodes leaving only a fraction of the field available to induce voltages within the working bipolar electrode. Therefore, to achieve the required electric field strength in solution that will induce the potential needed to drive an electrochemical process of interest, the voltage applied to the feeder electrodes will have to be increased. This increased voltage, potentially several hundred volts depending on the size of the bipolar electrode and the electrolyte concentration, can cause significant challenges in terms of corrosion of the feeder electrode that is positively biased. An alternating AC voltage can also be applied [3] or, like wireless phone charging, an alternating magnetic field can be used to wirelessly induce a voltage in a remote coil and if electrodes are connected to either end, redox reactions can be driven wirelessly.

Achieving a homogeneous electric field depends strongly on the geometry of the system, e.g., using a bipolar electrode that is narrower than the feeders, or placing it too close to either feeder, can cause inhomogeneities, especially at the edges of the bipolar electrode. Transport mechanisms beyond diffusion also need to be considered. Typically, at least one oxidation state is charged, and any charged species can migrate in the electric field, with Ox and Red possibly moving in different directions, especially when the electrolyte concentration is low. Moreover, current flow through the BPE can change the induced potential locally. These effects can alter faradaic processes ranging from electrochemiluminescence intensity to analyte detection sensitivity and thicker deposits of conducting polymers.

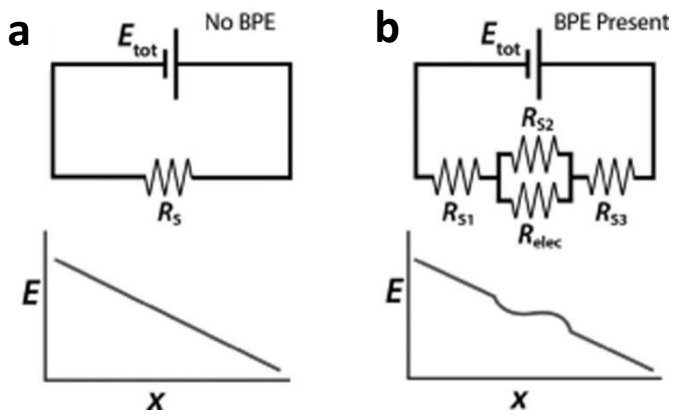


Fig. 2. a) Circuit diagram and potential distribution plot showing an ionic current mediated linear decay in potential across the feeder terminated bipolar cell. **b)** Circuit diagram and potential distribution plot showing a modulated potential distribution across the BPE surface between both poles of the BPE through which electrons can move. Reproduced from Crooks, R. M. Principles of Bipolar Electrochemistry. ChemElectroChem 2016, 3 (3), 357–359. Doi:10.1002/celc.201500549.

3. Detection of Biologically Active Molecules

Measuring the current flow through a bipolar electrode, e.g., in response to the binding of a redox-active target or the binding of a probe strand or secondary antibody labelled with a redox-active probe, generally requires a more complex geometry, e.g., a split bipolar electrode with the two sections bridged by a high impedance ammeter. This challenge has led to a significant increase in wireless electrochemiluminescence (ECL) detection where the light intensity depends on the concentration of the target analyte [4,5]. Significant progress has been made for selective and sensitive (multi-)analyte detection including new luminophores and co-reactants as well as the optimisation of the cell geometry, e.g., miniaturised cells for applications where the sample volume is restricted [6,19–21]. The key advantages of ECL, i.e., a high signal-to-noise ratio due to a dark background leading to low limits of detection, high analytical sensitivity, wide dynamic range, simplified instrumentation since a calibrated light

source is not required and short sample-to-answer times, are preserved, while the bipolar approach enables multianalyte analysis at independent electrodes and avoids the need for individual wired connections and multi-potentiostats.

The early detection of disease biomarkers is associated with improved patient outcomes and improved quality of life years. The clinical sensitivity (true positive rate, individual has disease) and clinical specificity (true negative rate, individual does not have disease) of some biomarkers, such as prostate-specific antigen (PSA) does not allow them to make a definitive diagnosis. However, the ability to conveniently, e.g., in a patient's home, monitor changes in their concentration over time could significantly improve contemporary medicine especially when populations are becoming older. PSA has been detected with wireless ECL [22]. For example, using gold nanoclusters functionalised with 6-aza-2-thiothymine as the luminophore. In an antibody sandwich assay, the binding of a cerium oxide-poly(ethylenimine) composite functionalised with a secondary antibody triggers energy transfer quenching of the ECL. The linear dynamic range is from 1×10^{-5} ng/mL to 200 ng/mL and a LOD of 2.2 fg/mL is reported. Cytokeratin 19 fragment 21-1 (CYFRA 21-1), which is an emerging effective biomarker of lung cancer, has also been detected using a similar bipolar electrochemiluminescence, BPECL, strategy at concentrations from 10 fg/mL to 100 ng/ml [23].

The concentration of alkaline phosphatase, ALP, in serum can be a valuable tumour marker with high specificity for cancers such as liver and sarcomas, especially osteosarcoma. The ability to measure biomarker concentrations at increasingly lower levels has the promise of earlier disease detection, but many BPECL systems achieve LODs in the µM range and there is a need for greater sensitivity. Fig. 3 illustrates an attractive strategy for enhanced analytical performance developed by Zhang and co-workers [24]. When an appropriate voltage is applied to the feeder electrodes, a complete electrochemical cell is generated through electron and ion transfer in solution. The ALP catalysed the conversion of p-APP to 4-aminophenol (p-AP) which was then oxidised at the anode of the BPE leading to ECL at the anode of the driving electrode. Thus, ALP was detected through the oxidation reaction of p-AP ultimately leading to ECL generation. The analytical performance is excellent with signal amplification of approximately 1000-fold compared to conventional strategies leading to an attomolar LOD. ALP could be detected in different types of cells, e.g., single Hep G2 cells which

could have significant benefits for understanding heterogeneity in (cancer) cell populations. Other “small molecule” biomarkers that have been detected using BPECL include tryptamine [25].

An attractive strategy for the rapid development of sample-to-answer devices is to combine 3D printing and smartphone camera detection within a bipolar ECL system. For example, Goel and co-workers [26] developed a six-well 3D-printed closed bipolar ECL for the detection of glucose and choline using luminol/peroxide-based enzymatic reactions.

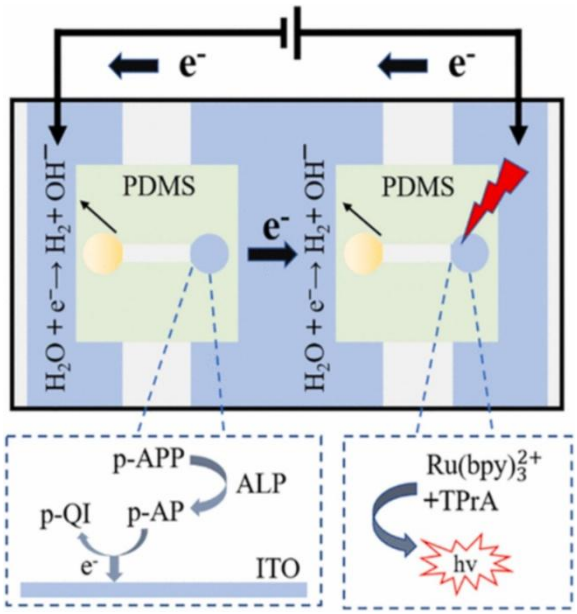


Fig. 3. Electrochemiluminescence detection of ALP based on a closed bipolar cell. Reproduced from Yang, X.-Y.; Bai, Y.-Y.; Huangfu, Y.-Y.; Guo, W.-J.; Yang, Y.-J.; Pang, D.-W.; Zhang, Z.-L.; Ultrasensitive Electrochemiluminescence Biosensor Based on Closed Bipolar Electrode for Alkaline Phosphatase Detection in Single Liver Cancer Cell, Anal. Chem. 2022, 93, 1757–1763, Doi:10.1021/ acs.analchem.0c04517.

A smartphone camera was used to image the ECL emission from which the concentration-dependent ECL intensities could be extracted, as well as using the phone to power the system. The dynamic range was from 0.1 to 10 mM for glucose and 0.1 to 5 mM choline, with LODs of 24 µM and 10 µM, respectively. Preliminary spiking measurements in blood serum suggest significant point-of-care potential for the device, especially for low-resource environments.

Bipolar ECL has also been applied to the detection of biological cells which has important implications for disease detection, e.g., circulating cancer tumour cells and sepsis causing bacterial infections. For example, a nanocomposite comprising luminol-chitosan-platinum nanoparticles has been combined with an aptamer that binds selectively to B lymphoma cells to enable their rapid detection at concentrations as low as 31 cells/mL [27]. BPECL has also been developed as a powerful tool for investigating living cells. For example, as shown in Fig. 4, Sojic and co- workers demonstrated the measurement of intracellular hydrogen peroxide, glucose as well as the sphingomyelinase activity [28]. Their elegant strategy involves a nanopipette tip where the walls are functionalised with platinum that is used as an open bipolar ECL device to achieve intracellular wireless electroanalysis. The combination of the nanopipette geometry and the bipolar ECL generation lead to spatially confined ECL emission from luminol. The porosity of the platinum deposit allows intracellular molecules to move into the nanopipette that are then coupled to enzymatic reactions. Significantly, when compared to classical geometries this device operates at a remarkably low potential thus minimizing the prospect of the voltage influencing cellular activity.

The ECL intensity correlates with the concentration of glucose between 0.1 and 10 mM with an LOD of 0.1 mM which effectively addresses the physiologically relevant range. More significantly, in agreement with results averaged over many cells, measurements on *single* living HeLa cells indicated a hydrogen peroxide concentration of 4 ± 3 mM. BPECL has been developed into a distinct branch of microscopy and applied to biological cells to image biological cells and even sub-cellular structures [29].

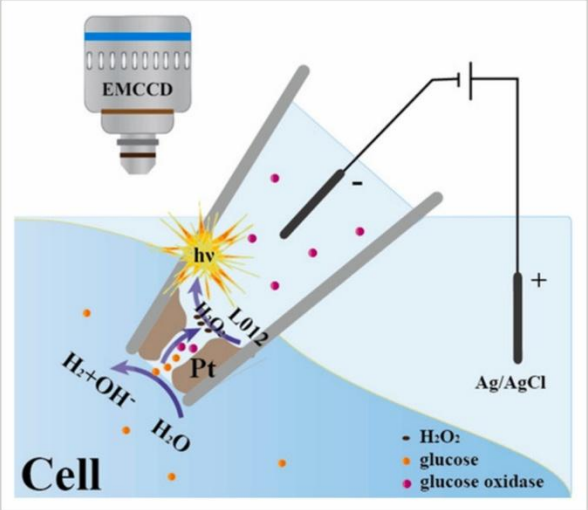


Fig. 4. Representation of the bipolar ECL detection at the porous Pt deposit inside a nanopipette, which is inserted into the cytosol for intracellular wireless electroanalysis. Reproduced from Wang, Y.; Jin, R.; Sojic, N.; Dechen Jiang, D.; Chen, H.-Y.; Intracellular Wireless Analysis of Single Cells by Bipolar Electrochemiluminescence Confined in a Nanopipette, Angew. Chem. Int. Ed., 2020, 132(26), 10502–10506, Doi:10.1002/ange.202002323.

4. Electrodeposition of Nanomaterials

The formation of thin films and nanomaterials using instrumental and chemical methods is pivotal to diverse health-related challenges from sensors for biomarker detection to on demand drug release systems and electroceutical platforms for the electrical and electrochemical stimulation of cells and tissue. Conducting polymers play a central role in all of these for health- oriented applications and as shown in Fig. 5, the ability to control the thickness, morphology, biocompatibility and stability of thin films is particularly important. Electrodeposition using conventional 3-electrode cells allows *uniform* films of conducting polymers to be deposited and when templates, e.g., 2D and 3D arrays of particles (nanosphere lithography), are used, shaped conducting polymer (CP) films/3D structures and (nano)wires can be created [30].

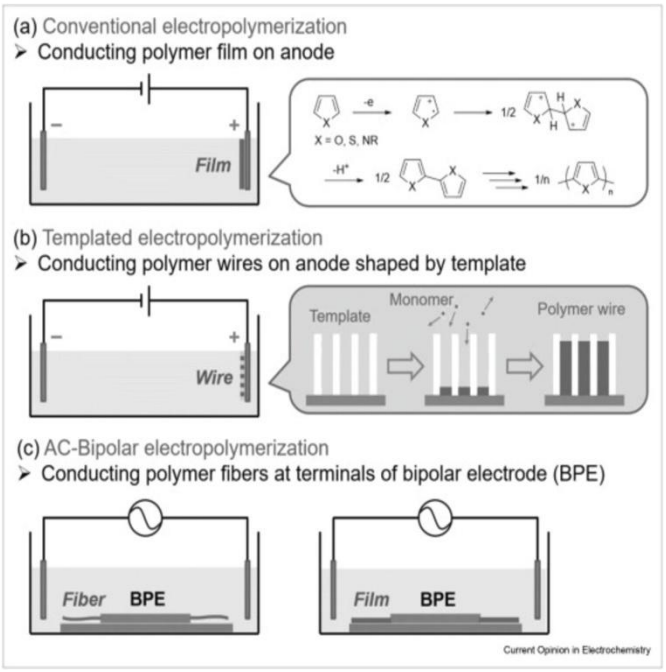


Fig. 5. a) Deposition of a conducting polymer film on the surface of the wired anodic feeder electrode using electrically induced chemical oxidation and subsequent polymerization of the monomer species in an electrolyte solution. **b)** Formation of conducting polymer wires spatially dictated by an inert template located on the anodic feeder electrode surface. **c)** Schematic illustration of fibre-conducting polymer depositions (left) and film deposition (right) at the anodic terminal of the immersed wire-free bipolar electrode (BPE) facilitated by the modified electric field housed by the wired feeder electrodes. Reproduced from Chen, Z.; Villani, E.; Inagi, S. Recent Progress in Bipolar Electropolymerisation Methods toward One-Dimensional Conducting Polymer Structures. Curr. Opin. Electrochem. 2021, 28, 100702. Doi:10.1016/j.coelec.2021.100702.

Significantly, *wireless* electrochemistry allows films with both thickness and composition gradients to be created on diverse bipolar electrode materials and shapes from plates to spherical nanoparticles and 3D-printed scaffolds [31]. If the potential-dependent rate of heterogeneous electron transfer influences the rate of film formation, then for a fixed electrodeposition time, the film thickness is different for different locations on the electrode because the potential is not uniform across the BPE surface. Moreover, its "*as synthesised*"

redox composition, and perhaps its morphology (due to different deposition rates) will vary across the surface. These variations could be used as a kind of "*2D barcode*" to quickly identify the optimum thickness, chemical composition and redox state for a given application, e.g., sensors, drug release systems, cell culture surfaces and valving in microfluidic systems. In addition, Fig. 6 shows that complex CP branching patterns may be formed without the use of a template [32]. Additionally, dendrite-inspired CP fibres form at both terminals of a BPE by using AC-bipolar electropolymerisation. This AC approach periodically swaps the anode and cathode giving very different materials compared to DC fields. It provides an excellent demonstration of the direct connection between the electric field distribution in space and time and the materials properties. It also shows how novel materials with different thicknesses, redox compositions and structures, e.g., porosity as controlled by the deposition rate, can be created using bipolar electrochemistry.

From a production standpoint, it is significantly easier to produce large numbers of films using BPE since multiple bipolar electrodes can be immersed in parallel between a single pair of feeder electrodes without the need for dedicated, individual interconnects allowing many identical coatings to be produced simultaneously.

5. Wire-free Release of Active Pharmaceutical Ingredients

Healthcare is moving away from blockbuster drugs and a 'one-size fits all' approach to personalised medicine where drug selection and dosage are based on an individual's unique genome, metabolism, and immune response. There are significant opportunities for advanced Drug Delivery Systems (DDS) that can release APIs on demand, ideally informed by a sensor-based measurement of the systemic concentration for closed-loop control. These systems could avoid the cumulative and life-threatening side effects of some therapies (it is estimated that there are more than 200,000 deaths annually in the EU due to side effects of medicines costing more than €80 billion annually). Some electrodeposited CPs are highly biocompatible and can be loaded with APIs that can be effectively released by oxidising the film. The total loading depends on the quantity of CP deposited and the release kinetics are highly sensitive to the CP composition, the micro- and nano-scale structure of the layer (influenced by the electrodeposition conditions), and the oxidation state of the polymer film [33]. Wirefree

electrochemistry has attractive properties for the electrodeposition of the CP- based DDS, e.g., the ability to generate films with mixed chemical composition/structure and different drug loadings along their length, as well as Janus drug-loaded particles.

Also, from the perspective of release, they offer the possibility of achieving different API release rates along their length because of a different structure or the potential gradient that is established by the feeders. These properties could improve the outcome of cancer patients, e.g., by delivering a high dose of an antineoplastic drug close to the centre of a tumour and a lower concentration further away to reduce side effects. The ability to deliver a drug locally, e.g., miRNA, or neuro-growth factors in the brain to treat neurodegenerative conditions such as Parkinson's, Alzheimer's and Huntington's and overcome the blood–brain barrier is likely to be especially impactful. Effective wireless release of a neuro-growth factor, brain-derived neurotrophic factor (BDNF) was successfully demonstrated by Qin and co-workers [34] whereby the BNDF particles embedded in a PPy-PMAS conducting polymer film were released following the application of wireless bipolar electrical stimulation, this led to enhanced neurite outgrowth of human neuroblastoma (SH-SY5Y) cells.

6. Electrostimulation of Biological Cells

The implantation of cells represents a significant emerging therapeutic intervention to treat diseases ranging from diabetes to neurodegeneration and nerve cell regrowth. It has become increasingly clear that electrochemical processes play a key role in many physiological and biochemical processes from nerve impulse transmission and mediating electrolyte balance to enabling antioxidant defence mechanisms and acting as a driving force for metabolic pathways and redox signalling. The ability to manipulate cellular responses and invoke phenotypic alterations of target cells through electrochemical stimulation is of utmost

importance, not only for elucidating disease mechanisms, but also to more precisely mimic biological systems and to optimise the performance of implantable bioelectronic devices [35]. Cell stimulation can drive cell proliferation, differentiation and interconnection of nerve-related cells.

Bipolar electrochemical stimulation, BPES, allows cells immobilised on a conducting platform to be stimulated wirelessly with potentials whose spatial and temporal properties can be

controlled. Electronically conducting polymers (CP) are very attractive for the creation of biocompatible, implantable devices and have proven useful in tissue engineering and controlled drug release systems [33]. A particularly important material is poly(3,4-ethylene dioxythiophene) (PEDOT) that can be doped with a diverse range of synthetic or biological counter-ions, with the most common being polystyrene sulfonate (PSS) [36]. PEDOT was used in the very first coated neural probes in 2003 [37] and the first PEDOT electrodes were placed in the human brain approximately a decade ago [38]. A significant challenge for translating implantable devices into clinical practice is FDA approval but this was successfully achieved for PEDOT in 2016 through the 'Amplicoat', technology and there is good reason to be optimistic about other CPs in the future.

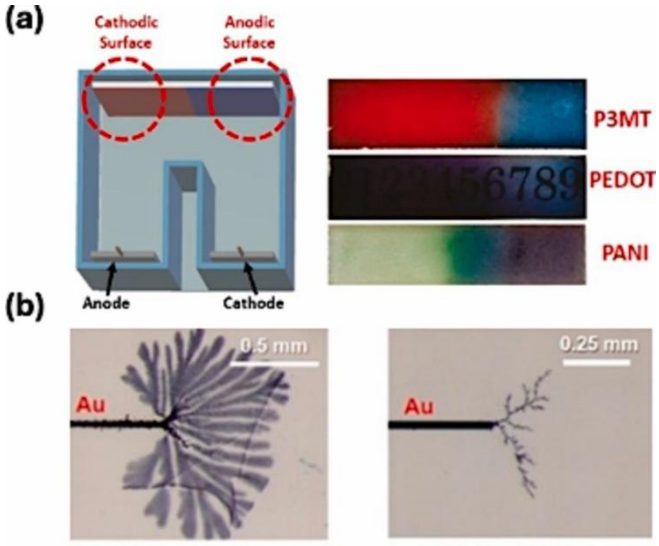


Fig. 6. a) A U-shaped bipolar cell with split anode and cathode feeder electrode placed opposite a BPE platform all immersed in monomer-electrolyte solution (left) and optical images of the resulting doped gradient CP films of Poly(3,4-methylthiophene), PEDOT and PANI following the application of an applied voltage (right). b) Optical images of PEDOT film (right) and PEDOT fibre (left) at different frequencies 5 Hz and 50 Hz respectively, originating from the anodic terminal of a gold BPE nanotube. Reproduced from Watanabe, T.; Ohira, M.; Koizumi, Y.; Nishiyama, H.; Tomita, I.; Inagi, S.; In-Plane Growth of Poly (3,4-ethylenedioxythiophene) Films on a Substrate Surface by Bipolar Electropolymerisation, ACS Macro Lett. 2018, 7(5), 551–555. Doi:10.1021/ acsmacrolett.8b00170.

6.1. Bipolar Electrochemical Stimulation – in vitro

As shown in Fig. 7, Qin et al. demonstrated effective bipolar electrical stimulation of PC 12 nerve cells embedded on soft (free-standing) PPy-PMAS-collagen/PEDOT-PSS films [39]. Intermittent, wire-free electrostimulation over a week dramatically increased the total number of cells alongside a notable increase in both neurite length and interconnectivity leading to the formation of complex neural networks.

Cells tend to inherit specific genotype/phenotype characteristics to effectively perform their desired function. For example, RBCs have a biconcave disc shape to increase the available surface area and optimize oxygen and CO2 uptake. These characteristics may be enhanced or altered through a multitude of physical and chemical-related cues, such as electrochemical stimulation. Shifting from 2D bipolar stimulation platforms (e.g. planar electrodes coated with conducting polymers) to complex 3D bio-mimetic structures could allow accurate physiological architectures to be created that replicate in vivo cellular behaviours.

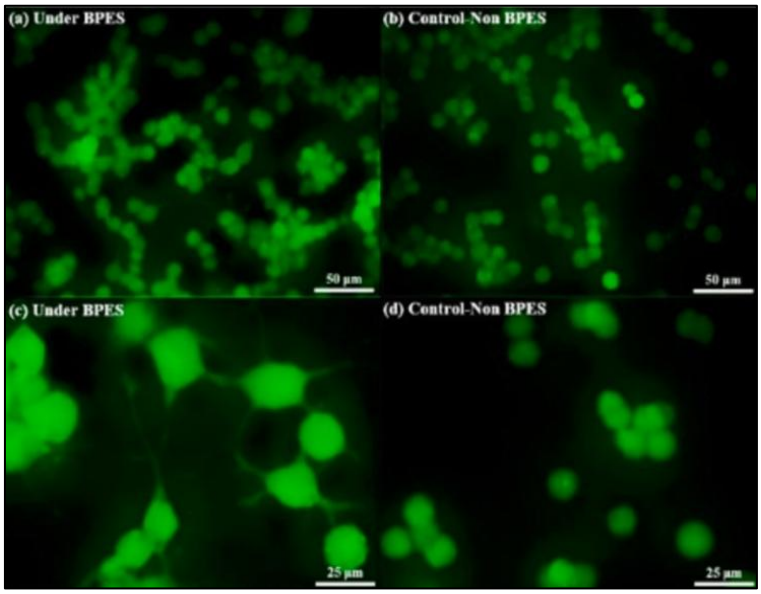


Fig. 7. (a) Fluorescent images on Day 7 via live/dead assay using calcein AM (green: live) and PI(red: dead) staining method of PC 12 clusters embedded on PPy-PMAS-DS/collagen under BPES, displaying increased cell number and neural neurite growth. (b) Fluorescent images on Day 7 of the PPy-PMAS-DS/ collagen platform without BPES implementation are to be used as a control sample for cell number and neurite growth comparison. (c) Fluorescent image

Day 7 of PC 12 cells showcasing extensive neurite growth/branching induced through BPES. (d) Fluorescent image Day 7 of undifferentiated PC 12 cells through the absence of BPES. Reproduced from Qin, C.; Yue, Z.; Huang, X.-F.; Forster, R. J.; Wallace, G. G.; Chen, J. Enhanced Wireless Cell Stimulation Using Soft and Improved Bipolar Electroactive Conducting Polymer Templates. App. Mat. Today 2022, 27, 101481. Doi:10.1016/j.apmt.2022.101481.

6.2. Biomimetic 3D Architectures

Rawson and co-workers developed a novel composite material consisting of pentaerythritol triacrylate (PETrA) and multiwalled carbon nanotubes (MWCNTs) [40]. This biocompatible material was 3D printed into a bio-inspired structure of stacked myofibrils for incorporation of human-induced stem cell-derived cardiomyocytes (hPSC-CMs). As illustrated in Fig. 8, the effects of the physical structure/topography, its chemical composition and the effects of wireless electrical stimulation were investigated. PETrA and composite materials promote hPSC-CMs maturation and organisation, but more importantly, the 3D architecture further amplified this effect. The coupling of wireless electrochemical stimulation with 3D anatomically correct structures not only enhances cell stimulation but presents a unique opportunity to develop bio-inspired bioelectronics. Biomimetic platforms, if integrated successfully, could offer synergistic effects regarding efficient cell stimulation and combating rejection issues of implants aided by their unique design.

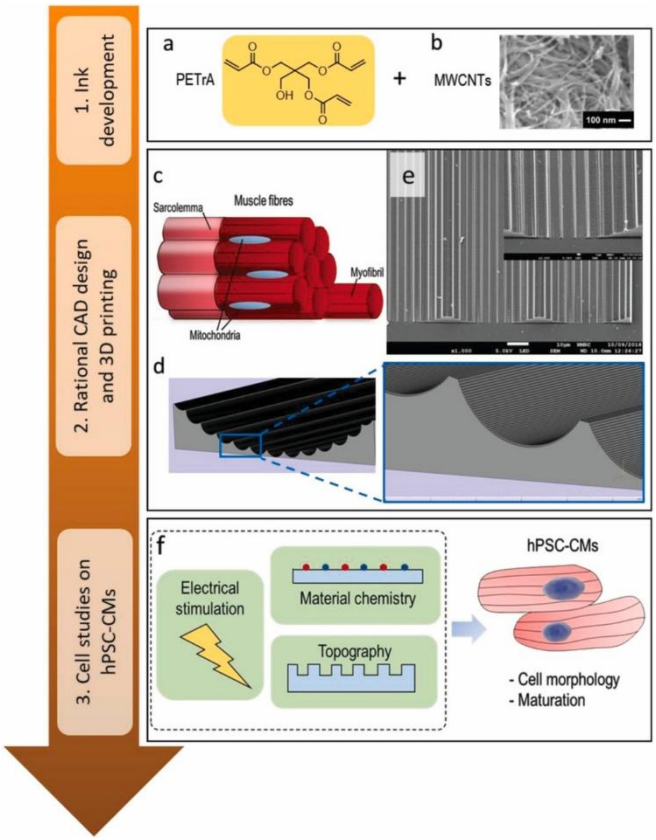


Fig. 8. Processes involved in ink development, 3D printing and stimulation of human-induced stem cell-derived cardiomyocytes. 1) Biocompatible ink material was comprised of both a) pentaerythritol (PETrA) and b) multi-walled carbon nanotubes (MWCNTs). 2) 3D printed structure impaired by c) *in vivo* structure of stacked myofibrils designed using d) CAD modelling and characterised through e) SEM-imaging. Reproduced from Vaithilingam, J.; Sanjuan-Alberte, P.; Campora, S.; Rance, G. A.; Jiang, L.; Thorpe, J.; Burroughs, L.; Tuck, C. J.; Denning, C.; Wildman, R. D.; Hague, R. J. M.; Alexander, M. R.; Rawson, F. J. Multifunctional Bioinstructive 3D Architectures to Modulate Cellular Behavior. Adv. Func. Mats. 2019, 29 (38), 1902016. Doi:10.1002/ adfm.201902016.

Retrospect and Prospects.

Bipolar electrochemiluminescence, BP-ECL, has developed from a somewhat obscure and under-utilised technique 10 to 15 years ago into a cutting-edge strategy for the highly sensitive and selective electrochemical detection of disease biomarkers. Current state-of-the-art devices address diverse disease detection and diagnosis issues from low-cost point-of-care devices to measurements within single biological cells. BP-ECL lends itself uniquely to multianalyte detection, e.g., by placing electrodes of different lengths in a single bipolar cell, the voltage induced at the tips of each electrode depends on their length and can therefore be used to drive light- generating reactions selectively, e.g., by tuning the redox potential of the ECL luminophore. However, there remains much to be understood about bipolar systems, e.g., the spatial distribution along the bipolar electrode is increasingly recognised as not being fully described by a simple linear decay model, but is structured and time-dependent, as processes, such as local ion depletion occur, e.g., due to faradaic reactions or neutralisation reactions. There are opportunities for detailed finite element modelling of the electric field distribution for even relatively simple geometries and certainly for models that integrate mass transport by diffusion *and* migration as well as the effects of heterogeneous electron transfer and the impact of the electric field on homogenous chemical reactions, e.g., the reaction of a ground state label and an electrogenerated co-reactant. Overall, there are strong reasons to believe the future is bright, the future is wirefree!

References

[1] L. Bouffier, Z. Dodzi, Bipolar (bio) electroanalysis, Anal. Chem. 14 (2021) 65–86, https://doi.org/10.1146/annurev-anchem-090820-093307.

[2] E. Villani, S. Inagi, Mapping the distribution potential gradient in bipolar electrochemical systems through luminol electrochemiluminescence imaging, Anal. Chem. 93 (23) (2021) 8152–8160, https://doi.org/10.1021/acs.analchem.0c05397.

[3] K.L. Rahn, R.K. Anand, Recent advancements in bipolar electrochemical methods of analysis, Anal. Chem. 93 (1) (2021) 103–123, https://doi.org/10.1021/acs.analchem.0c04524.

[4] X. Qin, J. Gao, Closed bipolar electrode array for optical reporting reaction-coupled electrochemical sensing and imaging, Chemistry Europe 29 (8) (2022) 1–8, https://doi.org/10.1002/chem.202202687.

[5] C. Mwanza, S.-N. Ding, Newly developed electrochemiluminescence based on bipolar electrochemistry for multiplex biosensing applications: a consolidated review, Biosensors 13 (2023) 1–36, https://doi.org/10.3390/bios13060666.

[6] J. Woo, J. Kim, J. Kim, Indium tin oxide bipolar electrodes modified with pt nanoparticles encapsulated inside dendrimers as sensitive electrochemiluminescence platforms, Electroanal. Chem. 906 (2022) 1–8, https:// doi.org/10.1016/j.jelechem.2021.115998.

[7] S. Eldabe, E. Buchser, R.V. Duarte, Complications of spinal cord stimulation and peripheral nerve stimulation techniques: a review of the literature, Pain Med. 17 (2016) 325–336, https://doi.org/10.1093/pm/pnv025.

[8] F. Cortes, F. Nourhash´emi, O. Gu´erin, C. Cantet, S. Gillette-Guyonnet, S. Andrieu, P.-J. Ousset, B. Vellas, REAL-FR Group, Prognosis of Alzheimer's disease today: a two-year prospective study in 686 patients from the REAL-FR study, Alzheimers Dement. 4 (1) (2008) 22–29, https://doi.org/10.1016/j.jalz.2007.10.018.

[9] C. Koch, G. Laurent, Complexity and the nervous system, Science 284 (1999) 96–98, https://doi.org/10.1126/science.284.5411.96.

[10] H. Lu, W.D. Le, Y.-Y. Xie, X.-P. Wang, Current therapy of drugs in amyotrophic lateral sclerosis, Curr. Neuropharmacol. 14 (4) (2016) 314–321, https://doi.org/10.2174/1570159x14666160120152423.

[11] I. Fyfe, Alzheimer disease mice improve with CRISPR–Cas9 gene editing, Nat. Rev. Neurol. 15 (5) (2019) 247, https://doi.org/10.1038/s41582-019-0172-6.

[12] D. Koní˘ckova, K. Men´˘síkova, L. Tu´˘ckova, E. H´enykova, M. Strnad, D. Friedecký, D. Stejskal, R. Mat˘ej, P. Kanovský, Biomarkers of neurodegenerative diseases:biology, taxonomy, clinical relevance, and current research status, Biomedicines 10 (7) (2022) 1760, https://doi.org/10.3390/biomedicines10071760.

[13] W. Noble, M.P. Burns, Challenges in neurodegeneration research, *Front.* Psychiatry 1 (2010) 7, https://doi.org/10.3389/fpsyt.2010.00007.

[14] G. García-Alías, J. del Valle, I. Delgado-Martínez, X. Navarro, Chapter 14 - Electroceutical therapies for injuries of the nervous system, in: A.J. Salgado (Ed.), Handbook of Innovations in Central Nervous System Regenerative Medicine, Elsevier, 2020, pp. 511–537, https://doi.org/10.1016/B978-0-12-818084- 6.00014-3.

[15] A. Szczakowska, A. Gabryelska, O. Gawlik-Kotelnicka, D. Strzelecki, Deep brain stimulation in the treatment of tardive dyskinesia, J Clin Med 12 (5) (2023) 1868, https://doi.org/10.3390/jcm12051868.

[16] R.J. Forster, Wirefree Electroceuticals: 3D electrical and electrochemical stimulation of biological systems, Curr. Opin. Electrochem. 39 (2023) 101297, https://doi.org/10.1016/j.coelec.2023.101297.

[17] R.M. Crooks, Principles of bipolar electrochemistry, ChemElectroChem 3 (3) (2016) 357–359, https://doi.org/10.1002/celc.201500549.

[18] S.E. Fosdick, K.N. Knust, K. Scida, R.M. Crooks, Bipolar electrochemistry, Ange. Chem. Int. Ed. 52 (40) (2013) 10438–10456, https://doi.org/10.1002/ anie.201300947.

[19] L. Xiuxiu, Z. Qin, T. Zhaoyan, Gold nanowires array-based closed bipolar nanoelectrode system for electrochemiluminescence detection of -fetoprotein on cell surface, Anal. Chem. 94 (20) (2022) 7350–7357, https://doi.org/10.1021/acs. analchem.2c00785.

[20] Y. Su, W. Lai, Y. Liang, C. Zhang, Novel cloth-based closed bipolar solid-state electrochemiluminescence (CBP-SS-ECL) aptasensor for detecting carcinoembryonic antigen, Anal. Chim. Acta 1206 (2022) 339789, https://doi.org/ 10.1016/j.aca.2022.339789.

[21] L. Zhu, X. Lv, H. Yu, X. Tan, Y. Rong, W. Feng, L. Zhang, J. Yu, Y. Zhang, Paper- based bipolar electrode electrochemiluminescence platform combined with pencil- drawing trace for the

detection of M.SssI methyltransferase, Anal. Chem. 94 (23) (2022) 8327–8334, https://doi.org/10.1021/acs.analchem.2c00803.

[22] H.-W. Shi, W. Zhao, Z. Liu, X.-C. Liu, M.-S. Wu, J.-J. Xu, H.-Y. Chen, Joint enhancement strategy applied in ECL biosensor based on closed bipolar electrodes for the detection of PSA, Talanta 154 (2016) 169–174, https://doi.org/10.1016/j. talanta.2016.03.059.

[23] X. Song, L. Zhao, C. Luo, X. Ren, X. Wang, L. Yang, Q. Wei, Bioactivity-protective electrochemiluminescence sensor using CeO2/Co4N heterostructures as highly effective coreaction accelerators for ultrasensitive immunodetection, Sens. Actuat. B: Chem. 355 (2022) 131158, https://doi.org/10.1016/j.snb.2021.131158.

[24] X.-Y. Yang, Y.-Y. Bai, Y.-Y. Huangfu, W.-J. Guo, Y.-J. Yang, D.-W. Pang, Z.- L. Zhang, Ultrasensitive electrochemiluminescence biosensor based on closed bipolar electrode for alkaline phosphatase detection in single liver cancer cell, Anal. Chem. 93 (2022) 1757–1763, https://doi.org/10.1021/acs. analchem.0c04517.

[25] L. Cai, J. Zhang, L. Teng, H. Wang, G. Fang, S. Wang, Ultrasensitive molecularly imprinted electrochemiluminescence sensor based on highly-conductive rGO- COOH synergically amplify TCPP luminophor signal in aqueous phase system for “switches-controlled” detection of tryptamine, Sens. Actuat. B: Chem. 366 (2022) 132004, https://doi.org/10.1016/j.snb.2022.132004.

[26] M. Bhaiyya, P.K. Pattnaik, S. Goel, Multiplexed and simultaneous biosensing in a 3D-printed portable six-well smartphone operated electrochemiluminescence standalone point-of-care platform, Mikrochim. Acta 189 (2) (2022) 79, https://doi. org/10.1007/s00604-022-05200-0.

[27] F. Fazlali, P. Hashemi, S.M. Khoshfetrat, R. Halabian, B. Baradaran, M. Johari- Ahar, P. Karami, A. Hajian, H. Bagheri, Electrochemiluminescent biosensor for ultrasensitive detection of lymphoma at the early stage using CD20 markers as B cell-specific antigens, Bioelectrochemistry 138 (2021) 107730, https://doi.org/ 10.1016/j.bioelechem.2020.107730.

[28] Y. Wang, R. Jin, N. Sojic, D. Dechen Jiang, H.-Y. Chen, Intracellular wireless analysis of single cells by bipolar electrochemiluminescence confined in a nanopipette, Angew. Chem. Int. Ed. 132 (26) (2020) 10502–10506, https://doi. org/10.1002/ange.202002323.

[29] D. Han, B. Goudeau, D. Jiang, D. Fang, N. Sojic, Electrochemiluminescence microscopy of cells: essential role of surface regeneration, Anal. Chem. 93 (3) (2021) 1652–1657, https://doi.org/10.1021/acs.analchem.0c05123.

[30] Z. Chen, E. Villani, S. Inagi, Recent progress in bipolar electropolymerization methods toward one-dimensional conducting polymer structures, Curr. Opin. Electrochem. 28 (2021) 100702, https://doi.org/10.1016/j.coelec.2021.100702.

[31] Y. Ishiguro, S. Inagi, T. Fuchigami, Gradient doping of conducting polymer films by means of bipolar electrochemistry, Langmuir 27 (11) (2011) 7158–7162, https://doi.org/10.1021/la200464t.

[32] T. Watanabe, M. Ohira, Y. Koizumi, H. Nishiyama, I. Tomita, S. Inagi, In-plane growth of poly(3,4-ethylenedioxythiophene) films on a substrate surface by bipolar electropolymerization, ACS Macro Lett. 7 (5) (2018) 551–555, https://doi.org/10.1021/acsmacrolett.8b00170.

[33] C. Qin, Z. Yue, G.G. Wallace, J. Chen, Bipolar electrochemical stimulation using conducting polymers for wireless electroceuticals and future directions, ACS Appl. Bio Mater. 5 (11) (2022) 5041–5056, https://doi.org/10.1021/acsabm.2c00679.

[34] C. Qin, Z. Yue, R.J. Forster, J. Chen, G.G. Wallace, On demand, wireless electrochemical release of brain derived neurotrophic factor, Electrochem. Commun. 157 (2023) 107626, https://doi.org/10.1016/j.elecom.2023.107626.

[35] Y. Zhou, G.H. Burgoyne Morris, M. Nair, Current and emerging strategies for biocompatible materials for implantable electronics, Cell Rep. Phys. Sci. (2024) 101852, https://doi.org/10.1016/j.xcrp.2024.101852.

[36] G. Li, P.G. Pickup, Ion transport in poly(3,4-ethylenedioxythiophene)–poly (styrene-4-sulfonate) composites, Phys. Chem. Chem. Phys. 2 (2000) 1255–1260, https://doi.org/10.1039/A908372C.

[37] F. Masdarolomoor, P.C. Innis, G.G. Wallace, Electrochemical synthesis and characterisation of polyaniline/poly(2-methoxyaniline-5-sulfonic acid) composites, Electrochim. Acta 53 (12) (2008) 4146–4155, https://doi.org/ 10.1016/j.electacta.2007.12.055.

[38] D. Khodagholy, J.N. Gelinas, T. Thesen, W. Doyle, O. Devinsky, G.G. Malliaras, G. Buzsaki, NeuroGrid: recording action potentials from the surface of the brain, ´ Nat. Neurosci 18 (2) (2015) 310–315, https://doi.org/10.1038/nn.3905.

[39] C. Qin, Z. Yue, X.-F. Huang, R.J. Forster, G.G. Wallace, J. Chen, Enhanced wireless cell stimulation using soft and improved bipolar electroactive conducting polymer templates, App. Mat. Today 27 (2022) 101481, https://doi.org/10.1016/j. apmt.2022.101481.

[40] J. Vaithilingam, P. Sanjuan-Alberte, S. Campora, G.A. Rance, L. Jiang, J. Thorpe, L. Burroughs, C.J. Tuck, C. Denning, R.D. Wildman, R.J.M. Hague, M.R. Alexander, F.J. Rawson, Multifunctional bioinstructive 3D architectures to modulate cellular behavior, Adv. Func. Mats. 29 (38) (2019) 1902016, https://doi.org/10.1002/ adfm.201902016.

The preceding chapter highlighted both the significant progress and the fundamental limitations of contemporary bipolar electrochemistry systems, particularly within biomedical contexts. While a range of applications have been successfully demonstrated, from biosensing at ultralow concentrations and electrochemiluminescence based detection to drug delivery and cellular stimulation, these systems are still largely designed and interpreted using simplified assumptions regarding electric field behaviour and spatial potentials distributions. Consequently, although bipolar electrochemistry has demonstrated considerable promise, the ability to rationally predict and engineer electrochemical behaviour remains limited, representing a major barrier to the broader development of wireless electrochemical technologies.

Most analyses of bipolar electrochemical systems rely on idealised or quasi linear descriptions of the electric field, despite growing experimental evidence that real systems exhibit complex, spatially heterogenous and time-dependent field distributions. These deviations become increasingly significant in biologically relevant environments, where electrolyte composition, electrode geometry, mass transport and interfacial processes all contribute to local potential gradients.

As the field moves towards more advanced applications in sensing, bioelectronics and electroceuticals, there is a clear and growing need for predictive tools capable of accurately describing electric field behaviour in realistic geometries. However, modelling such systems remains challenging, particularly when extending from simplified two-dimensional architectures towards more representative systems that incorporate coupled transport, reaction kinetics and heterogenous material properties. As a result, the rational design of bipolar electrochemical devices based on predictive field engineering is still an emerging and unresolved challenge.

With that in mind, this chapter introduced a finite element modelling framework for investigating electric field distributions in bipolar electrochemical systems. The objective is to move beyond simplified analytical descriptions and develop a more physically well rounded and representative understanding of how geometry, conductivity and systems configuration influence local field strength and spatial electrochemical activity. By establishing a quantitative understanding of field formation, this chapter provides the theoretical foundation upon which the subsequent experimental chapters are built, enabling electric fields to be treated not merely as a consequence of cell design but as controllable design parameters for wireless electrochemical engineering.

Chapter 3

Advancing Bipolar Electrochemistry for Targeted Deposition of Biocompatible Polymers in Electrolyte-Free Solutions *via* Finite Element Modeling

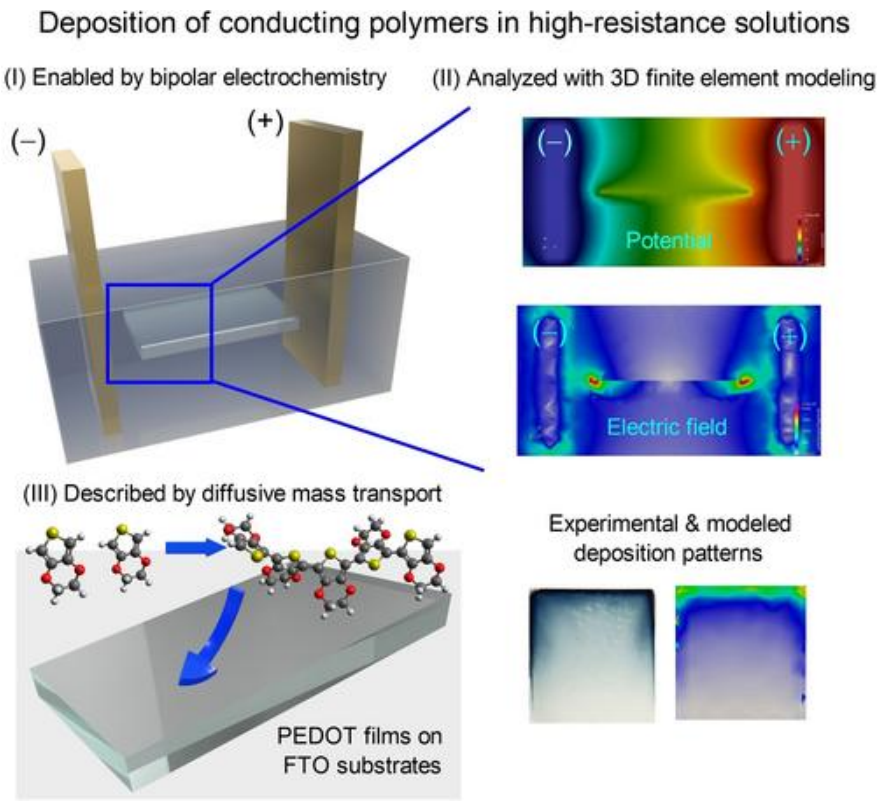
ChemElectroChem2025,12,6 *doi.org/10.1002/CELC.202400506*

Advancing Bipolar Electrochemistry for Targeted Deposition of Biocompatible Polymers in Electrolyte-Free Solutions *via* Finite Element Modeling

Michal Wagner,*[a] Áine Brady,[a] Oisín F. Doyle,[a] and Robert J. Forster*[a, b]

a. School of Chemical Sciences, Dublin City University, Glasnevin, Ireland
b. FutureNeuro, SFI Research Centre for Chronic and Rare Neurological Diseases, Dublin City University, Dublin 9, Ireland

Graphical Abstract



Modeling and experimental data for the synthesis and deposition of conducting polymers in high-resistance solutions enabled by bipolar electrochemistry indicate the reaction control via homogenous rather than heterogeneous electron transfer conventionally postulated for bipolar electrochemical systems.

Abstract

The spatially controlled, template-free, deposition of electro-active and biocompatible materials on 3D objects is of great interest for wireless cell stimulation intended for diverse applications ranging from electroceuticals to advanced sensor development. Bipolar electrochemistry provides the possibility of depositing electrically conducting polymers controlled through the (shaped) electric field distribution. A second advantage is that electrochemistry can be performed in electrolyte-free media potentially removing the "interfering" effect of added electrolyte. Here, poly(3,4-ethyldioxythiophene) (PEDOT) films have been deposited on bipolar electrodes directly in ultrapure water. Significantly, the deposition patterns cannot be fully explained using a linear change in the solution-phase potential, which is a common assumption for bipolar electrochemical systems. 3D finite element modelling and diffusive mass transport considerations have been combined to map the electric field distribution in this very low conductivity medium and demonstrate that homogenous rather than heterogenous electron transfer is likely to play an important role in polymer deposition. Moreover, modelling predictions were compared to electrochemical impedance and cyclic voltammetry results and non-linear behaviours qualitatively matched, through film capacitances and deposition patterns. The proposed framework opens significant opportunities for the template-free deposition of various electroactive materials on bipolar electrodes in low-conductivity solutions.

Introduction

Electrical stimulation of biological cells is an ever-increasing approach in applied medicine[1] and mechanistic studies,[2] since it can effectively influence the intracellular environment and signal transduction pathways[3] in a non-destructive manner. Electrostimulation devices can greatly benefit from implementing wireless approaches where no physical contact is needed between stimulus electrodes and driver circuits, thus further extending their adaptability for specific *in vivo* applications. Among prospective approaches, bipolar electrochemistry offers a versatile framework for minimally invasive, cost-effective, and adaptable biological cell stimulation.[4] Bipolar electrochemical systems typically consist of two working 'feeder' electrodes (FEs) immersed in the desired medium and spaced with the third 'floating' bipolar electrode (BPE).[5] The latter electrode is subjected to polarization without direct electronic contact *via* an electric field generated by FEs. In biological studies, it is preferential to interface cell cultures and BPE with biocompatible materials while the electroactivity of the interlayer is preserved. Electrically conducting polymers are a group of materials that can provide this dual function.[6] Moreover, electronic and ion-to-electron transduction properties of conducting polymers can be altered to enhance electrochemical "communication" between cells and BPE.[7] Conducting polymers such as sulfonated polyaniline along with more common polypyrrole and poly(3,4-ethylenedioxythiophene) (PEDOT) are extensively applied in biomedical settings.[8,9] Importantly, listed here polymers can readily be made by anodic electropolymerisation, thus opening possibilities for deposition on various conducting 2D and 3D objects whose shape can trigger certain cell culture responses such as proliferation, adhesion, and differentiation.[10]

Since the electric field distribution is mainly controlled by the geometry of the system,[11] the electrochemical deposition of conducting polymers can be confined to a specific region of BPE. For planar BPE centered midway between FEs, the electric field distribution typically results in a gradual change in solution overpotentials along the surface of BPE, with anodic and cathodic polarization of opposing BPE sides.[11] Therefore, anodic polymerization of conducting polymers in such a system result in asymmetric deposition patterns and regions of preferential deposition. Exemplary controlled patterning of conducting polymers with submillimetre precision *via* bipolar electrochemistry has been achieved,[12] as well as the fabrication of

conducting polymer wires driven by dendritic growth in bipolar systems,[13,14] all being promising for bioelectronic applications. To gain control over the asymmetric deposition of conducting polymers, *i.e.*, to ultimately develop a template-free approach to the spatially controlled electrodeposition, (I) mass transport and interfacial kinetics, as well as (II) the relation of the BPE system geometry with electric field theory, need to be well understood. Significant efforts have been undertaken toward modeling the electrode-electrolyte solution interface in bipolar electrochemical systems, such as faradaic (de)polarization,[15,16] charging-discharging dynamics and kinetics,[17,18] as well as generalized algorithms for solving potential and current distributions.[19] Importantly, the local distribution of various electrochemical quantities can be modeled with the finite element method (FEM).[20] This technique was successfully applied to map potential distributions in proximity to BPE surfaces and confirmed by experimental potential measurements.[21,22] However, these investigations have been focused on electrochemical systems with relatively high ionic strengths where ions are freely available.

In this work, we explore the electrochemical synthesis and deposition of the PEDOT process in bipolar systems in the absence of deliberately added electrolyte, *i.e.*, where the solution only contains ultrapure water and the monomer. This strategy seeks to address one of the main disadvantages of electrochemistry compared to spectroscopy, *i.e.*, that the sample must be "contaminated" with supporting electrolyte. Specifically, in the case of the deposition of conducting polymers, it opens the possibility of creating novel underdoped materials and could provide deep insights into the relative importance of ionic *vs.* electronic conductivity in these systems. Moreover, for wirefree electroceuticals purely aqueous, electrolyte-free media can minimize aggregation of proteins,[23] as well as kosmo- and chaotropic effects.[24] Encapsulation of function-specific proteins in conducting polymer matrix is highly attractive for understanding and controlling electrochemical communication with biological cells. Thus, a thorough understanding of the potential distribution and the factors that control the synthesis and deposition of electroactive materials in high-resistance solutions is needed. Ultralow ion concentrations are expected to significantly influence the potential distribution at the electrode-solution interface.[25] Therefore, we conducted a systematic 3D FEM modeling of both potential and potential gradient distributions in bipolar systems and subsequently

estimated limitations for diffusive mass transport important for experimental PEDOT deposition on BPEs in ultrapure water. The experimentally observed PEDOT film deposition patterns are in excellent qualitative agreement with the modeling predictions and cannot be fully explained using conventional approaches describing bipolar electrochemistry in the presence of electrolyte. We believe that our modeling approach represents a significant opportunity to *a priori* predict the complex potential distributions that can occur in bipolar systems allowing, for example, different regions of a 3D cell culture array to receive different electrical, electrochemical and chemical stimuli simultaneously.

Methods

Modelling

Three different lengths (1.4, 2.0, and 2.6 cm) of BPE samples were chosen for FEM simulations, referred to in this work as **1.4 cm BPE**, **2.0 cm BPE**, and **2.6 cm BPE**, respectively. Each BPE is 1.0 cm in width and 0.23 cm in height consisting of a glass slide coated with a 550 nm thick fluorine-doped tin oxide (FTO) layer, Figure 1. In the model, the FTO-coated glass BPEs are placed between two titanium FEs (WE1 and WE2) spaced by 3.0 cm and with the following dimensions: length = 0.2 cm, width = 1.2 cm, and height = 2 cm. The electrical conductivities (s) of FEs,[26] the medium, glass body,[27] and FTO are set to 2.38×10^{6}, 5.5×10^{-6}, 1×10^{-11}, and 2.6×10^{5} S m^{-1}, respectively. Significantly, these values reflect the very large differences in conductivity of the electrodes compared to the medium which has profound implications for the potential distribution and current flow pathways. Both BPEs and FEs were placed within a continuous medium (length = 9.4 cm, width = 7.2 cm, height = 8.0 cm) whose outer surfaces represent a Dirichlet boundary of 0 V. The same boundary type was applied to the surfaces of FEs which were 'electrified' by ± 5, 10, 15, and 20 V, to create the desired electric field ($\vec{E}$) in the studied systems. Additionally, the system where the BPE is absent is referred to as **0 cm BPE** and was also analysed with the same set of potentials to gain insights into the impact of the presence of the BPE on potential and electric field distributions. The BPEs are positioned with a central axis located at the interface between the FTO layer and the medium. 3D models were built using Free CAD 0.21.1 and meshed in Salomé 9.12.0 with 'NETGEN 1D-2D-3D' algorithm. For all FEM simulations, Elmer solver[28] was used, and data were visualized using

Para View 5.11.2 software. The electric potential (ϕ) and the modulus of potential gradient ($|\phi| = \nabla \varphi$) were calculated utilizing Elmer's static current conduction and flux computation modules, through the following Poisson's equation describing the total charge density (ρ_t) based on the electric field relationships with current density ($\vec{J} = \sigma\vec{E}$) and potential gradient ($\vec{E} = -\nabla \varphi$) :

$$-\nabla \cdot \sigma \nabla \varphi = \rho_t \quad (1)$$

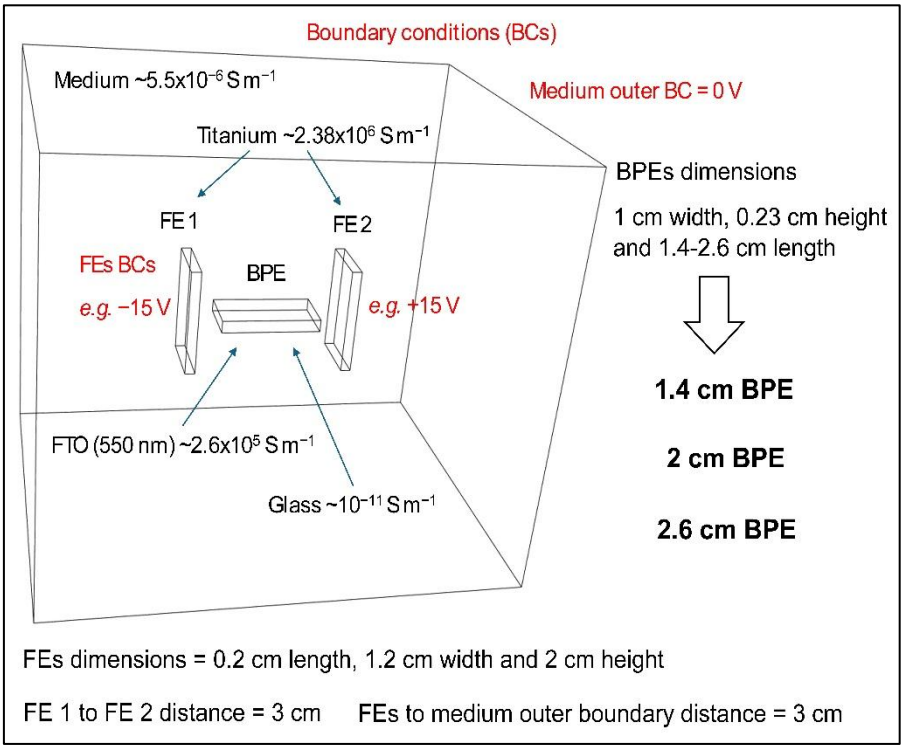


Figure 1. The schematic of studied BPE systems used for FEM simulations.

Empirical Verification

FTO glass slides with 550 nm coating having a sheet resistance of ~7 Ω sq^{-1} were obtained from Sigma-Aldrich and cut into dimensions equivalent to **1.4 cm BPE**, **2.0 cm BPE**, and **2.6 cm BPE** modeled samples. Before polymer deposition, the samples were ultrasonicated in isopropyl alcohol for 10 min and dried with nitrogen gas. The chemicals 3,4-ethylenedioxythiophene (EDOT, 97%) and lithium perchlorate (95%) were obtained from Sigma-Aldrich and used as

received. All aqueous solutions were prepared with freshly deionized water (18.2 MΩcm resistivity) obtained with the Mili-Q ultrapure water system. For electrochemical polymerization of PEDOT *via* the bipolar approach, two polished titanium feeder electrodes, FEs, with dimensions like modeled electrodes were inserted into inhouse 3D printed cells made of acrylonitrile butadiene styrene. The Ti FEs were separated by 3 cm, and BPE samples were placed midway between the two FEs marking the centre of the bipolar system. In each 10-minute deposition run, 3 mL of 10 mM EDOT (aq) was used, and potential difference ($\Delta\varphi_{app}$) of 10, 20, 30, and 40 V were applied across the FEs using DC laboratory power supply (max. 200 V, EA-PS 5200-02A, ElektroAutomatik).

After deposition, PEDOT films were rinsed with ultrapure water to remove any residual monomer and left to dry at ambient conditions. Subsequently, the PEDOT/ FTO samples acted as working electrodes (WEs) in conventional 3electrode cells for cyclic voltammetry (CV) and electrochemical impedance spectroscopy (EIS) experiments (utilizing Metrohm Autolab PGSTAT204 potentiostat/ galvanostat controlled by Nova 2.1 software). These measurements were carried out in 0.1 M $LiClO_4$ (aq) to obtain film capacitance (C_f) and Warburg admittance (Y_0) values. WEs were masked using Teflon tape so that a 1 cm^2 area was analysed (*vide* Figure S1c). A platinum wire coil and an Ag/AgCl (1 M KCl) acted as counter electrode (CE) and reference electrode (RE), respectively. All samples were cycled from - 0.1 to + 0.5 V at 5, 10, 20, 50, and 100 mV s^{-1} scan rates, *i.e.*, they were doped with perchlorate anions. Before and after CV studies, potentiostatic EIS measurements were conducted within the 100k – 0.1 Hz frequency range (61 data points per one measurement) at 10 mV excitation amplitude and a fixed potential of 0.2 V. The latter potential was selected for C_f estimations for both CV and EIS since it represents a clear current plateau region where the PEDOT film response is dominated by capacitance (*vide* Figure S1a). In the case of EIS, obtained impedance spectra were fitted to the following equation (Randles circuit in series with C_f):

$$Z(\omega) = R_S + \left(j\omega C_{dl} + \frac{1}{R_{ct} + W_c (1-j)/\sqrt{\omega}}\right)^{-1} + \frac{1}{j\omega C_f} \quad (2)$$

where, ω is angular frequency, R_S is solution resistance, C_{dl} is double-layer capacitance, R_{ct} is charge transfer resistance, and Y_0 ($1/W_C$) is the magnitude of admittance (in S $s^{0.5}$) of the

Warburg element. For C_f estimation from CV, both anodic and cathodic currents were considered and plotted against the applied scan rate values, followed by linear regression to obtain slopes of the fitting lines (*i.e.* C_f). Triplicates for PEDOT deposition on each BPE (1.4, 2.0, and 2.6 cm) were independently fabricated and subjected to CV and EIS analysis. All experiments were performed at room temperature (21.5± 1.5°C).

Results and Discussion

First, the experimental deposition of PEDOT using bipolar electrochemistry in the absence of deliberately added electrolyte is considered. In the conventional model, the potential induced in the BPE by the electric field is expected to decay linearly across electrode length. This distribution gives the largest potential at the BPE edges closest to the FEs and the linear decay would be expected to give a film thickness that decreases uniformly towards the centre of the BPE if electrodeposition is controlled by overpotential dependent heterogeneous electron transfer, resulting in "wedge" shape films. Figure 2a shows that the wireless electrodeposition of PEDOT on FTO glass BPEs in ultrapure water was successful for all the applied voltages and selected electrode lengths. The presence of PEDOT films was confirmed by comparative CV and EIS experiments with PEDOT made in a standard 3-electrode system (*vide* Figure S1). As can be seen from Figure 2a some aspects predicted by the linear decay model are present, *e.g.*, the film is thickest at the edges and becomes thinner towards the centre of the BPE. However, the film is significantly more structured than expected, since preferential deposition occurs at all the edges within the anodic region of BPE. Similar intensity distribution maps were obtained *via* electrochemiluminescence (ECL) imaging of luminol in bipolar systems,[29] while more uniform patterns were observed for fluorescence monitoring of "microfluidic" BPEs at very high field strengths (around 200 kV m^{-1}).[30] However, optical assessments alone are not sufficient for the characterization of the material deposition process.

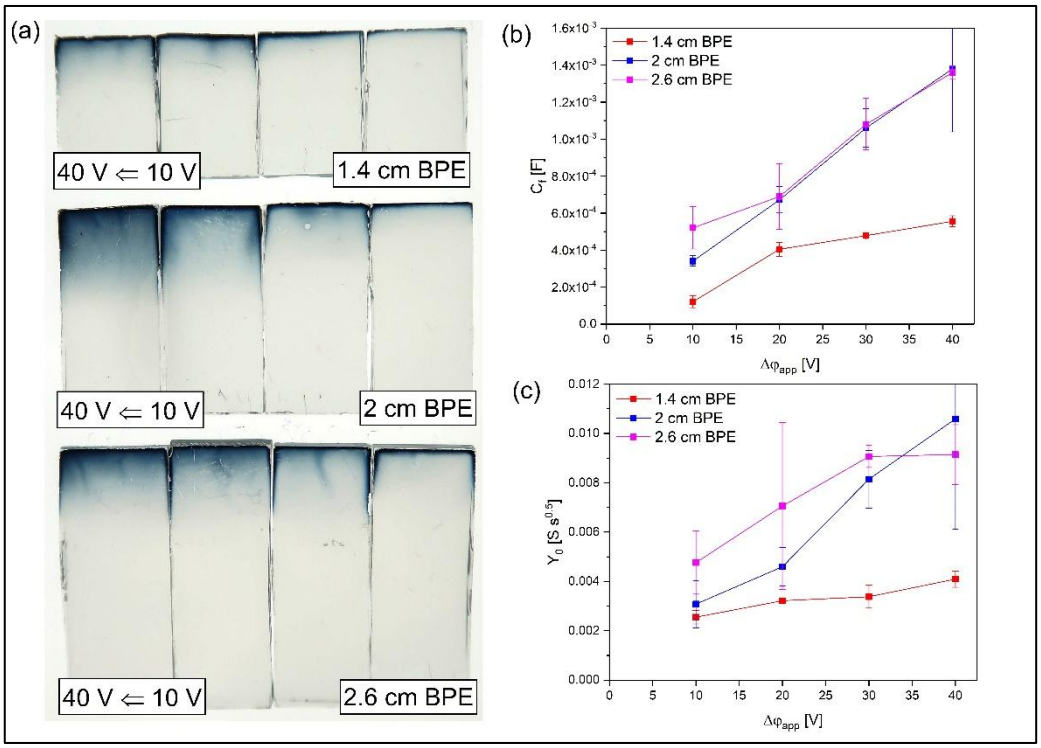


Figure 2 - Photographs of exemplary PEDOT samples deposited on FTO glass (a). Estimated PEDOT film capacitance (C_f) values from CV (b) and admittance (Y_0) from Equation 2 (c) as a function of applied voltage (3 replicas).

Importantly, electrodeposited PEDOT films on BPEs were subjected to both CV and EIS techniques to obtain C_f values which is a useful measure of the quantity of PEDOT deposited. Capacitance values were obtained by calculating slopes of the fitting lines for both anodic and cathodic currents *vs.* applied scan rate, as well as applying the Randles-based equivalent circuit model (*vide* Equation 2) to impedance spectra. The summary of this analysis is presented in Figure S2, while refined C_f *vs.* $\Delta\varphi_{app}$ plots are shown in Figure 2b. The capacitance is expected to increase proportionally to the amount of the material deposited which, if potential-dependent heterogeneous electron transfer is rate determining step, should depend on the voltage applied to FEs. However, for the **1.4 cm BPE** sample, the obtained profile does not follow the expected linear dependence, while the **2.0 cm BPE** and **2.6 cm BPE** samples exhibit unexpectedly similar capacitance characteristics. Additionally, the approximation of the general trends in mass diffusivity in the studied PEDOT films can be derived from the

analysis of the magnitude of admittance (Y_0) characteristic for the Warburg element, Figure 2c. For an electrochemical system, this electrical quantity can be related to the diffusional time constant and thus to the diffusion coefficient.[31] Since the deposition of PEDOT on BPEs results in films with significant thickness inhomogeneity, the Y_0 values represent average quantities across the film. The Y_0 *vs.* $\Delta\varphi_{app}$ profiles for **2.0 cm BPE** and **2.6 cm BPE** samples exhibit relatively high levels of nonlinearity and are similar to capacitance profiles shown in Figure 2b when considering variability in the dataset.

In the frequently used approximation of polarization of conducting BPE due to applied voltage ($\Delta\varphi_{app}$),[5,11] the magnitude of the combined solution overpotentials (anodic and cathodic, $\Delta\varphi_{BPE}$) changes linearly with $\Delta\varphi_{app}$ according to the proportionality factor in the form of BPE length/cell length ratio. The floating potential of BPE (φ_{BPE}) reside within $\Delta\varphi_{BPE}$ bounds and reflect the equilibrium state. On the other hand, at a microscopic level, the effective capacitance of the Stern layer plays a significant role in the potential and charge distributions at the BPE – solution interface.[17] The potential drop across the Stern layer at the reaction plane is connected with local electric field strength.[32,33] Therefore, for a reaction to occur *via* electron tunnelling, the interfacial potential difference between BPE and solution ($\varphi_{BPE} - \varphi$) needs to be adequately significant in the proximity of the Stern layer. The kinetics of a reaction can be then described within the Frumkin–Butler–Volmer theory[34] and the resultant Faradaic current linked with local surface charge dependent on both Stern layer thickness and $\varphi_{BPE} - \varphi$ magnitude. For the electrochemical deposition of PEDOT on BPE in ultrapure water very large Debye lengths are expected (> 30 nm). Hence, the surface charge density and resultant polarization of BPE seem to be not sufficient for electron transfer to occur directly at the BPE/solution interface. Moreover, the significant drop of around 1 V (for $\Delta\varphi_{app}$ = 10 V) in solution potential near BPE edges measured above 100 and 300 µm corroding stainless steel surface[22] suggests rather low solution potential values at the length scale of the electric double layer.

It is therefore apparent that a theoretical analysis of induced electric fields in bipolar electrochemical systems with significant differences in conductivity between the BPE material and the surrounding solution phase is required. Multiphysics simulations of electrodynamics on 3D objects can be performed utilizing the FEM technique addressing geometry/boundary

constraints and material conductivities. Overall, four 3D models of bipolar systems were built representing **1.4 cm BPE**, **2.0 cm BPE**, and **2.6 cm BPE** samples including a "reference" system where no BPE is present, referred to as **0 cm BPE**. In the model schematic presented in Figure 1, both FEs were equidistant to the outer boundary by 3 cm. This choice of geometry enabled the unimpeded development of the electric field in the opposite direction to the BPE, since the focus of the work was to study and quantify the interaction of BPE with FEs and thus resultant PEDOT film formation mechanism without the interference of other structural components. Moreover, the potential on the outer boundary was fixed at 0 V to provide conditions resembling electric continuity extending to infinity. Since the total charge density is proportional to the potential gradient *via* the electric conductivity of a specific medium (*vide* Equation 1), the distribution of electrical quantities is clearly governed by the composition and geometry of both the model and actual BPE systems.

Typical φ and IϕI distributions within both the medium and BPE are shown in Figure 3b. The presence of the BPE results in significant changes in the potential distribution associated with the non-zero gradual asymmetric distribution of electric field within the underlying glass and near the surface of FTO, Figure S3. The FTO is only approximately one order of magnitude less conducting than the Ti FEs, therefore effectively no net electric field is expected within the FTO layer. This results in $\varphi = 0$ (in respect to infinity) directly along the FTO/ medium interface in contrast to non-zero and near linear potential profile in **0 cm BPE** case, Figure 3c. Consequently, as shown in Figure 3d, two major features in the IϕI *vs.* x plots can be observed, one present near the edge of BPE and the second one in close proximity to the surface of the feeder electrode. The insert in Figure 3d shows that, the latter feature is also observed in **0 cm BPE** model samples. As the BPE length is increased, these two features merge as the BPE and FE become closer to one another resulting in higher absolute field strengths in this increasingly narrow gap, Figures S4a and b. These features in the IϕI *vs.* x plots can be further investigated by analysing the vector components of the potential gradient. When no BPE is present (Figure S4c) only the negative values in the x-direction contribute to the overall gradient being a consequence of the relatively homogeneous distribution of the current flow except the edges of FEs. In the exemplary case of the **1.4 cm BPE** model sample (Figure S4d), the significantly conducting surface of FTO becomes the major current pathway resulting in inhomogeneous current distribution within an overall system, especially at the corners of BPE.

Therefore, the dominant contribution in the x-direction with a negative gradient exhibits two features in IϕI *vs.* x plots governed by the distance between BPE and FE edges. This predicted behaviour closely mirrors the experimental observations shown in Figure 2a, *i.e.*, enhanced PEDOT deposition close to the edges of the BPE. At the BPE edges, both positive and negative gradients in the z-direction are found with ϕ_Z minimum at BPE surface in anodic ($\phi < 0$) and ϕ_Z maximum in cathodic ($\varphi > 0$) regions of BPE. However, the specific pattern in IϕI is clearly dominated by electric field vectors pointing in the x-direction. Consequently, the equipotential BPE surface imposes increasingly positive solution overpotentials (φ_{BPE} $\varphi > 0$) in the anodic region as the distance in the z-direction from BPE increases.

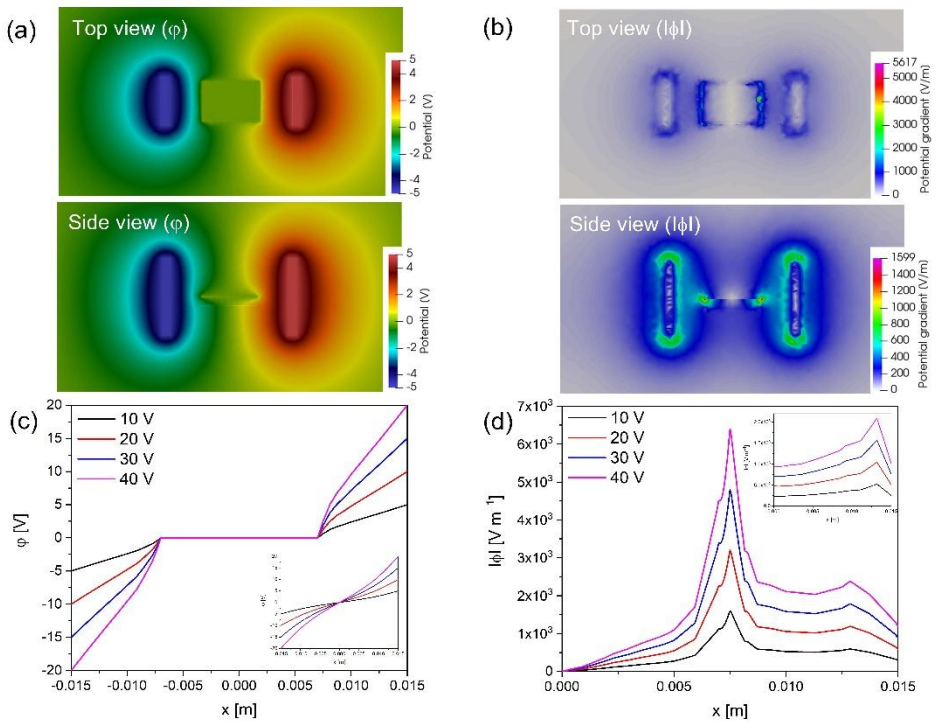


Figure 3. Exemplary ϕ (a) and IϕI (b) distribution maps for 1.4 cm BPE, together with cross-sectional profiles for ϕ (c) and IϕI (d) at the centre and surface of BPE for different applied potentials. Inserts: corresponding ϕ (c) and IϕI (d) profiles taken in the absence of BPE.

In order to quantify the effect of the inclusion of BPE on the whole FTO/medium interfacial area, IϕI *vs.* x plots for all the studied systems were subjected to integration. The resulting potential values were plotted against the total applied voltage divided by two, Figure 4a. For the **0 cm BPE** model sample, the calculated slopes of the fitting lines are close to unity

representing relatively high homogeneity in the electric field distribution. In the case of BPE model samples, higher than unity slopes were obtained (**1.4 cm BPE** = 1.30, **2 cm BPE** = 1.52, and **2.6 cm BPE** = 1.89). The increase as the BPE is moved closer to the feeder electrode arises from decreasing homogeneity in the electric field distribution in the system. Figure 4b shows the global distribution of slopes. For all BPE model samples, the lowest slopes are observed at the centre of the long axis of the BPE (0.000 m) and peak at the BPE edges (± 0.005 m). At 0.1 cm beyond BPE edges the drop in slope is substantial, but it does not become unity, suggesting a significant enhancement in the electric field strength at relatively large distances (from a diffusion perspective) away from the long BPE edges.

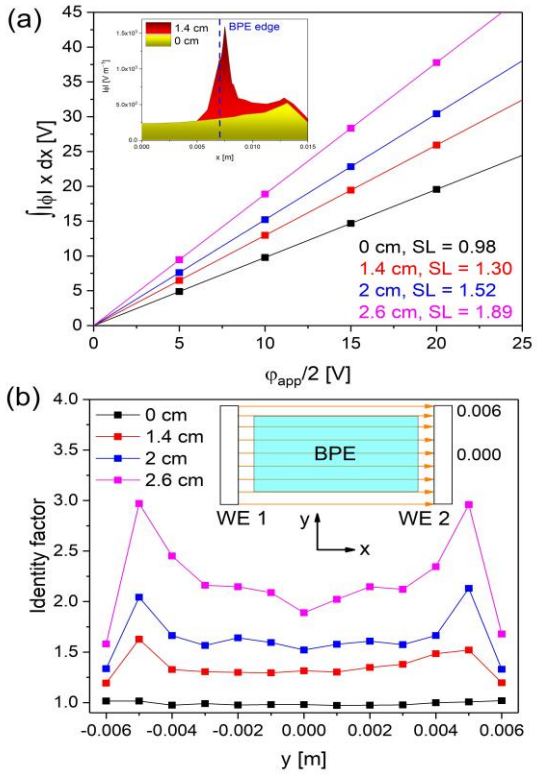


Figure 4 - Integrated areas under IϕI vs. x curves (from BPE or cell centre to WE) as a function of half of the applied potential to calculate the slope (SL) of the fitting lines (a). SL distribution for all studied samples at 0.001 m intervals covering BPE and edges of WEs (b). Inserts: visual comparison of integrated areas between 1.4 cm BPE and 0 cm BPE samples (a), and schematic representation of BPE system geometry (b).

Figure 5a shows plots of IϕI vs. distance/ location on the BPE (x = centre → edge, y= ± 0.005 m) and demonstrates the significant effect of the BPE edges on the local field strength. Specifically, there is approximately a two-fold increase in IϕI at the long BPE edges even as the BPE length is increased from 2.0 to 2.6 cm. In all cases, the IϕI distribution exhibits slight irregular features in proximity to the central axis. Previous FEM investigations [35,36] on inhomogeneous dielectric interfaces have shown that various surface defects can have notable effect on local electric fields. Different mesh sizes were tested for the **1.4 cm BPE** model sample and demonstrated the importance of having a sufficiently fine mesh to avoid mesh-related artifacts. To quantify the rate of change of the electric field strength with position, single exponential decays were fitted to the IϕI vs. x profiles to give a distance-dependent field strength decay factor that could be conveniently compared for different BPE lengths and feeder voltages. The following equation was used:

$$f(x) = Aexp\,(Bx) \tag{3}$$

where, A is IϕI value at the BPE centre (in V m^{-1}) and B is the rate factor (in m^{-1}). Exemplary fitting ($\Delta\varphi_{app}$=10 V, y = 0.000 m) to Equation 3 is presented in Figure S5. Rate factors, B, of 595, 415, and 480 m^{-1} were obtained for the 1.4, 2.0, and 2.6 cm long BPEs, respectively. The obtained rates are independent of applied voltage and likely reflect the "mid-range" position of **2.0 cm BPE** among studied model samples in terms of its effect on φ and IϕI distributions. To obtain "smooth" datasets of the global distribution of field strengths, firstly, the calculated A and B values were used to construct the following derivative of Equation 3 for all considered systems:

$$f'(x) = ABexp(Bx) \tag{4}$$

where, AB is the initial value of the rate of change (in V m^{-2}). Representative distribution plots according to Equation 4 can be seen in Figure S6b. Secondly, all of the BPE systems expressed with Equation 4 were integrated with respect to *x*-direction (*vide* insert in Figure 4b) to

construct voltage-dependent distribution plots of field strength, Figure 5b. Notably, the resultant distribution patterns are visually consistent with actual PEDOT/FTO samples (Figure 2a), thus predicting enhanced PEDOT deposition at BPE edges and corners due to enhanced electric field strengths and hence a greater driving force for EDOT oxidation.

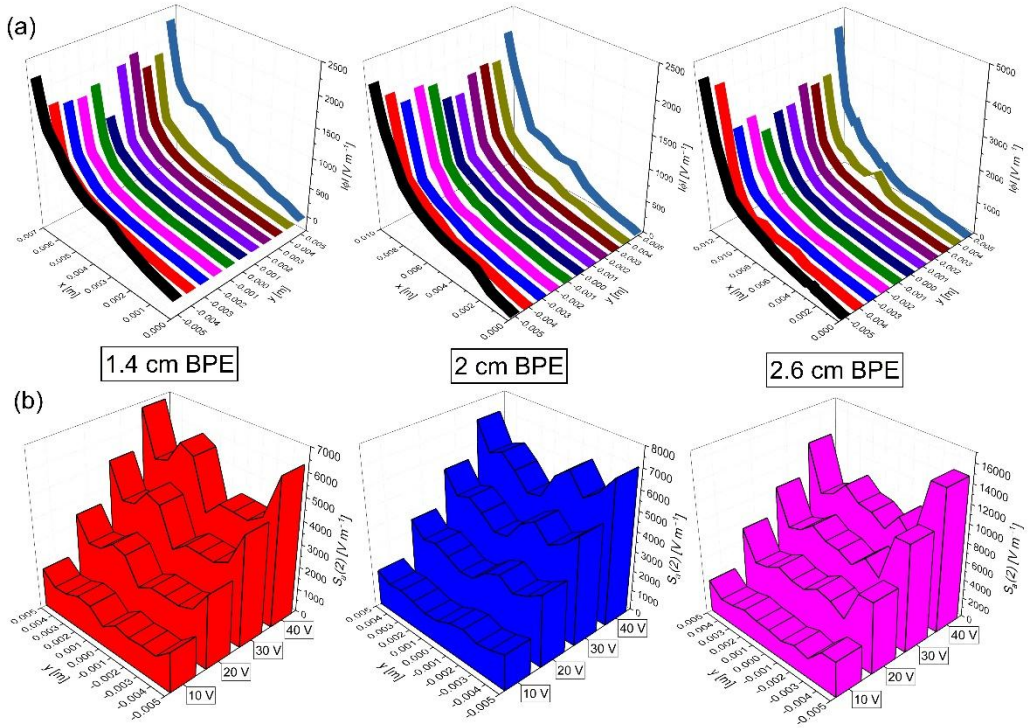


Figure 5 - Exemplary IϕI distribution plots ($\Delta\phi_{app}$= 10 V) at BPE surfaces in x and y directions (a). Field strength distributions on BPE surfaces (± y) at different applied potentials obtained from integration of Equation 4 (b).

The theoretical limitation of the linear model discussed earlier when no electrolyte is present, as well as relatively small, calculated solution potential values in close proximity to the BPE surface (*vide* Figure S3), indicated a need for alternative explanations of the obtained non-linearities in PEDOT deposition patterns. We therefore speculate that homogeneous reactions driven by the significant potential difference between the BPE and solution, along with subsequent diffusive mass transport of the products play a dominant role. To determine the

region where the potential is sufficient to oxidize EDOT in the vicinity of the BPE, both φ and IϕI values were calculated for different heights above the BPE for distances, Δz, up to 1x10^{-3} m and the results obtained are shown in Figures 6a and b. The potential range values increase significantly (approximately proportionally) with increasing distance in the direction perpendicular to the BPE surface, while IϕI profiles and their ranges of magnitude remain the same up to Δz = 1x10^{-4} m. Predictably, φ maximizes at the BPE edges, with the highest values being observed for the **2.6 cm BPE** followed by **2.0 cm BPE** and **1.4 cm BPE** model samples. As can be seen from Figure 5c, the vector field lines are evenly distributed along the BPE surface with the most intensity in proximity to the BPE edge (*vide* overlaid colour map). Since $\vec{J} = \sigma\vec{E}$ the presented field lines reflect all possible current pathways in the system. Due to the significant difference between the electrical conductivity of the FTO layer and medium (~10^{10} ratio), the majority of the current passes through the FTO layer. On the other hand, notable current flow occurs in solution at the corners/edges and through the edge facing the feeder electrode.

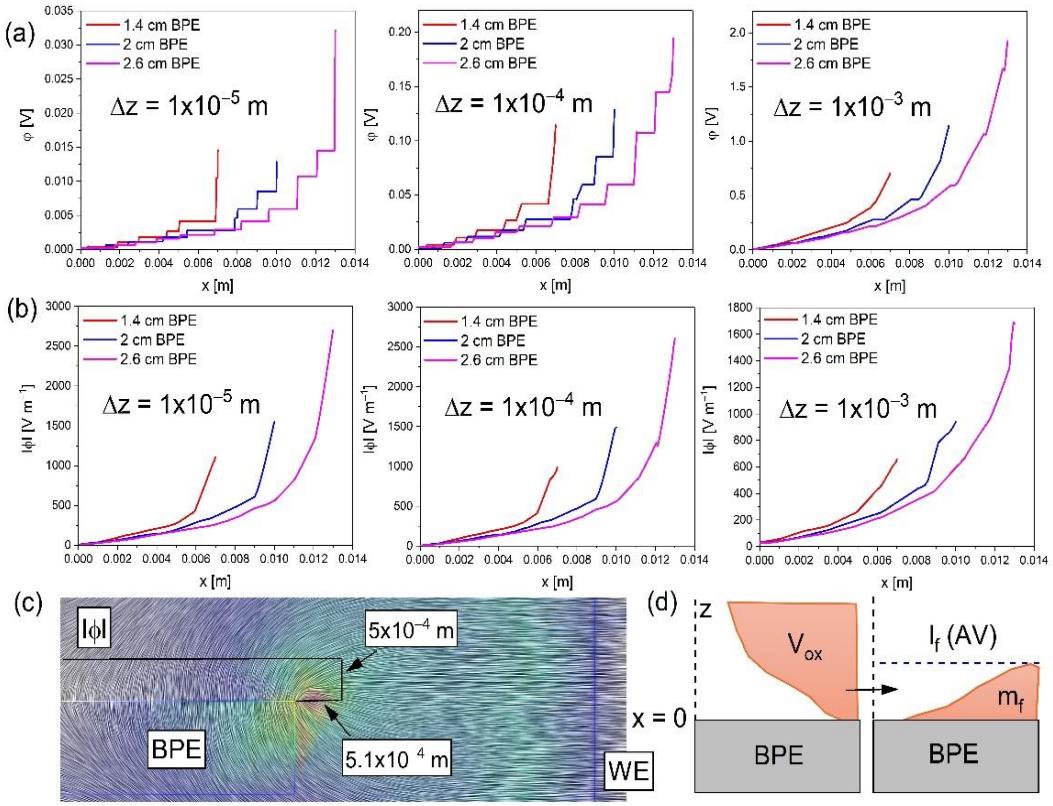


Figure 6 - Representative ϕ (a) and IϕI (b) profiles ($\Delta\phi_{app}$ = 10 V) at the centre of BPE for three different distances along the z-axis (Δz). Potential gradient map of studied systems with indicated vector field lines and unscaled marking (black lines) of the region near BPE considered in mass transport of EDOT entities (c). Schematic representation of the hypothetical volume of oxidized EDOT (V_{ox}) above BPE, together with the profile of deposited film with marked average film thickness (l_f) and total mass (m_f) characteristics (d).

In the simplified oxidative PEDOT polymerization process, the initiation reaction is a radical cation formation (EDOT → $EDOT^{+}\cdot$) followed by radical-radical coupling ($EDOT^{+}\cdot$ + $EDOT^{+}\cdot$ → 2EDOT). The polymerization continues with the oxidation of dimer/oligomers occurring at successively lower oxidation potential, *i. e.*, the effective driving force increases as polymerization proceeds. At a certain chain length, the product becomes insoluble in the medium and thus deposits on the electrode surface.

Due to the significant complexity of the electrochemical polymerization of conducting polymers, at this stage of research, we consider only the initial steps, as well as exclude dynamic changes in solution conductivities originating from generated and/or reacted hydronium ions. Independent experiments in a conventional 3-electrode system indicate that the oxidation potential of EDOT is approximately 0.8 V.[37] Therefore, this value was set as a threshold limit to estimate the fraction of oxidized EDOT molecules within the relevant vicinity of BPE. Firstly, the maximum thickness of the layer of solution in which 2EDOT can be oxidized within the experimental time is calculated assuming diffusion control. The diffusion coefficient (D) for 2EDOT was estimated to be approximately $4.34\text{x}10^{-10}$ m^2 s^{-1}. The diffusion length (l_D) was calculated using $l_D \approx \sqrt{Dt}$. For a deposition time, t, of 10 min, l_D is $5.1\text{x}10^{-4}$ m. Therefore, the considered volume of the medium above BPE and the hypothetical 'volume' of oxidized EDOT (V_{ox}) were limited by $5.1\text{x}10^{-4}$ m in the *x*-direction and $5\text{x}10^{-4}$ m in the z-direction, Figure 6c. The latter limitation was selected to accommodate six vertical intervals for calculations of (Δx)(z) surface areas (*vide* Figure S7a).

Herein, the Δx notation represents a fraction of oxidized EDOT along the x-axis above 0.8 V in φ *vs*. x plots. For each vertical interval, two fractions were considered totalling Δx: at the plane

of BPE (Δx_1) and beyond the BPE edge (Δx_2). For V_{ox} calculations two integrations were conducted along the x, y, and z dimensions, Figures S7 and S8. Resultant V_{ox} values were used to estimate the average film thickness (l_f) and mass of deposited film (m_f), Figures 7a and b. The analysis of the plots used for the first integration step in V_{ox} estimations reveals an interesting rationale for the non-linear deposition profile (*vide* Figure 2b) obtained for the **1.4 cm BPE** samples. As can be seen from Figure S7b, at $\Delta\phi_{app}$ = 10 V the oxidized fraction of EDOT expressed as $\Delta x = \Delta x_1 + \Delta x_2$, is only above zero for y = 0.003, 0.004, and 0.005 m. Moreover, in those cases, the Δx_2 contribution is significant in sharp contrast to **2.0 cm BPE** and **2.6 cm BPE** model samples, Figures S7 c and d. For **1.4 cm BPE**, non-zero Δx fractions for all y values are only obtained when $\Delta\varphi_{app} \geq 20$ V.

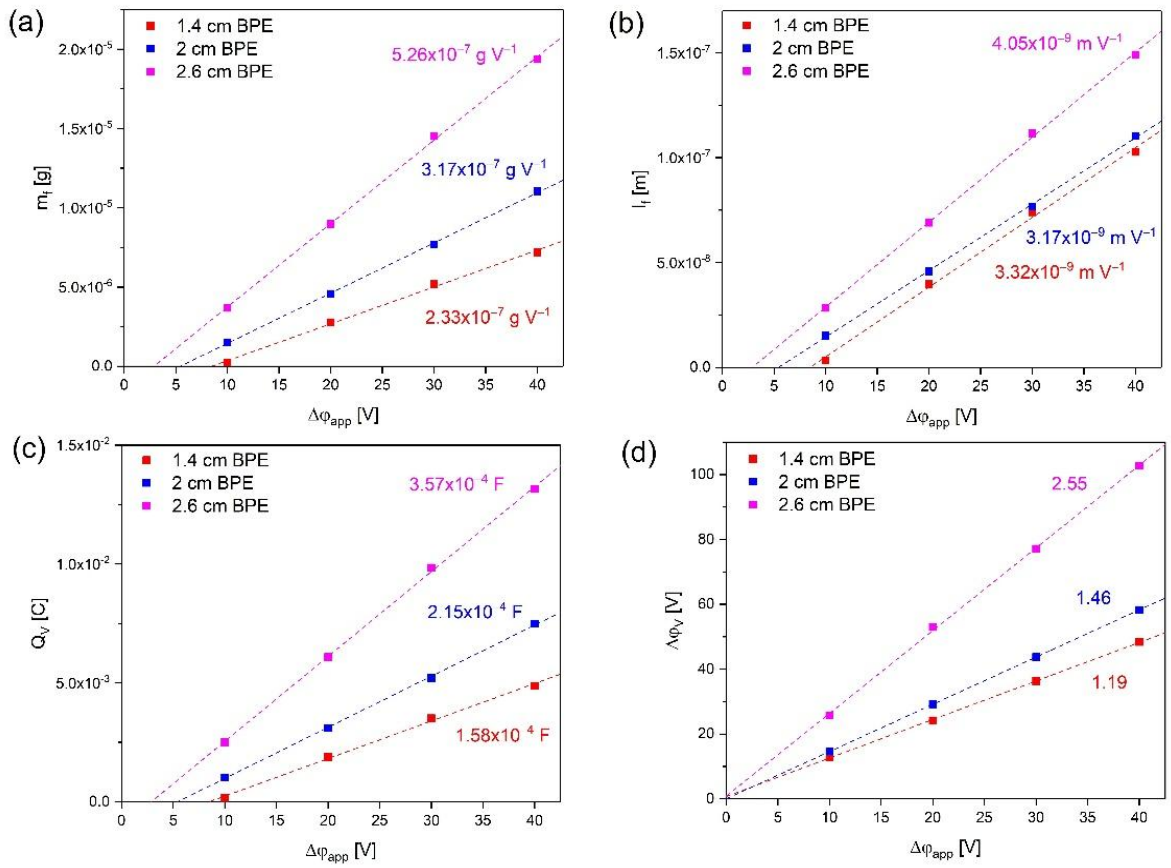


Figure 7 - Calculated change in film mass based on V_{ox} (a) and corresponding average film thickness (b) as a function of applied potential, together with marked SL values. Hypothetical charge (Q_V) values based on calculated total V_{ox} (c) and conceptual "volumetric voltage" ($\Delta\phi V$) obtained from integration of plots in Figure 5b (d) as a function of applied potential, together with marked SL values.

Importantly, the calculated V_{ox} values can be used for both m_f and l_f estimations, Figure 6d. All of the resultant m_f *vs.* $\Delta\varphi_{app}$ plots (*vide* Figure 7a) are linear, displaying increasing slope values with increasing lengths of BPE (**1.4 cm BPE** = 2.33×10^{-7} g V^{-1}, **2.0 cm BPE** = 3.17×10^{-7} g V^{-1}, and **2.6 cm BPE** = 5.26×10^{-7} g V^{-1}). The corresponding l_f *vs.* $\Delta\varphi_{app}$ plots can be constructed assuming a PEDOT film density of 1 gcm^{-3}, Figure 7b. The obtained slope values (**1.4 cm BPE**= 3.32×10^{-9} m V^{-1}, **2.0 cm BPE**= 3.17×10^{-9} m V^{-1}, and **2.6 cm BPE**= 4.05×10^{-9} m V^{-1}) indicate the proximity of average l_f values for **1.4 cm BPE** and **2.0 cm BPE** model samples. The average l_f value obtained for a **2.0 cm BPE** sample electrodeposited at $\Delta\varphi_{app}$ = 30 V and 20 min is around 1.54×10^{-7} m, Figure S9. Significantly, this value is very close to the calculated l_f for **2.0 cm BPE** (i.e. 1.53×10^{-7} m) based on 3.17×10^{-9} m V^{-1} slope and considered deposition time.

When assuming the theoretical specific charge of EDOT to be 679 C g^{-1} (for single electron transfer), film mass can be converted to the charge stored in the film (Q_V), Figure 7c. The obtained Q_V values were used for the calculation of hypothetical film capacitances for studied BPE systems. The corresponding voltage ($\Delta\varphi_V$) values were found from the integration of the results presented in Figure 5b with respect to the y-axis. The resultant $\Delta\varphi_V$ *vs.* $\Delta\varphi_{app}$ plots (*vide* Figure 7d) exhibit the same trends as m_f and thus Q_V plots. As can be seen from Figures 7c and d, the slope values in both cases are indeed closely proportional. The exact physical interpretation of $\Delta\varphi_V$ is an open question. This quantity is based on the consideration of potential gradient distribution at the BPE/medium interface, while film mass and charge quantities include consideration of potential distribution at both the interface and the electrode vicinity limited by diffusion. It can be speculated that $\Delta\varphi_V$ represents the area-dependent voltage at the BPE surface exerted by an electric field controlled by the specific geometry of the BPE system. The calculated $Q_V/\Delta\varphi_V$ ratios representing hypothetical C_f values as a function of applied voltages are shown in Figure 8.

The resultant profiles for all studied BPE systems are in good agreement with deposition profiles obtained *via* electrochemical measurements (*vide* Figure 6d). The non-linear profile for the **1.4 cm BPE** sample is reproduced, as well as, to a notable extent the intertwined profiles for the **2.0 cm BPE** and **2.6 BPE** samples. Moreover, the model-derived film capacitance profiles are also similar to calculated admittance profiles that are related to diffusivity in the PEDOT films, Figure 2c.

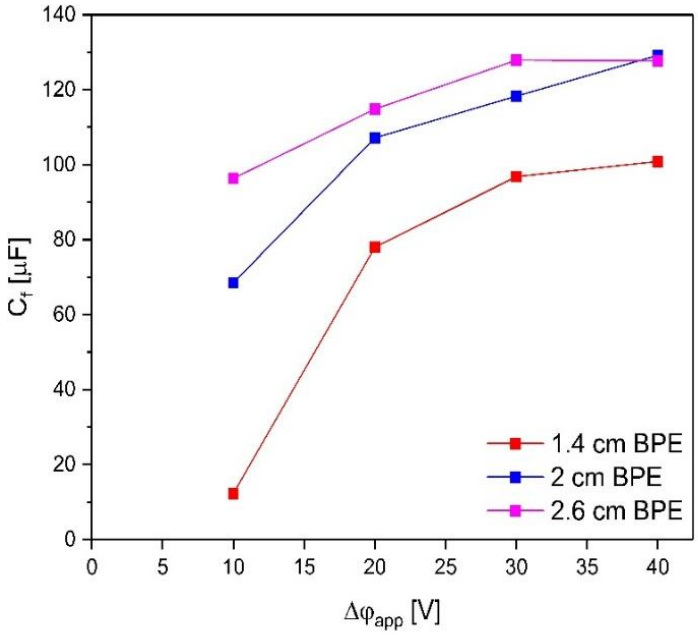


Figure 8 - Hypothetical film capacitance (C_f) values based on $Q_V/(\Delta\phi_V)$ ratios.

Due to the expected very large Debye lengths at BPE/ medium interfaces in high-resistance solutions, the nature of BPE reactions deserves attention. *i.e.*, because of the low ion concentration, the Debye length may exceed the distance over which it is reasonable to expect heterogeneous electron transfer. On the other hand, the reactions at titanium FEs are rather straightforward to identify. At the positively charged FE, the growing TiO_2 layer occurs driven by a tandem of two anodic reactions: (i) $Ti^{0} \rightarrow Ti^{4+} + 4\bar{e}$ and (ii) $Ti^{4+} + 2H_2O \rightarrow TiO_2 + 4H^+$.[38] Freshly polished titanium surfaces readily oxidize at ambient conditions forming *ca.* 1.5 nm thick layers, and further anodic oxidation results in significant TiO_2 growth in the order of tens of nm.[39] At negatively charged FE cathodic reduction of TiO_2 at acidic conditions proceeds as follows, $TiO_2 + 4H^+ + \bar{e} \rightarrow Ti^{3+}_{(aq)} + H_2O$.[40] Listed here titanium FE reactions are confirmed by consecutive observations and are important determinants for dielectric properties of the medium in studied systems, yet their temporal evolution does not affect effective FE potentials nor electric field distribution in the vicinity of BPE. As can be seen from Figure S10a, anodic passivation of Ti FEs in both monomer-free and EDOT ultrapure water solutions during bipolar experiments is apparent. The oxidation of the monomer and subsequent PEDOT film formation is impeded by TiO_2 layer development. The estimated pH values before and after PEDOT deposition on BPEs are *ca.* 6, which implies a preference for cathodic reduction of TiO_2 to Ti^{3+} cations at negative FE. Based on utilized FE dimensions the estimated complete TiO_2

layer disintegration with a hypothetical thickness of 1.5 nm would result in only ~ $1.2x10^{-5}$ M extra titanium ions that could contribute to overall ionic strength. Control studies of PEDOT deposition at BPEs in a series of increasing electrolyte content from 10^{-9} to 10^{-1} M $NaClO_4$ reveal that from 10^{-3} M, severe corrosion at anodic FE occurs (*vide* Figure S10b) accompanied by hydrogen gas generation at both cathodic FE and cathodic extremity of BPE. As a result, overoxidized PEDOT films are formed at the anodic part of BPEs even at relatively low applied potentials, Figure S10c. Notably, no gas evolution was observed at any electrode surface during experiments presented in Figure 2a, as well as control experiments with $NaClO_4$ concentrations from 10^{-9} to 10^{-4} M.

FEs taking part in bipolar experiments (10 mM EDOT in ultrapure water solutions) with **2.0 cm BPE** samples exposed to 30 V for 40 min were subjected to EIS measurements to estimate the specific capacitance of deposited PEDOT film, Figure S10d. The obtained value of *ca.* 0.6 $mFcm^{-2}$ constitutes only 10% of all PEDOT deposited since concurrent PEDOT film on BPE in this system exhibits around 5 $mFcm^{-2}$ capacitances. Therefore, indeed anodic passivation of positive FE significantly inhibits PEDOT film formation on itself. Anodic oxidation of EDOT on both positively charged FE and BPE surface starts with the following reactions: (i) EDOT → $EDOT^{+*}$ + ē and (ii) $EDOT^{+*}$ + $EDOT^{+*}$ → 2EDOT + $2H^+$ *etc.* When the growing polymer chain attains a certain length it loses solubility and deposits on the electrode surface. Generated protons from dimerization steps and already mentioned titanium ions from the cathodic reduction of the oxide layer on negative FE contribute to specific ionic characteristics of the bipolar electrochemical system. In order to gain insight into apparent electrolytic characteristics we measured the solution conductivities at different polymerization times from 5 to 40 min for **2.0 cm BPE** samples in ultrapure water exposed to 30 V with and without 10 mM EDOT, Figure S11. Recorded solution conductivity values for different concentrations of EDOT in ultrapure water samples are significant (*vide* Figure S11a), arriving at the value of *ca.* 8 µS cm^{-1} for 10 mM concentration. As can be seen from Figure S11b, which presents conductivity sensor calibration, the maximal EDOT concentration in our systems roughly corresponds to 10^{-4} M equivalent of KCl in terms of conductivity.

Interestingly, it was observed that polymerization solution conductivities decrease as electrodeposition proceeds which is in sharp contrast to the control study where the conductivity increases when the BPE is polarized in monomer-free ultrapure water samples,

Figure S11c. It can be speculated that in the case of monomer-free samples, a slight and non-linear increase in conductivity is predominantly related to a cathodic reduction of the oxide layer at negative FE since the previously estimated value of 1.2 x10 $^{-5}$ M titanium ions roughly match the "concentration-conductivity" region of interest. Importantly, despite proton generation at each dimerization step, there is a clear linear decrease in conductivity with polymerization time likely reflecting PEDOT formation kinetics. Results presented in Figure S11 suggest that the studied bipolar electrochemical systems in this work are within the 10 $^{-5}$ to 10 $^{-4}$ M range, leading to very large Debye lengths between 90 to 30 nm. The electron tunnelling probability through the distance of ~1 nm of the water layer yielding a 2eV energy barrier is empirically estimated[41] to be around 6x10^{-6} and consistent with the Gamov tunnelling equation.

Oxidation of EDOT via heterogeneous electron transfer at BPE surfaces is evident at 10 $^{-3}$ M concentrations of supporting electrolyte, in studies before[17,18] and also in this work. Therefore, a significantly large interfacial potential difference is created in close proximity to the Stern layer already at this concentration level. We did not include charging conditions at electrode boundaries in the FEM modeling but estimated the hypothetical maximum polarization voltage (~φ_{BPE}) based on the calculation of potential at BPE extremities induced by increasing the conductivity of the medium. Those FEM simulations were conducted on 1.4 cm BPE model sample with medium conductivity values equivalent to KCl in the 10 $^{-5}$ to 10 $^{-1}$ M range with ~ φ_{app} =10, 20, and 40 V, Figure 9. It is conspicuous that within the 10 $^{-3}$ to 10 $^{-1}$ M range the induced polarization of ~ 10 to 360 mV at e.g. ~ φ_{app} = 40 V is enough to drive EDOT oxidation via heterogeneous electron transfer if the effective capacitance of electric double layer and thus the local surface charge of BPE are considered. On the other hand, estimated 10 and 20-fold lower polarization potential values at 10 $^{-5}$ and 10 $^{-4}$ M (in reference to polarization induced at 10 $^{-3}$ M) suggest very low probability for electron tunnelling, e.g., using 2 eV energy barrier.

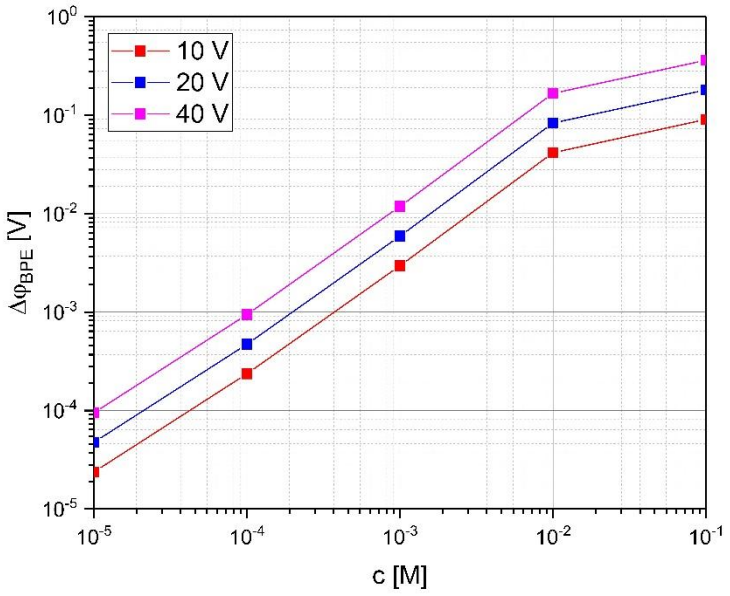


Figure 9 - Hypothetical maximum polarization voltage of the exemplary 1.4 cm BPE ($\Delta\phi_{BPE}$) calculated for different medium conductivities equivalent to KCl concentrations in the 10^{-5} – 10^{-1} M range.

Thus, in pure milli-Q water one would not expect significant heterogeneous electron transfer to be possible based on the Debye length and the voltage induced in the BPE, but a relatively small increase in solution concentration, *e. g.*, arising for protons released during EDOT oxidation or dissolution or titanium oxide at the feeder cathode. It appears that there is significant scope for further investigations into electron transfer dynamics when the electric double layer is underdeveloped using wirefree methods that avoid iR drop effects, as well as including scanning probe methods to measure the potential drop when approaching the BPE surface.

Overall, the presented theoretical framework qualitatively replicates observed non-linearities in film capacitance profiles for the wirefree deposition of conducting polymers. The successful prediction of deposition patterns for a highly complex process of conducting polymer film formation constitutes an important first step toward understanding bipolar electrochemistry in high-resistance solutions. Significantly, the modeled non-linear change in solution overpotentials imposed by the equipotential surface of BPE combined with calculated

relatively low electric field strengths (< 6 kV m^{-1}) in close proximity to the BPE-solution interface indicates that PEDOT electrosynthesis is likely to involve homogeneous electron transfer where the double layer is not well developed. In the future, we plan to build a model that accounts for the influence of growing PEDOT film layers on the physicochemistry of the BPE-solution interface as well as radical cation transport and acceleration due to the presence of the interfacial and feeder-driven electric fields. Additionally, since a well-developed electrical double layer is needed to screen the charge resulting from BPE polarization induced by an electric field, new theoretical considerations (aided with quantum and molecular dynamics simulations) are needed to model various interfacial electric field effects at suboptimal ion concentrations.

Conclusion

We have successfully fabricated electrically conducting polymer PEDOT films in ultrapure water utilizing bipolar electrochemistry. Such deposition would not be possible in "traditional" 3electrode systems where the presence of a supporting electrolyte is needed. We demonstrated that the PEDOT deposition profiles cannot be fully explained by commonly assumed linear decay of the electric field through the solution driven by the feeder voltages. Our FEM model provides a rationale for the observed preferential deposition areas and provides deep insights into mass transport and quantifies the volume of solution above the BPE that could be available for deposition. Importantly, we have been able to calculate both the hypothetic film charge and BPE voltage that depends markedly on the physical location on the BPE. Taken together, this model successfully replicates the film capacitance profiles of studied PEDOT-BPE systems obtained experimentally. The proposed alternative framework provides a valuable starting point for understanding the electrochemical deposition process on BPEs in high-resistance media. We envision further investigations where polymer layers are modeled to target various charge transfer and polarization effects on hetero- and homogeneous reactions in dynamic bipolar systems with low ion content.

References

[1] P. Sanjuan-Alberte, M. R. Alexander, R. J. M. Hague, F. J. Rawson, *Bioelectron Med* **2018**, *4*, 1–7.

[2] M. R. Love, S. Palee, S. C. Chattipakorn, N. Chattipakorn, *J. Cell. Physiol.* **2018**, *233*, 1860–1876.

[3] M. R. Cho, H. S. Thatte, M. T. Silvia, D. E. Golan, *The FASEB Journal* **1999**, *13*, 677–683.

[4] R. J. Forster, *Curr. Opin. Electrochem.* **2023**, *39*, 101297.

[5] S. E. Fosdick, K. N. Knust, K. Scida, R. M. Crooks, *Angew. Chem. Int. Ed.* **2013**, *52*, 10438–10456.

[6] C. Qin, Z. Yue, Y. Chao, R. J. Forster, F. Maolmhuaidh, X. F. Huang, S. Beirne, G. G. Wallace, J. Chen, *Appl Mater Today* **2020**, *21*, 100804. [7] C. Qin, Z. Yue, X. F. Huang, R. J. Forster, G. G. Wallace, J. Chen, *Appl Mater Today* **2022**, *27*, 101481.

[8] B. Guo, P. X. Ma, *Biomacromolecules* **2018**, *19*, 1764–1782.

[9] R. Balint, N. J. Cassidy, S. H. Cartmell, *Acta Biomater.* **2014**, *10*, 2341– 2353.

[10] K. Duval, H. Grover, L. H. Han, Y. Mou, A. F. Pegoraro, J. Fredberg, Z. Chen, *Physiology* **2017**, *32*, 266–277.

[11] F. Mavré, K. F. Chow, E. Sheridan, B. Y. Chang, J. A. Crooks, R. M. Crooks, *Anal. Chem.* **2009**, *81*, 6218–6225.

[12] Y. Ishiguro, S. Inagi, T. Fuchigami, *J. Am. Chem. Soc.* **2012**, *134*, 4034– 4036.

[13] Y. Koizumi, N. Shida, M. Ohira, H. Nishiyama, I. Tomita, S. Inagi, *Nat. Commun.* **2016**, *7*, DOI 10.1038/ncomms10404.

[14] J. Lee, T. W. Yoon, S. Chung, K. Cho, G. Zhang, B. Kang, *Adv. Funct. Mater.* **2024**, DOI 10.1002/adfm.202406229.

[15] J. F. L. Duval, G. K. Huijs, W. F. Threels, J. Lyklema, H. P. Van Leeuwen, *J. Colloid Interface Sci.* **2003**, *260*, 95–106.

[16] J. F. L. Duval, *J. Colloid Interface Sci.* **2004**, *269*, 211–223.

[17] A. Eden, K. Scida, N. Arroyo-Currás, J. C. T. Eijkel, C. D. Meinhart, S. Pennathur, *J. Phys. Chem. C* **2019**, *123*, 5353–5364.

[18] A. Eden, K. Scida, N. Arroyo-Currás, J. C. T. Eijkel, C. D. Meinhart, S. Pennathur, *Electrochim. Acta* **2020**, *330*, 135275.

[19] A. N. Colli, H. H. Girault, *J. Electrochem. Soc.* **2017**, *164*, E3465–E3472.

[20] T. Nann, J. Heinze, *Electrochem. Commun.* **1999**, *1*, 289–294.

[21] C. Ulrich, O. Andersson, L. Nyholm, F. Björefors, *Anal. Chem.* **2009**, *81*, 453–459.

[22] N. Pébère, V. Vivier, *ChemElectroChem* **2016**, *3*, 415–421.

[23] J. Song, *FEBS Lett.* **2009**, *583*, 953–959.

[24] A. Dér, L. Kelemen, L. Fábián, S. G. Taneva, E. Fodor, T. Páli, A. Cupane, M. G. Cacace, J. J. Ramsden, *J. Phys. Chem. B* **2007**, *111*, 5344–5350. [25] K. B. Oldham, *J. Electroanal. Chem.* **2008**, *613*, 131–138.

[26] G. Meaden, in *Electrical Resistance of Metals*, Springer, Boston, MA, **1965**. [27] *Handbook of Chemistry and Physics*, CRC Press, **1997**.

[28] M. Malinen, P. Råback, in *Elmer Finite Element Solver for Multiphysics and Multiscale Problems, Multiscale Modelling Methods for Applications in Material Science* (Eds.: I. Kondov, G. Sutmann), **2013**, pp. 101–113.

[29] E. Villani, S. Inagi, *Anal. Chem.* **2021**, *93*, 8152–8160.

[30] K. Scida, A. Eden, N. Arroyo-Currás, S. Mackenzie, Y. Satik, C. D. Meinhart, J. C. T. Eijkel, S. Pennathur, *ACS Appl. Mater. Interfaces* **2019**, *11*, 13777– 13786.

[31] B. A. Boukamp, *Solid State Ion* **1986**, *20*, 31–44.

[32] A. Bonnefont, F. Argoul, M. Z. Bazant, *J. Electroanal. Chem.* **2001**, *500*, 52–61.

[33] E. M. Itskovich, A. A. Kornyshev, M. A. Vorotyntsev, *Physica A* **1977**, *39*, 229–238.

[34] M. Van Soestbergen, *Russ. J. Electrochem.* **2012**, *48*, 570–579. [35] S. M. Risser, K. F. Ferris, *Mater. Lett.* **1992**, *14*, 99–102.

[36] K. F. Ferris, S. M. Risser, *Chem. Phys. Lett.* **1995**, *234*, 359–366.

[37] L. Pigani, A. Heras, Á. Colina, R. Seeber, J. López-Palacios, *Electrochem. Commun.* **2004**, *6*, 1192–1198.

[38] M. Brocklebank, H. Feltham, J. J. Noël, L. V. Goncharova, *Electrochim. Acta* **2022**, *435*, 141342.

[39] D. Prando, A. Brenna, M. V. Diamanti, S. Beretta, F. Bolzoni, M. Ormellese, M. P. Pedeferri, *J Appl Biomater Funct Mater* **2018**, *16*, 3–13.

[40] T. Ohtsuka, M. Masuda, N. Sato, *J. Electrochem. Soc.* **1987**, *134*, 2406– 2410.

[41] W. Schmickler, *Surf. Sci.* **1995**, *335*, 416–421.

Finite element modelling within the context of two-dimensional bipolar configurations in low-conductive media suggest that electric fields should not be viewed solely as passive consequences of cell design and architecture but rather as parameters that can be deliberately engineered to directly influence electrochemical behaviour. Having established a more well-rounded view of field formation and distribution, the next logical step is to investigate whether fields can be actively manipulated through structural design. While the modelling framework demonstrated how geometry influences electric field localisation, it also raised the important question of whether these theoretical predictions could be experimentally exploited to enhance wireless electrochemical performance.

Conventional bipolar electrochemical systems typically employ planar feeder electrodes that generate relatively uniform field profiles. While effective, such configurations inherently limit the degree of control that can be exerted over the resulting electrochemical environment. Consequently, a key objective of this thesis is to determine whether modification of feeder electrode geometry can be used to intentionally redistribute electric fields and thereby regulate local electrochemical activity.

This chapter therefore explores the use of three-dimensional feeder electrode architectures as a strategy for electric field engineering. By introducing geometric complexity into the field generating elements of the system, new opportunities emerge for field localisation, amplification and spatial confinement. The work presented here examines how complex, organised structures can be used as a powerful tool for controlling electrochemical activity. In doing so , this chapter represents the first experimental validation of the central hypothesis that deliberate manipulation of fields can be used to engineer wireless behaviour.

Chapter 4

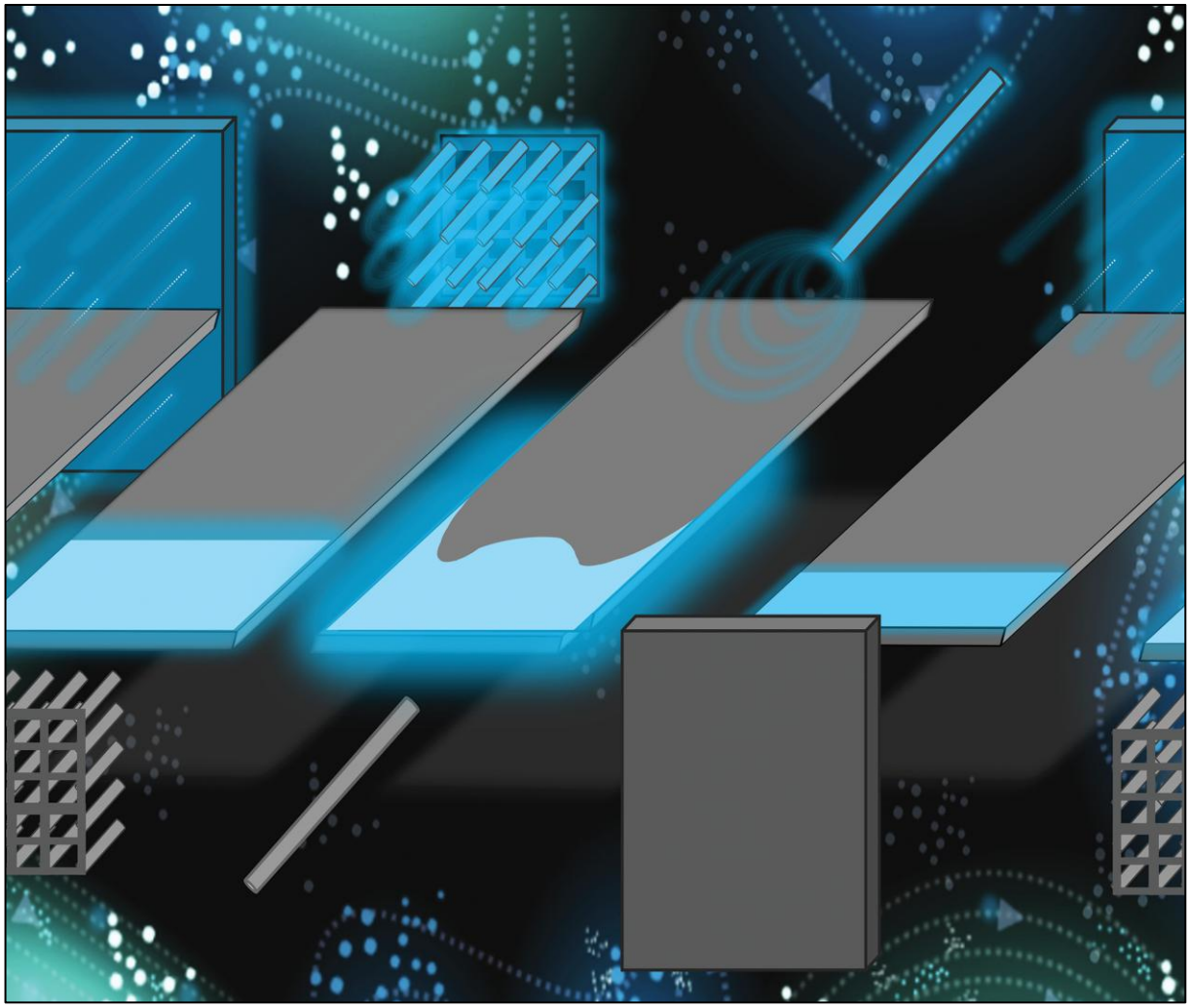
Directing the glow : 3D feeder geometric to enhance planar bipolar electrochemiluminescence

Volume 61
Number 97
18 December 2025
Pages 19135–19322

ChemComm

Chemical Communication

rsc.li/chemcomm



ISSN 1359-7345

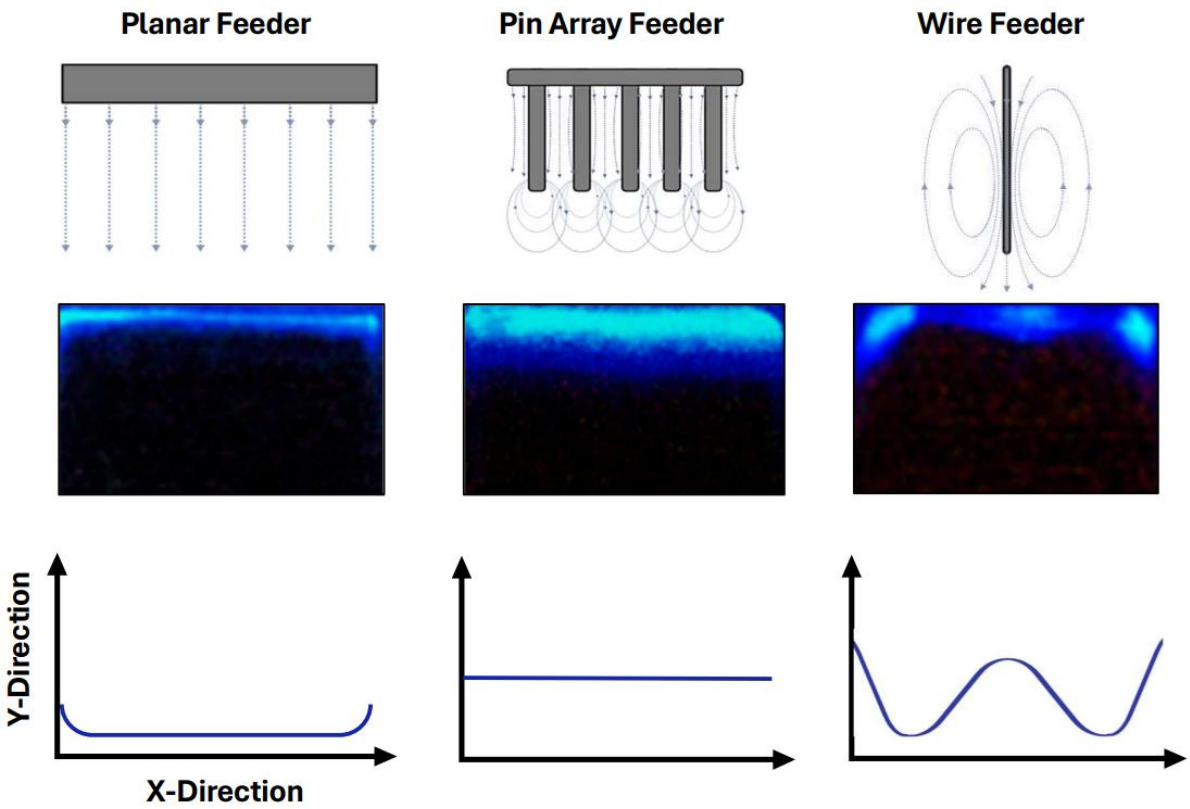
Chem.Comm.2025, 61, 19221 *doi.org/10.1039/D5CC04706D*

Directing the glow: 3D feeder geometries to enhance planar bipolar electrochemiluminescence

Oisin Foley Doyle [a], Gordon G. Wallace [c], Zhilian Yue [c], Jun Chen [c], Stephen Beirne [c], and Robert J. Forster [ab].

a. School of Chemical Sciences, Dublin City University, Dublin 9, Ireland. E-mail: robert.forster@dcu.ie
b. FutureNeuro, SFI Research Centre for Chronic and Rare Neurological Diseases, Dublin City University, Dublin 9, Ireland
c. Intelligent Polymer Research Institute, Faculty of Engineering and Information Science, University of Wollongong, Innovation Campus, North Wollongong, NSW, 2500, Australia

Graphical Abstract



Abstract

Using 3D-printed pin arrays or single wires as feeders in open bipolar cells enhances luminol bipolar electrochemiluminescence (BP-ECL) and allows light to be generated in localised regions of planar stainless-steel bipolar electrodes (BPEs). Spatially resolved ECL mapping shows that both pin arrays and single wires outperform planar feeders, yielding approx. 2-fold and 2.6-fold more intense ECL, respectively. Strikingly, single-wire feeders produce a symmetrical three-spot emission pattern, while planar and pin array feeders generate uniform bands of ECL. These findings demonstrate that compact feeder architectures can localise and intensify BPECL, enabling efficient wire-free electrochemical activation without the need for size matching of the feeder and the BPE.

Introduction

Controlling the spatial distribution of the induced potential and the current flow within bipolar electrochemical cells is key to developing next-generation wireless electrochemical technologies, including multianalyte sensors, adaptive (4D) materials, microreactors, and electrocatalytic platforms.[1,2] The local potential difference that drives redox reactions at a bipolar electrode, BPE, does not exclusively arise from a static electric field in a uniform dielectric medium, but from an electric potential gradient controlled by ionic current flow through the electrolyte. This gradient reflects the combined effects of the applied voltage between feeder electrodes, the solution conductivity, and the faradaic or capacitive processes at both the feeders and the BPE surface. Thus, the potential induced in the BPE depends critically on the dynamic current flow, rather than simple geometric field lines generated by the potential difference between the feeders.

In planar configurations, where two extended feeder electrodes are positioned on either side of a planar BPE, the potential difference across the electrolyte develops gradually along the cell across the electrode width (y-direction) is approximately uniform. Under these conditions, the potential difference within the BPE reflects the local distribution of solution potential along its length, which in turn depends on the spatial pattern of ionic current flow between

the feeders. By deliberately shaping the feeder electrodes or varying their separation, the current paths, and therefore the solution potential, can be tailored to achieve controlled, spatially selective polarisation within the BPE.

Three-dimensional feeder electrodes, such as 3D-printed Ti_4Al_6 pin arrays, allow the potential and current distribution within the electrolyte to be controlled. Local curvature, field focusing, and fringing effects around the protruding pins on each feeder array can introduce anisotropic potential gradients that modulate the direction and magnitude of ionic fluxes.[4] In turn, they control the induced voltage not only along the traditional *x*-axis, but also in the transverse *y*-direction. By controlling these gradients, it becomes possible to tune where and at what rate redox reactions occur across the BPE surface, potentially enabling spatially resolved electrocatalysis, reagent generation, or sensing zones on a single, continuous electrode.

To visualise and quantify how variations in feeder geometry and current pathways shape the local potential and reaction zones on a BPE surface, several wireless mapping techniques have been developed. Wireless electropolymerisation of conducting monomers such as EDOT or pyrrole has been used as a qualitative indicator of local potential distribution.[5] Polymer deposition occurs close to those regions where the interfacial potential exceeds the oxidative threshold, thereby identifying regions of high anodic polarisation. However, the spatial resolution of this method is limited by the fact that polymer may not necessarily deposit exactly where radicals are electrogenerated, due to diffusion, ionic migration, and convection, effects that are especially pronounced in complex 3D geometries where the potential distribution is strongly non-uniform.

Bipolar electrochemiluminescence (BP-ECL) offers a complementary, non-destructive approach with superior spatial and temporal resolution.[6–8] Because light emission occurs only when the local interfacial potential surpasses the activation threshold for ECL generation, BP-ECL can allow zones of electrochemical activity to be visualised in real time without altering the electrode surface. When combined with image-based analysis, the spatial intensity profiles provide a more quantitative insight into the underlying potential and current

distributions and can help discriminate whether the rate-determining step is mass transport or heterogeneous electron transfer.

Here, a custom-designed electrochemical cell was created via CAD and 3D-printed using tough PLA filament. The internal cell volume was approximately 3.0 cm^3. The cell contains 3 cm^3 of 10 mM Luminol and 30 mM H_2O_2 in 0.1 M NaOH solution. The nominal electric field strength was kept constant at 3.33 V cm^{-1}, typically 10 V dropped across 3 cm ignoring ohmic losses. Differences in the ECL generating regions and ECL intensity can be used to elucidate how different feeder geometries affect the potential in solution and hence within the BPE. Here, the ECL intensity along five separate line plots from the BPE terminal (0 cm) towards the centre of the BPE (1 cm) were used to map the local ECL intensity.

Experimental

Materials

Luminol (3-aminophthalhydrazide), hydrogen peroxide (30 wt%), and sodium hydroxide were obtained from commercial suppliers and used without further purification. A 10 mM luminol and 30 mM hydrogen peroxide solution was prepared in 0.1 M NaOH using ultrapure deionised water (18.2 MΩ cm). 304S15 stainless steel (Radionics Ltd.) was used as the bipolar electrode (BPE). Feeder electrodes consisted of planar stainless steel, Ti6Al4V pin arrays, and stainless-steel wires.

Bipolar Electrochemical Setup

The bipolar electrochemical cell was designed using FreeCAD and fabricated using an Ultimaker S5 3D printer with Acrylonitrile Butadiene Styrene (ABS) filament. The layer height and skin thickness were 0.15 mm, with an infill density of 20%, and printed at 230 °C.

The feeder electrodes were positioned vertically at opposite ends of the cell with a separation distance of 3 cm. The stainless-steel BPE was positioned centrally between the feeder electrodes. Different feeder geometries were investigated using planar, pin-array, and wire configurations. An EA PS 2384-03 B power supply was used to apply the required voltage across the feeder electrodes.

Bipolar Electrochemiluminescence Measurements

The bipolar cell contained 3 mL of 10 mM luminol, 30 mM hydrogen peroxide, and 0.1 M NaOH solution with the prepared BPE and feeder electrodes. A constant potential difference was applied across the feeder electrodes to induce bipolar electrochemical reactions. Electrochemiluminescence emission was recorded using a Nikon CCD camera under dark conditions.

Image Analysis

Image analysis was performed using ImageJ software. Greyscale intensity profiles were extracted from ECL images to determine spatial emission distributions along the BPE surface. Integrated ECL intensity values were calculated following background subtraction.

When a planar BPE is placed between two planar, perpendicular feeders, the solution potential varies progressively across the electrode in accordance with the imposed current flow.[9] Fig. 1 shows a typical experimental ECL intensity profile across a planar electrode where the feeders are two vertical, planar electrodes. Several key observations can be made. First, no light is observed for distances greater than approximately 0.12 cm from the tip of the bipolar anode. Cyclic voltammetry experiments using a traditional 3-electrode cell and a highly sensitive PMT for ECL detection indicate that a potential of 0.33 V is required to generate luminol ECL under these conditions. The BPE is 2.0 cm long and the voltage at its centre is at 0 V while at 0.872 cm (1 – 0.128 cm, the first location light is observed), it is 0.33 V. Thus, while the nominal field strength is 3.33 V cm $^{-1}$, the actual field strength is approximately 0.38 V cm $^{-1}$.

In part, the significantly reduced field reflects iR drop between the feeder and bipolar electrodes. Second, the variation in ECL intensity with *x*-distance is not linear for any *y*-position on the bipolar electrode. Non-linearity is expected if the rate of heterogeneous electron transfer, k, is rate limiting since k depends exponentially on the overpotential. It is also important to consider the possibility that mass transport may limit the ECL response closer to the anode tip where the overpotential, and consequently the rate of heterogeneous electron transfer, are largest. However, the potential at the tip of the bipolar electrode is expected to be approximately 0.38 V, i.e., 0.38 V cm $^{-1}$ 1.0 cm, giving a maximum overpotential driving heterogeneous electron transfer of only about 50 mV. The luminol ECL reaction involves bond breaking and formation, and it is highly likely that the reorganisation energy is of the order of 0.5 – 1.0 eV.[10] Therefore, slow heterogeneous electron transfer rather than mass transfer by diffusion/migration is the most likely rate determining step, RDS, across the entire BPE where ECL is generated, i.e., a change of RDS in ECL generation does not contribute to the nonlinear dependence of I_{ECL} on distance.

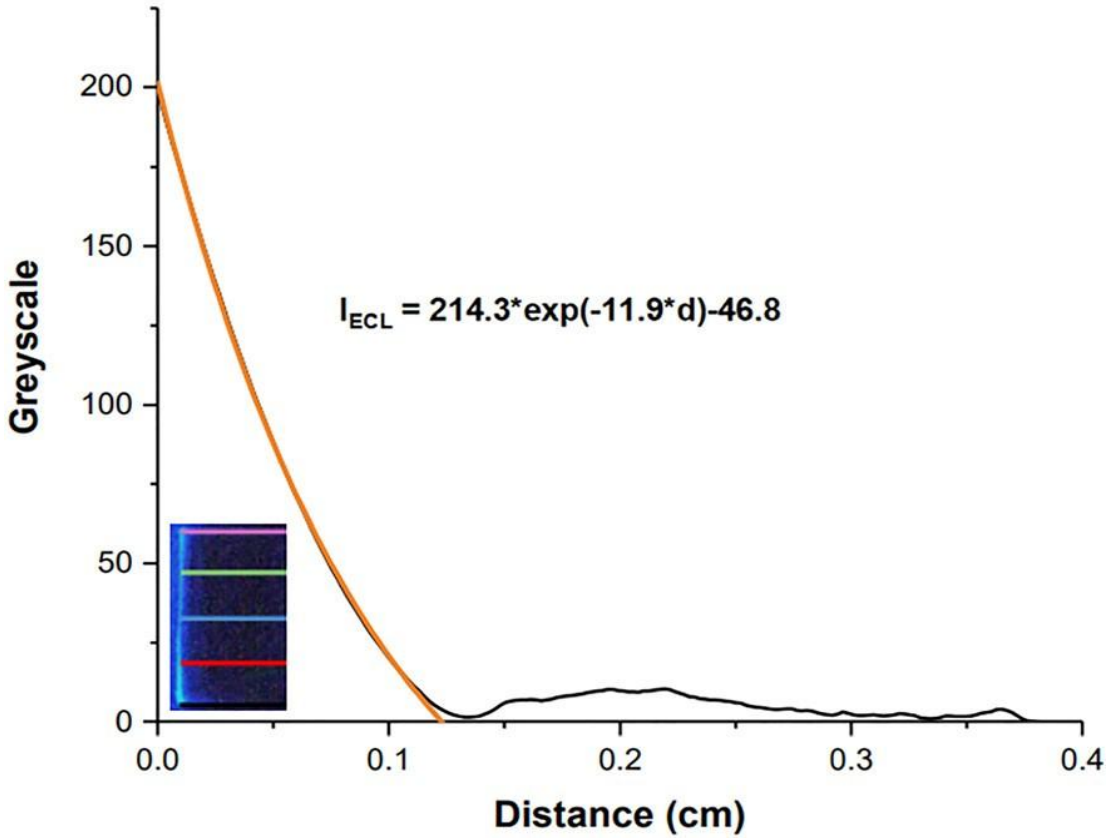


Fig. 1 - An averaged ECL intensity (greyscale) vs. distance plot across the 2 cm long (*x*) by 1 cm wide (*y*) centred, planar BPE. The inset shows a top-down view of the ECL generated at the BPE and the location of the experimentally indistinguishable, individual traces that were averaged to obtain the black line of the main figure.

Marcus theory predicts an exponential dependence of the current density or rate of heterogeneous electron transfer on the overpotential, Z, (= $E_{app} - E^{\circ'}$, where E_{app} is the applied potential and $E^{\circ'}$ is the operational formal potential) at least when the overpotential is small.[11] Fig. 1 shows that a very high quality fit (R^2 = 0.9995) is obtained for the experimental I_{ECL} vs. distance (voltage) profile for the bipolar cell with a planar BPE and planar feeders using I_{ECL} = 214.3 ± 72.1 exp(- 11.9± 1.2 x *d*) - 46.8 ± 20.0, where *d* is the distance measured from the tip of the BPE anode, i.e., where the overpotential is largest. The high-quality fit further suggests that the ECL profile is controlled by heterogeneous electron transfer kinetics, influenced by the voltage induced across the bipolar electrode.

The electrochemiluminescence (ECL) intensity along a bipolar electrode decreases exponentially with distance from the anode tip because even if the local interfacial potential difference decreases linearly under a uniform electric field the redox reaction rate governing ECL depends exponentially on the (over)potential. Significantly, the best fit equation can be used to accurately determine the distance from the tip over which ECL is generated. This value, 0.128 cm, agrees with that found by measuring the distance from the ECL image using Image J, but has the significant advantage of using the bright ECL response, (S/N ratio is > 20) to accurately determine the distance rather than trying to identify the first ''bright'' pixel where the S/N ratio can be less than 1. The observation that the best fit requires a negative offset, - 46.8 ± 20.0 a.u., likely arises because the standard heterogeneous electron transfer rate, k°, is not zero, but other effects, such as limited detector sensitivity (8-bit), ambient light, non-uniform electric fields, reagent depletion/transport or excited state quenching, may also be important. Numerical integration gives an overall ECL intensity, ϕ, of 16.1 ± 3.6 for the planar feeder systems which can provide a convenient way to compare alternative systems using different feeder electrode types.

Three-dimensional feeder structures, such as a single pin electrode oriented in the same plane as the BPE, could give a highly localised, intense potential distributions since it should act as a point-like electric field source, creating a strongly radial electric field that dissipates sharply in a lateral (*y*) direction. The ability to localise ECL could significantly impact sensor development. For example, the detection region could be switched when the analytical performance degrades locally or different analytes could be detected at different physical locations on the BPE, i.e., spatially resolved multianalyte detection, but where the detector performance can be optimised for each analyte without having a bright adjacent emission due to another analyte.

Significantly, as shown in Fig. 2, a single wire feeder creates a focused polarisation region in the BPE directly facing the wire feeder tip, but two additional bright ECL regions are observed at the lateral edges of the BPE. Line scans of the ECL intensity vs. *x*-distance at different *y*-locations can provide a deeper insight into the electric field distribution and how feeder electrode configuration can be used to spatially manipulate ECL active regions on the BPE.

Fig. 2 demonstrates that there are significant differences in the ECL intensity line scans between the centre of the BPE that is directly opposite the single wire feeder, 2.5 mm away from the centre and the edges. For example, like the full-width planar feeder, the intensity of the line scans at the middle of the BPE, and the two either side (2.5 mm away) decrease exponentially from the edge of the BPE facing the wire feeder. Fitting all three of these traces close to the centres of the BPE indicates that the width of the ECL generating region is 0.198 ± 0.02 cm, corresponding to a field of 0.41 ± 0.01 V cm $^{-1}$, which is approximately 10% higher than that found for the planar feeders. In contrast, while significant ECL is observed at the edges of the BPE where there is no opposing feeder, I_{ECL} is initially high, but is independent of the *x*-distance for the first 0.11 cm before decaying exponentially with increasing distance. Significantly, ECL is observed for substantially longer distances at the edges, 0.30 and 0.39 cm for the right and left edges, respectively, corresponding to fields of 0.46 ± 0.05 and 0.54 ± 0.06 V cm^{-1}. It may be important to note that the asymmetry may arise due to the single wire feeder not being placed in the exact centre of the BPE.

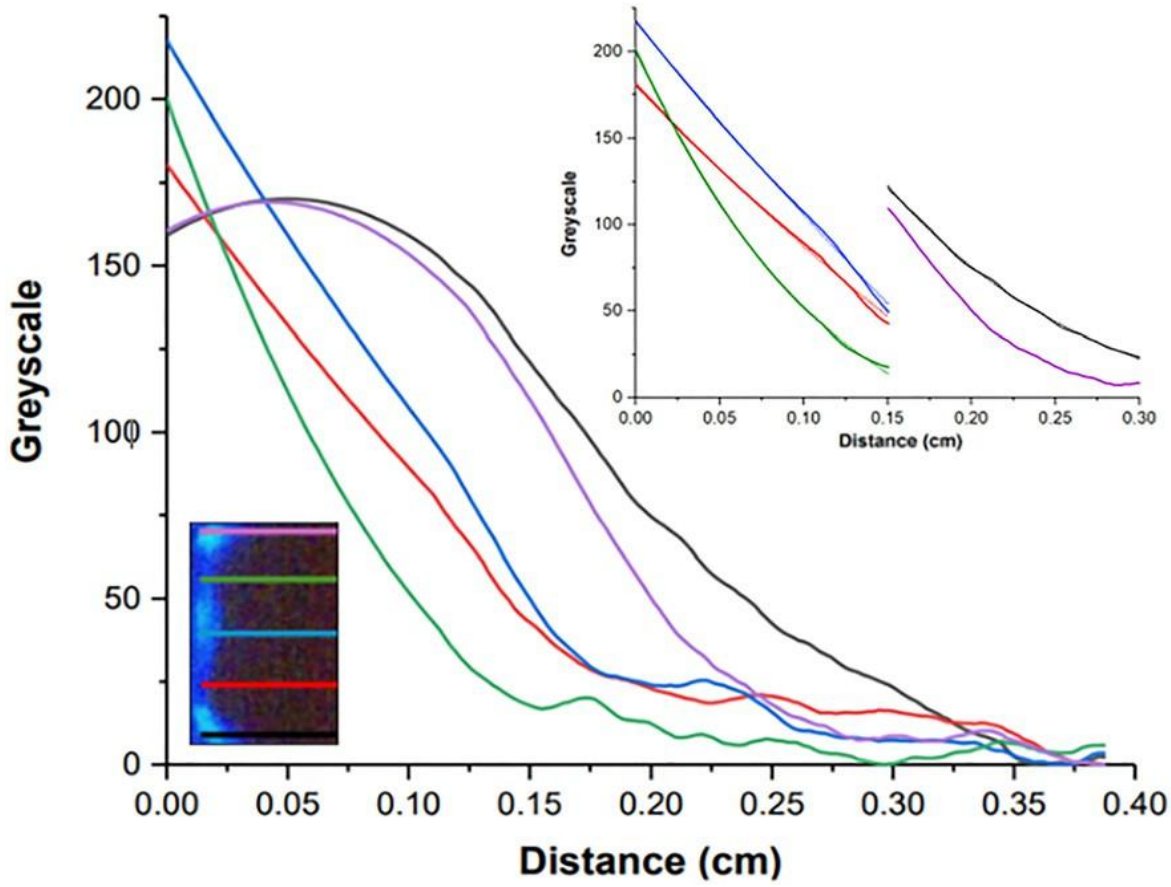


Fig. 2 - ECL intensity (greyscale) vs. distance plots (n = 3) at five different positions across the surface of a 2 cm long by 1 cm wide planar BPE where the feeder electrodes are single titanium wires (0.1 cm dia) located in the same plane as the BPE and centred. The inset shows a top-down view of the ECL generated at the BPE and the locations of the ECL profiles are colour coded to the graphs.

These are the highest field strengths observed and exceed the planar feeder values by 20 to 40%. While the predicted overpotential is relatively larger, e.g., 0.21 V at the left edge, this is unlikely to be sufficient to observe a Marcus inverted region effect even if mass transport limitations (due to diffusion and migration in the field) were absent. The observation of isolated ECL at the corners of the BPE, even though there is no physical feeder opposite arises because the electric fields at the lateral edges of the feeder wire (left and right edges), fringe outwards. This fringing increases the normal component of the electric field at those edge locations, leading to localised enhancements in the current flow and potential drop across the BPE–solution interface. These effects are amplified by the sharp corner and the small thickness of the BPE, 0.1 cm. Fringing is especially prominent in this configuration due to the highly non-uniform electric field distribution caused by the miniaturised (0.1 cm diameter cylinder) feeder. The central placement and symmetry of the single wire feeder promote a mirror-symmetric potential distribution across the BPE, encouraging approximate equivalent activation of both terminal regions.

Finally, the path of least resistance for ionic current flow from the feeder to the BPE is not strictly linear and the current paths can curve laterally through the electrolyte, resulting in spatially diffuse field lines that can reach terminal regions with sufficient strength to drive bipolar reactions. Significantly, using a single wire feeder results in the highest integrated ECL intensity, ϕ, among all feeder configurations investigated at 41.6 ± 4.9 AU. The higher total emission intensity observed arises in large part due to a larger emitting region because of the potential distribution. Thus, using a single 3D pin feeder can give heterogeneous potential distributions in solution, allowing the polarisation to be spatially confined at the BPE and enabling lower feeder voltages to be used for a given ECL system.

To probe the effect of using multiple pins as feeders, an array was used as the feeder electrode where the long axis of the pins is in the same plane as the bipolar electrode. The array comprises 25 round cylinders (0.015 cm radius, 0.3 cm long) that are evenly separated on a 0.48 cm x 0.48 cm square-porous base (total geometric area of 1.32 cm^2). Importantly, the array is 0.48 cm wide compared to the 1 cm width of the BPE, and it is centrally located in both y and z. The pins are expected to act as point sources of electric field and the electric field lines could diverge radially from the pins and converge toward the BPE. However, fringing at the edges could extend the ECL generating region into areas where the feeder is not present as observed for the single wire system. The change in feeder material from pure titanium to Ti_6Al_4V is reasonable because both materials exhibit similar electrochemical stability and oxide-forming behaviour in aqueous media. The small alloying additions of aluminium and vanadium do not significantly alter the surface potential or conductivity under the conditions used, so the overall behaviour of the bipolar electrode remains largely unchanged.

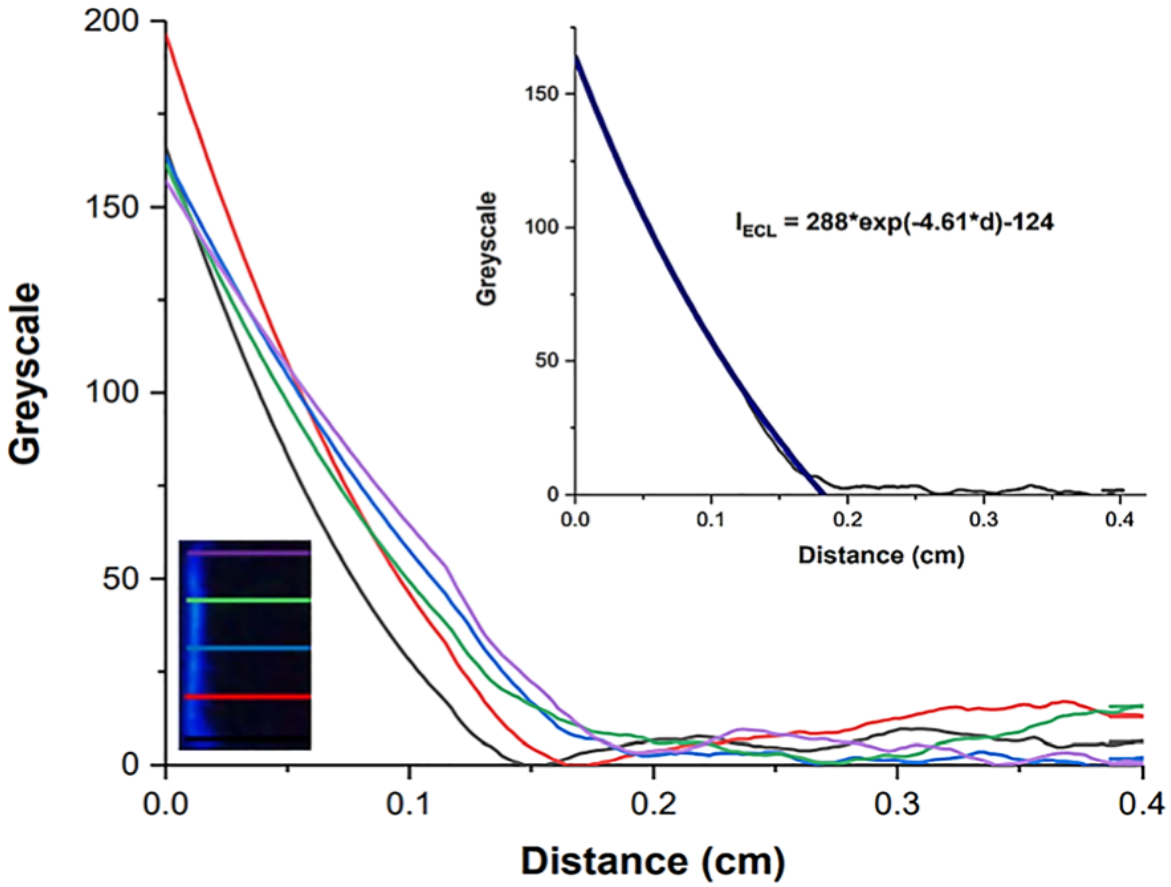


Fig. 3 - ECL intensity (greyscale) vs. distance plots (n = 3) at five distinct positions across the surface of a 2 cm long by 1 cm wide planar BPE where the feeder electrodes are 3D-printed Ti_4Al_6V pin arrays located in the same plane as the BPE and centred. The small lower inset to the left shows a top-down view of the ECL generated at the BPE and the locations of the ECL profiles are colour coded to the graphs. Inset to right shows the average of the five experimental traces and the best fit single exponential decay.

Fig. 3 illustrates five ECL intensity line scans obtained for the planar BPE surface, but where pin arrays are used as feeders. The ECL intensities measured at the anodic edge are clustered tightly within a narrow range, 178 13 and cannot be experimentally distinguished. This close grouping indicates that the potential distribution in solution and hence across the BPE is highly uniform (*y*-direction) and that fringing very significantly extends the width of the ECL generating region, i.e., the feeder array is only 0.48 cm wide, but uniform ECL is generated across the entire 1.0 cm width of the BPE. The striking uniformity of the ECL arises because the lateral arrangement of the pins causes the electric fields from neighbouring pins to converge when moving away from the pin array surface and, at the relatively remote (5 mm from the feeder) bipolar electrode the potential distribution is homogeneous. This superposition effect gives rise to broader and more spatially uniform ECL. Significantly, while the actual electric field strength obtained experimentally using the planar and pin array feeders, 0.380 and 0.395 V cm^1, respectively, and the maximum ECL intensities at the anode tips are indistinguishable, the integrated ECL intensity, ϕ, is approximately double (32.0 ± 2.5 vs. 16.1 ± 3.6) when the feeder is a pin array. This larger total light emission using a pin array as feeders arises due to a larger ECL emission region, 0.125 to 0.175 cm, i.e., a 40% increase in emitting area. However, it is important to consider the role of iR drop between the feeder and bipolar electrodes. While the area of each individual pin is relatively small, radial spreading significantly increases the volume through which current can effectively flow through solution. Each pin's radial current path addresses a large volume of electrolyte, effectively lowering the total solution resistance relative to the planar feeder electrodes of equivalent projected geometric area. This reduced iR drop changes the ECL intensity vs. distance profiles with the pin array feeder showing making the spatial decay rate lower and giving a brighter emission.

This work demonstrates that changing the geometry of the feeder electrode is a powerful approach to controlling the location and intensity of BP-ECL. Planar feeders, which have the same width as the bipolar electrode induce the same potential across the full width of the BPE which is ideal for applications requiring consistent light output across large areas, e.g., ultrasensitive detection since the total light intensity is high because of the large area. In striking contrast, a single wire feeder produces a focused ECL hotspot directly opposite its tip, with secondary emissions at the BPE edges due to localised current flow and fringing electric fields giving a spatial pattern that can be exploited to localise analytical responses. The location and relative intensity of the three emitting areas can be controlled by changing the size and position of the feeder relative to the BPE, as well as the width and thickness of the BPE itself. Pin arrays, despite being narrower than the BPE, generate ECL across the entire BPE width by distributing the electric field radially, activating more of the BPE through 3D field spreading.

Miniaturised 3D feeders and BPEs can harness lightning-rod field amplification to overcome the higher potentials normally required when miniaturised bipolar electrodes are used. In conclusion, feeder design emerges as a powerful lever for creating low-power, addressable and wire-free means of redefining what is possible in bipolar electrochemical sensing, bioassays, and light-generating devices.

The financial support of Research Ireland (SFI) under Grant Number 21/FFP-P/10255 and the EU under MSCA Doctoral Network ECLectic (101119951) is gratefully acknowledged. This publication has emanated from research supported in part by a research grant from Research Ireland (SFI) under 21/RC/ 10294_P2 and co-funded under the European Regional Development Fund and by FutureNeuro industry partners. The authors wish to acknowledge the use of facilities at the Australian National Fabrication Facility (ANFF) – Materials Node at the University of Wollongong.

References

1 Y.-L. Wang, et al., ChemistryOpen, 2022, 11(12), e202200163.

2 O. F. Doyle and R. J. Forster, Electrochem. Commun., 2024, 169, 107832.

3 M. Wagner, et al., ChemElectroChem, 2025, 12(6), e202400506.

4 Y. Koizumi, et al., Nat. Commun., 2016, 7(1), 10404.

5 A´. Brady, et al., Chem. Commun., 2024, 60(89), 13000–13003.

6 R. Zou, et al., Chem. Commun., 2025, 61, 11896–11906.

7 E. Villani, Electrochemistry, 2024, 92(10), 101007.

8 L. Bouffier and N. Sojic , 2019, pp. 1–28.

9 R. M. Crooks, ChemElectroChem, 2016, 3(3), 357–359.

10 C. Mariani, et al., Electrochim. Acta, 2024, 489(10), 144256. 11 J. Wang, et Nat.Commun., 2021, 12(1), 6333.

Chapter 4 above demonstrated that strategic modification of feeder electrode architecture provides an effective route for manipulating field distributions and tailoring the electrochemical environment experienced by a planar bipolar electrode. While this represents a significant advance in field engineering, the bipolar electrode itself remains an equally important component capable of influencing both field behaviour and the resulting electrochemical response. Accordingly, the principles established through feeder electrode engineering provide a natural platform from which to investigate whether similar control can be achieved through rational design of the bipolar electrode itself.

To date, many bipolar electrochemical studies have focused on strictly 2D planar BPE geometries despite the growing recognition that three-dimensional architectures can provide substantial advantages e.g. enhanced surface area and field distributions, effective mass transport. Furthermore, advances in additive manufacturing and microfabrication technologies now offer unprecedented opportunities to fabricate complex higher order electrode structures with precisely defined geometries. These developments present an opportunity to extend the concept of field engineering beyond the external cell architecture and towards the wireless electrode itself, further advancing the core blueprint of the thesis with regards to exploiting geometry to direct electrochemical function.

Building upon the principles established in the previous chapters, this collection of work investigates the development and application of three-dimensional modular BPE architectures. By extending the concept of field engineering from feeder electrodes to the BPE itself, this work explores how geometry can be exploited to achieve enhanced spatial control of electrochemical activity. Collectively, this chapter represents the culmination of the demonstrating the progression from understanding electric field behaviour, to engineering electric field distributions, and ultimately to designing wireless electrochemical systems in which geometry and local fields act together to control electrochemical function

Chapter 5

Spatially Controlled Wireless Electrochemistry *via* 3D Bipolar Electrodes

Electrochimica Acta, Volume 576, 2026,149658. *doi.org/10.1016/j.electacta.2026.149658.*

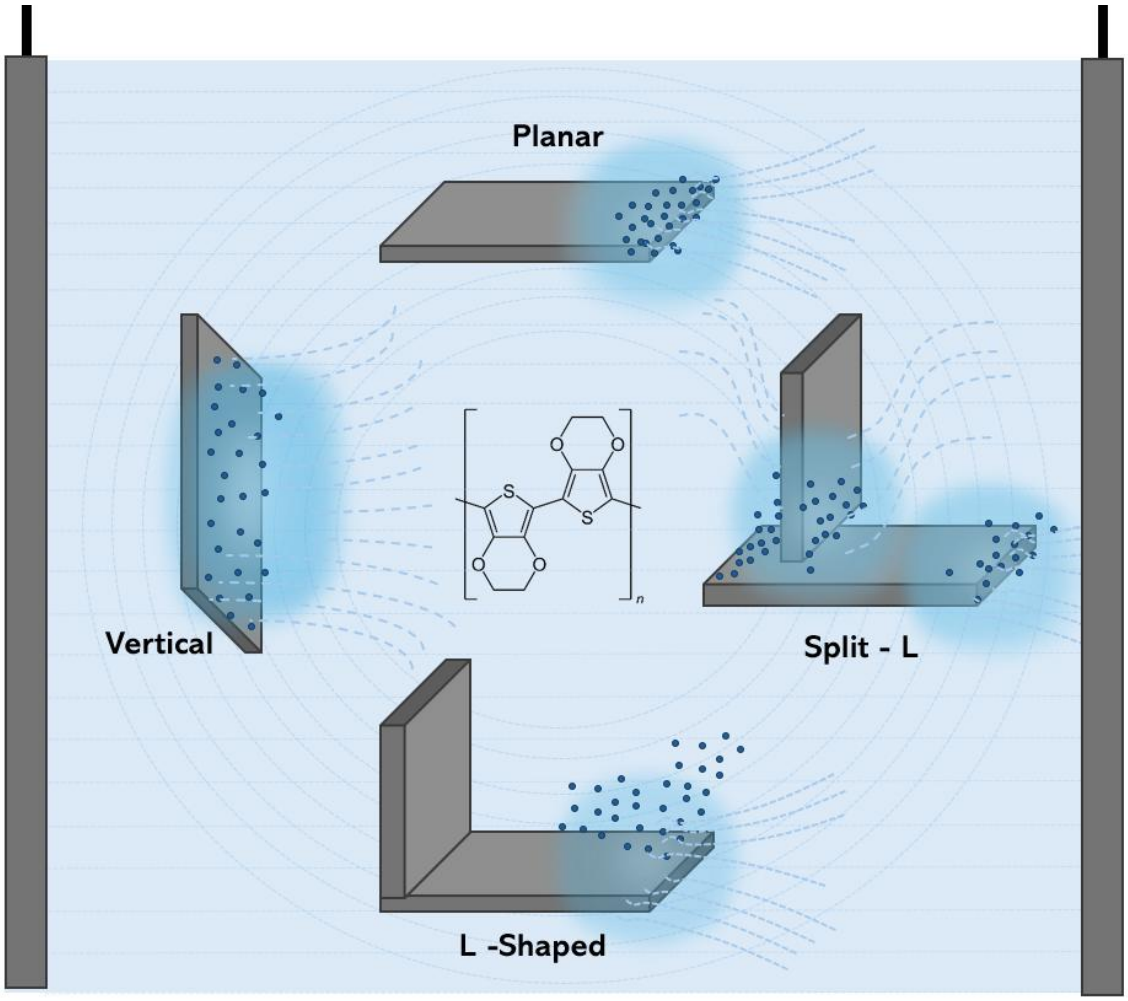
Spatially Controlled Wireless Electrochemistry *via* 3D Bipolar Electrodes

Oisín Foley Doyle [ab], Áine Brady [ab] and Robert J. Forster [ab]*

a. School of Chemical Sciences, Dublin City University, Dublin 9, Ireland

b. FutureNeuro, SFI Research Centre for Chronic and Rare Neurological Diseases, Dublin City University, Dublin 9, Ireland

Graphical Abstract



Abstract

The development of advanced electroactive materials for energy storage, electrocatalysis, and sensing is increasingly influenced by the need to spatially control redox activity and material growth. Programmable approaches to electrochemical materials synthesis that enable precise, localised control over structure and function remain a significant challenge. Here, we demonstrate that three-dimensional bipolar electrodes (3D BPEs) provide a versatile, wireless platform for regioselective electroactive materials synthesis by using electrode topology to reshape electric-field distributions. Using poly(3,4-ethylenedioxythiophene) (PEDOT) as a model system, spatially resolved electrodeposition across horizontal, vertical, split-L, and L-shaped BPE geometries reveals that 3D architectures generate highly localised and asymmetric polarisation that deviates strongly from classical one-dimensional field models. In electronically coupled split-L configurations, vertical elements act as field-amplifying "antennas", inducing cooperative dual-face and centre-focused polymerisation on adjacent horizontal electrodes. This topology-driven redistribution of redox activity enables spatially programmed conductive polymer growth without lithography or direct electrical addressing. These findings establish 3D BPE topology as a general design framework for field-directed electrochemical synthesis, enabling the programmable formation of electroactive material architectures. This approach offers new opportunities for engineering functional electrode materials with spatially controlled activity and structure.

1. Introduction

The development of advanced electroactive materials for applications in energy generation and storage,[1] electrocatalysis, bioelectronic interfaces[2,3,4] and sensors[5,6,7,8] increasingly depends on the ability to precisely control where and how redox-driven material growth occurs[9] and to create materials with unusual properties, e.g., through composition or structure. Spatially programmable electrochemical synthesis offers a powerful route to engineer functional architectures with localised activity, conductivity, and interfacial reactivity.[10,11] However, current approaches typically rely on multiple steps, complex templating strategies or lithography that limit scalability and design flexibility. Developing

wirefree electrochemical methods[12,13,14] to direct material formation with high spatial resolution is a key challenge in the field.[15,16,17,18]

Bipolar electrochemistry provides an attractive platform, relying on the polarisation of electrically floating conductors, or bipolar electrodes (BPEs), in an externally applied electric field generated by feeder electrodes.[19,20,21] This approach has enabled diverse applications, including the fabrication of nanotubes,[22] biocompatible conductive films,[23] wireless stimulation of biological systems, controlled drug release,[24] and ultrasensitive electrochemiluminescence-based detection[25,] Despite this progress, most studies have focused on planar horizontal BPE configurations, where redox activity is typically treated as a passive response to a linear imposed field.[26,27,28] As a result, the potential of bipolar electrochemistry as a tool for programmable materials synthesis remains underexploited.

Moving beyond horizontal BPEs[29,30] creates an opportunity to shift from passive conductors to treating BPEs as active design components in materials fabrication. Three-dimensional (3D) BPE architectures could be used to shape local electric-field distributions, enabling spatial control over polarisation and thus over the location, extent, and rate of electrochemical reactions. Such control could allow material properties to be encoded directly through electrode topology, providing a route to patterned conductive coatings, asymmetric catalytic interfaces, localised electrochemical actuation, and spatially addressable bioelectronic platforms.

Here, we demonstrate that the geometry, orientation, and electrical coupling of 3D BPEs can be systematically engineered to direct the spatial distribution of redox activity and thereby control electrochemical materials synthesis. Using modular 3D electrode architectures, including horizontal, vertical, split-L, and L-shaped configurations, we show that deviations from classical one-dimensional field distributions[31] lead to highly localised and asymmetric polarisation. In particular, vertically oriented elements act as field-amplifying “antennas”, enabling cooperative and spatially focused electrochemical activity in electronically coupled systems.

To visualise and quantify these effects, we employ wireless electropolymerisation of poly(3,4-ethylenedioxythiophene) (PEDOT) as a model electroactive material, where deposition

patterns directly map regions of sufficient local potential to drive polymer growth. PEDOT is especially relevant because its conductivity, biocompatibility, electrochemical stability, and mixed ionic–electronic transport make it widely used in electrodes for energy storage, sensing, actuation, and bioelectronics.[32] By systematically varying electrode geometry, orientation, and confinement within the electrochemical cell, we reveal how 3D BPE topology can be used to program electric-field distributions and, consequently, material formation. These findings establish a general framework for topology-directed electrochemical synthesis, providing a scalable and wiring-free strategy for constructing electroactive materials with spatially controlled structure and function.

2. Experimental

2.1 Materials

Bipolar Electrode: 304S15 Stainless Steel, Radionics Ltd. Feeder Electrodes: Titanium (99.6% purity, Goodfellow Metals UK), Supporting Solution: 3,4-Ethylenedioxythiophene, 97% purity, Merck. EDOT solutions were prepared using deionised water (resistivity of 18.2 MΩ cm^{-1}) in the absence of deliberately added electrolyte.

2.2 Bipolar Setup

The bipolar electrochemical cell was designed in-house using FreeCAD and printed using Acrylonitrile Butadiene Styrene (ABS) Ultimaker filament with an Ultimaker S5 3D printer. The layer height and skin thickness were 0.15 mm with an infill density of 20%, and printed at 230 °C. In all cases, the titanium feeder electrodes, L:2 cm × W:1 cm × D:2 mm, sit vertically, 3 cm apart within two slots and in contact with solution.

304S15 Stainless Steel (SS) was used for the BPEs. For a horizontal orientation the 2cm × 1cm × 0.1cm (L x W x D) BPE, (Figure 1), sits centrally between the two feeder electrodes within a slot to ensure reproducible alignment. For the vertical configurations (Figure 2), the BPEs were mounted using an insulated support that rested against the cell wall without contacting the solution. Two wells on either side of the inset BPE allow for easy removal using tweezers without damaging the polymer film. The internal width of the printed cell is 1.7 cm which

leaves 3.5 mm between the BPE edge and the adjacent cell wall. An EA PS 2384-03 B power supply was used to apply the required voltage to the feeder electrodes.

2.3 BPE & Feeder Anode Pre-Treatment

Mechanical polishing of both the titanium feeder electrode and stainless steel BPE surfaces was performed using a 400-grit (35 μm) sandpaper. Then, both BPE and feeder electrodes were electropolished in 0.1 M KCl using an Autolab (Metrohm) potentiostat, Ag/AgCl reference electrode and coiled platinum wire (≈ 3.6 cm^2) counter electrode with an applied potential window of +0.4 to +1.0 V, at 100 mV/s for 30 cycles. Finally, the electrodes were sonicated in alcohol and dried using a nitrogen stream before use.

2.4 Wireless Electropolymerisation of 3,4 -Ethylenedioxythiophene, EDOT.

The bipolar cell contained 3 mL of 10 mM 3,4-ethylenedioxythiophene dissolved in Milli-Q water, with a prepared BPE and titanium feeder electrodes. A constant 30 V potential difference was applied across the feeders for a fixed polymerisation period of 20 min. Consistent with conventional electrodeposition in a 3-electrode cell, the rate of PEDOT deposition increases with increasing feeder voltage. The film capacitance increases with polymerisation time before the rate decreases markedly after approximately 20 min, reflecting the maximum film thickness that can be deposited under these conditions.[16]

2.5 Electrochemical Characterisation

Cyclic voltammetry (CV) was performed using an Autolab (Metrohm) potentiostat in a conventional three-electrode configuration. For controls using conventional 3-electrode cells, the stainless-steel working electrode (2 x 1 cm) was masked with Teflon tape to define a geometric surface area of 2 cm^2 (1cm^2 per side). A coiled platinum wire (≈ 3.6 cm^2) and an Ag/AgCl (saturated KCl) served as the counter and reference electrode, respectively. CVs were recorded in aqueous 0.1 M $LiClO_4$ electrolyte within an applied potential window of -0.1 to +0.5 V at scan rates ranging from 5 to 100 mVs^{-1}. CVs were also recorded for both unmodified BPEs and following wireless deposition of PEDOT. Specific capacitance values were obtained

by numerically integrating the current potential curves. The capacitance associated with the PEDOT-coated electrode was corrected for the contribution of the unmodified BPE (less than 10%). All measurements were performed in triplicate (n =3). Capacitance values are reproducible to within 10%.

2.6 Surface Characterisation

2.6.1 SEM Analysis

A Jeol JSM-IT 100 InTouchScope electron microscope was used to image electrodes and PEDOT films using an accelerating voltage of 5.0 kV and a secondary electron detector.

2.6.2 ImageJ Analysis

Image analysis performed using ImageJ software. Greyscale intensity profiles were used to identify the onset of PEDOT deposition. Three-dimensional reconstructions were generated from the greyscale data using the ImageJ surface plot function to visualise variations in film topography.

3. Results & Discussion

3.1. Horizontal Bipolar Electrode

The onset potential for PEDOT electrodeposition has been determined from conventional three-electrode measurements to be +0.85 V vs Ag/AgCl. As polymer growth occurs only where the local interfacial potential exceeds the oxidation threshold, the spatial position of the deposit indicates where the BPE-solution potential difference exceeds + 0.85 V.

For the horizontal BPE with a pair of feeders, PEDOT deposition starts 0.54 cm from the centre, where the potential is 0 V. This gives a voltage gradient of 1.6 V cm^{-1} (0.85 V / 0.54 cm), which is significantly lower than the 10 V cm^{-1} (30 V / 3 cm) calculated for an ideal, loss-free field. Ohmic drop through the solution will decrease the voltage gradient, but based on the solution conductivity and current passed, the iR drop[33] is expected to decrease the voltage gradient by

only 15-20 % from the maximum value of 10 V cm^{-1}, not the 80-85% decrease determined from the position of the PEDOT deposition.

For a horizontal BPE placed perpendicular between a pair of feeder electrodes, the voltage gradient is expected to be approximately linear along its length.[19] As illustrated in Figure 1(a), this results in a progressively thicker polymer film toward the anodic pole. Significantly, the voltage gradient, 1.6 V cm^{-1} leads to a voltage of approximately 1.6 V at the anodic end of the BPE. Overoxidation of PEDOT occurs around +1.3 V,[34] which will inhibit electrodeposition close to the anodic tip.

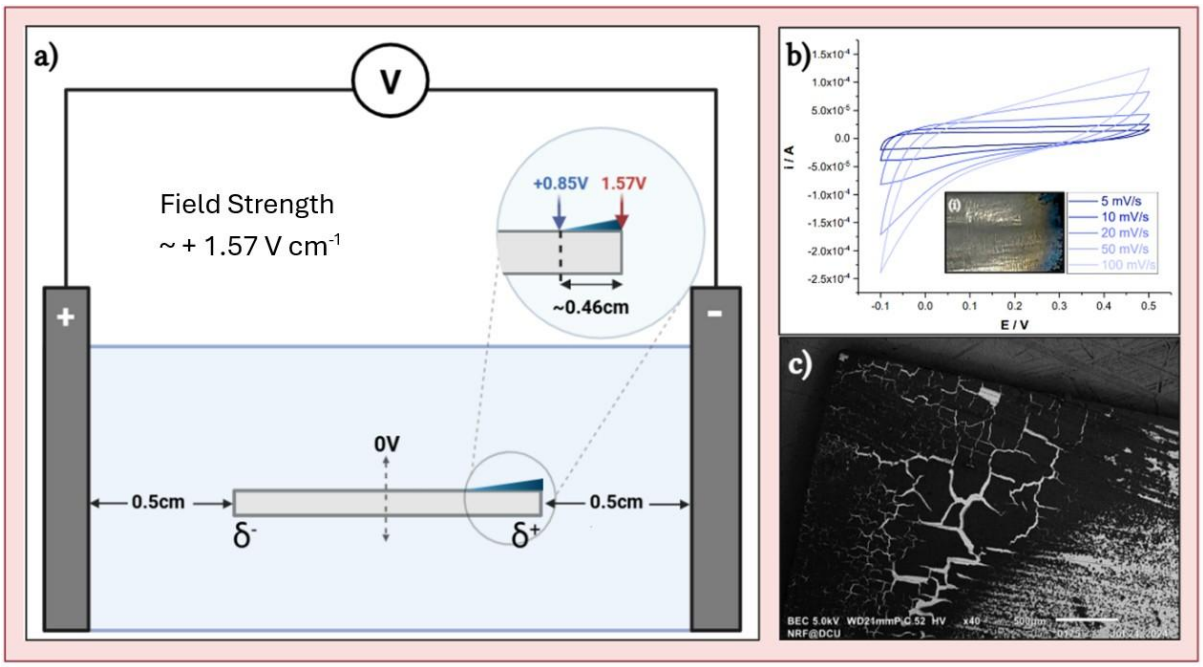


Figure 1. (a) Schematic of the BP polymerisation set-up using 10 mM EDOT in DI water. The bipolar electrode is a 2 cm x 1 cm x 0.1 cm stainless steel (SS) flag. The two vertically oriented feeder electrodes were 2 cm x 1 cm titanium plates. PEDOT film progressed ~ 0.46 cm from the anodic terminal, resulting in an estimated voltage top of 1.57 V (b) Scan rate study of a 1cm x 1 cm section of the SS BPE in 0.1 M $LiClO_4$. (i) Inset: Photo of the PEDOT film deposited on the positive terminal of the SS BPE. (c) SEM image of the positive terminal of the BPE depicting the PEDOT film.

PEDOT gains its electrical conductivity through p-type doping, which involves the removal of a π-electron upon oxidation to form polarons and, at higher doping levels, bipolarons.[35,36] This doping process not only enables electrical conductivity but also leads to a substantial capacitance due to charge-compensating counter-ions within the three-dimensional structure.

To quantify the amount of PEDOT wirelessly deposited under different BPE configurations (horizontal, vertical, split-L, and L-shape), scan-rate studies were performed in 0.1 M $LiClO_4$ using the polymer-modified BPEs as working electrodes. Figure 1(b) shows the characteristic box-like cyclic voltammograms observed within the non-faradaic potential window.[37] The capacitance of the horizontal PEDOT modified electrode is $4.00\pm 0.14\times10^{-4}$ F cm^{-2}. The volumetric capacitance is 80-100 F cm^{-3}, while the molar volume ranges from 90-100 cm^3 mol^{-1} depending on the density (polymer chain packing).[3839] These values give a surface coverage of $4x10^{-8}$ mol cm^{-2}. Three-electrode experiments show that the kinetics of PEDOT depend non-linearly on the applied potential, increasing ≈ 25-fold between + 0.85 V and + 0.90 V, but only ≈ 2-fold between 1.2 and 1.3 V before decreasing for more positive potentials, where the film over oxidizes and loses conductivity.[40] Thus, film deposition starts at 0.54 cm, and is thickest at 0.85 cm, with an average film thickness of approximately 2 μm. This value is consistent with that expected from conventional 3-electrode experiments. Taken together, these observations suggest that PEDOT deposition is governed by the local electrode potential, with the underlying mechanism and rate-determining step remaining consistent between both conventional three-electrode and bipolar configurations. In this context, the applied electric field functions primarily to establish the potential distribution along the BPE, rather than directly influencing the deposition kinetics, e.g., through electrophoretic transport.[41,42]

Figure 1(c) shows stress-induced cracking in the dried films.[43] As expected, the film thickness decreases toward the centre of the BPE, where the potential approaches 0 V, reflecting the dependence of polymer growth on the BPE-solution potential difference.

3.2. Vertical Bipolar Electrode

Changing the orientation of the bipolar electrode could represent a convenient way to change the electric field distribution. For example, rotating the bipolar electrode from the horizontal to the vertical orientation reduces the effective electrode dimension along the electric-field axis to its effective thickness, 0.1 cm. Therefore, in a 1D linear decay model, this would dramatically diminish the induced polarisation of the BPE and could make local edge-fringing effects much more important than pole-to-pole effects. Figure 2 shows the result for electrodeposition using a vertical BPE. Significantly, relatively uniform PEDOT deposits exclusively on the BPE surface facing the negative feeder electrode. Based on the potential gradient of ~1.6 V cm^{-1}, the expected voltage on the anodic face is only ~ 0.16 V, which is insufficient to drive PEDOT electrodeposition.

It is conceivable that radicals generated elsewhere, e.g., at the feeder electrodes, could play a role in the asymmetric (one-sided) PEDOT deposition. However, the lifetime of the radical cation, τ, is ≈100 μs, meaning that the distance the radicals could travel by diffusion/migration is approximately three orders of magnitude smaller than the feeder-to-BPE separation. These constraints exclude feeder-derived EDOT cation radical generation as a possible origin of PEDOT deposition on the BPE, and PEDOT formation must be initiated locally at the anodic pole of the BPE, driven by the induced bipolar overpotential.

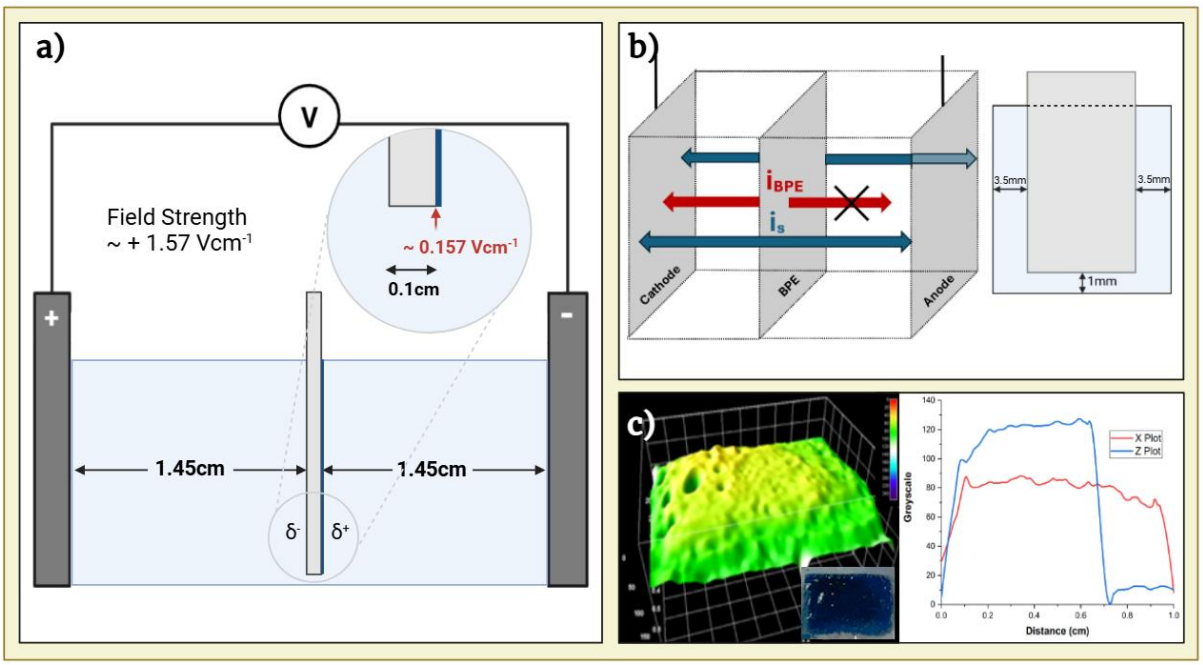


Figure 2. (a) Schematic of the electropolymerisation of EDOT on the centrally located, vertical stainless steel BPE (2 cm x 1 cm x 0.1 cm) configuration in a 10 mM EDOT milli-Q water solution. **b)** Schematic showing the BPE cathode and anode alignment, with ionic current (i_s, blue arrows) flowing through the electrolyte. **(c)** 3D PEDOT surface topography map (left) with a height-based colour scale from low (white) to high (yellow). Surface topography line scan profile of the PEDOT on vertical BPE along the x-axis (red) and z-axis (blue), deposition occurred at 30V for 20min.

Although the solution remains continuous, the vertical BPE occupies most of the cell width, leaving only a narrow pathway for ion transport. The constriction increases the local current density and corresponding ohmic potential drop in the solution, thereby steepening the local potential gradient. Although not a true closed-bipolar configuration, this geometry can be considered a functional analogue because ionic transport between the regions near the positive and negative feeder electrodes is severely restricted. This constriction increases the local solution resistance ($R \propto L/A$) and concentrates a disproportionate fraction of the ohmic potential drop into the slit region, thereby enhancing the local solution voltage gradient relative to the nominal field. Thus, relative to an open-cell configuration with a horizontally oriented BPE, the restricted ionic conduction pathway in the vertical geometry is expected to increase the local potential gradient in the solution adjacent to the BPE. This effect may be expressed as $E_{Local} = \beta E_{Horizontal}$, where $E_{Horizontal}$ is the nominal macroscopic field (horizontal BPE), and $\beta > 1$ is a geometry-dependent enhancement factor that accounts for current constriction arising from restricted ion transport. The corresponding induced polarisation across the BPE is then $\Delta V_{BPE} = E_{Local} L_{eff}$, where L_{eff} is the effective electrode dimension. For a nominal field of 1.6 V cm^{-1}, the enhancement factor required to generate an induced polarisation of + 0.85 V is therefore at least 5.4.

It is perhaps important to note that ion transport by migration is the dominant mechanism for exchange between the two “compartments”. Given a mobility of ≈ 6×10^{-8} m^2 V^{-1} s^{-1}, it would take more than an hour for the migration distance to approach the length of the cell. Thus, on the timescale of electrodeposition used here (20 min), electroneutrality is expected to be

maintained throughout most of the bulk electrolyte, with appreciable ion depletion and enrichment restricted mainly to interfacial transport layers near the electrodes.

For this PEDOT modified vertically oriented BPE, the capacitance is 6.0± 1.8x10^{-5} F cm^{-2}, corresponding to a layer thickness of approximately 600 nm. This result indicates that the bipolar electropolymerisation process yields a thin PEDOT film, most likely reflecting a modest overpotential for deposition, i.e., β is close to 5.4. An interesting observation is the pronounced difference in the quantity of PEDOT deposited on the anodic feeder electrode as a function of BPE orientation. For the horizontal BPE, the capacitance of the feeder electrode is 1.67×10^{-4} F cm^{-2}, whereas the vertical configuration it increases to 1.03×10^{-3} F cm^{-2}. This approximately 10-fold difference in deposition suggests that the vertical geometries appear to cause a redistribution of the electric field, increasing the contribution at the feeder electrode while reducing localisation at the bipolar interface. Taken together, these initial observations suggest that BPE orientation strongly influences the spatial partitioning of electrochemical activity.

3.3. Split-L Bipolar Electrode

L-shaped BPEs move bipolar electrochemistry from a single-axis problem into a 3D architecture, and when the upright and horizontal segments are electrically connected, new cooperative polarisation pathways could occur. In contrast, when electrically disconnected, effects associated with vertical and horizontal components can be combined in a single system. Split L-shaped BPEs are of particular interest because they give unique insight into how electrode architecture governs bipolar behaviour, specifically whether non-linear, segmented geometries can reshape local field distributions and ionic conduction pathways sufficiently to alter the spatial separation, symmetry, and efficiency of redox reactions. Here, the split-L configuration consisted of two stainless steel BPEs (2.0 x 1.0 x 0.1 cm). As shown in Figure 3a, a horizontal BPE was centred between feeder electrodes (0.5 cm between BPE tips and the feeders), while a vertical BPE was positioned 1 mm above it at the anode tip (2.5 cm from the negative feeder).

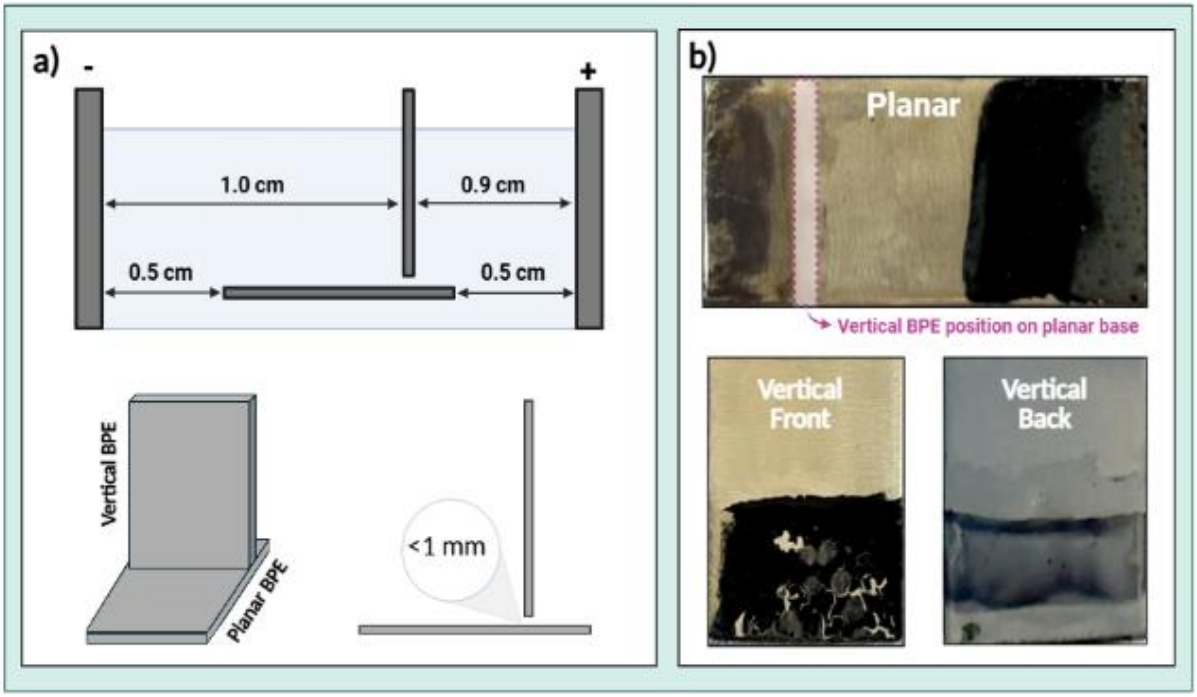


Figure 3 (a) Schematic of the Split-L BPE polymerisation set-up. It comprises two stainless steel BPEs (2.0 cm x 1.0 cm x 0.1 cm). The vertical BPE was positioned approximately 1 mm above the underlying horizontal BPE surface. **(b)** Images of the horizontal BPE surface (Top View) and front/back of the vertical BPE post bipolar electropolymerisation.

Significantly, as shown in Figure 3(a), under identical conditions, this pair of BPEs produces a very different deposition pattern compared to that observed for the two components alone. In contrast to the single-sided PEDOT deposition at a single upright BPE (Figure 2), PEDOT was deposited on both sides of the vertical BPE when the horizontal BPE was present. Moreover, deposition on the horizontal BPE was heavily influenced by the presence of the vertical BPE, with PEDOT being deposited at both the positive and negative ends. Also, the film deposited at the **anodic pole shows an inverted thickness gradient**, with maximum film towards the centre of the BPE rather than towards the tip as was observed for the horizontal BPE alone.

This result is significant in that it represents direct evidence that the two BPEs influence and shape the electric field distribution in solution, making the two BPEs electrochemically coupled so that each electrode actively reshapes the profile of the BPE-solution potential difference of the other. The split-L pair does ***not*** behave as the sum of two independent BPEs. In contrast, it exhibits *cooperative field coupling* that generates a new deposition profile. For

a single floating conductor, oxidation cannot occur over the entire area of both faces because the electrode is equipotential overall, and anodic and cathodic faradaic currents must be balanced. The observation of PEDOT deposition on *both* faces indicates that the spatial distribution of the interfacial driving force is no longer one-dimensional or uniform. It appears that the horizontal BPE distorts the surrounding solution potential so strongly that the vertical BPE no longer behaves like a simple two-sided plate polarised across its thickness. Instead, different parts of each face experience different local solution potentials, so that anodically biased regions can develop on both faces simultaneously, even though the conductor overall still maintains charge balance. It is perhaps important to note that the EDOT oxidation and water reduction are likely to be the dominant oxidation and reduction processes. Given the very much lower concentration of EDOT, it is not unreasonable to have water reduction occur at a relatively small fraction of the total area of the vertical BPE to maintain the current balance. Equally, the vertical BPE distorts the local solution-potential distribution experienced by the *horizontal* BPE, disrupting the end-dominated bipolar response characteristic of an isolated horizontal element and creating new regions of anodic and cathodic activity. The vertical BPE effectively partitions the local potential distribution along the horizontal BPE, making it into two spatially distinct anodic/cathodic pole pairs. This is evidenced by the emergence of a second anodic PEDOT-growth region adjacent to the vertical BPE, in addition to the primary anodic tip, indicating that field redistribution by the upright element creates a distinct new pattern of bipolar reactivity within one continuous electrode.

Once PEDOT nucleates, a further positive-feedback mechanism likely amplifies this behaviour, with the growing polymer changing the local interfacial resistance and accelerating deposition at those sites. Thus, multi-BPE architectures lead to electric field distributions that are emergent rather than additive, and demonstrate a powerful design principle for bipolar electrochemistry, i.e., electrode geometry and proximity can be used to create polarisation hotspots and achieve regioselective redox reactions in a way that is not possible in simpler systems.

The capacitance per unit deposited area provides quantitative evidence of cooperative polarisation between the horizontal and vertical BPEs. For isolated electrodes (Figures 1 & 2), the horizontal BPE exhibits a capacitance of 8.7×10^{-4} F cm^{-2}, while the vertical BPE shows only 6×10^{-5} F cm^{-2}. In contrast, in the split-L configuration, the horizontal segment shows a reduced

capacitance per deposited area of 3.8×10^{-4} F cm^{-2} (deposition area ≈ 0.84 cm^2), or approximately 44% of the isolated horizontal value. This marked decrease indicates that the split-L architecture notably redistributes PEDOT formation. Simultaneously, the vertical segment has a higher capacitance, increasing to 1.7×10^{-4} F cm^{-2} (deposition area of ~ 1.2 cm^2), compared to its isolated vertical counterpart. These results support the conclusion that adjacent BPEs couple through the solution, redistributing the local solution-potential field and thereby reshaping the spatial pattern of bipolar faradaic activity. Consequently, the response is no longer localised to a single dominant electrode region but extends across a broader interfacial area due to a greater potential difference between the BPE and solution.

3.4 Connected L-Bipolar Electrode

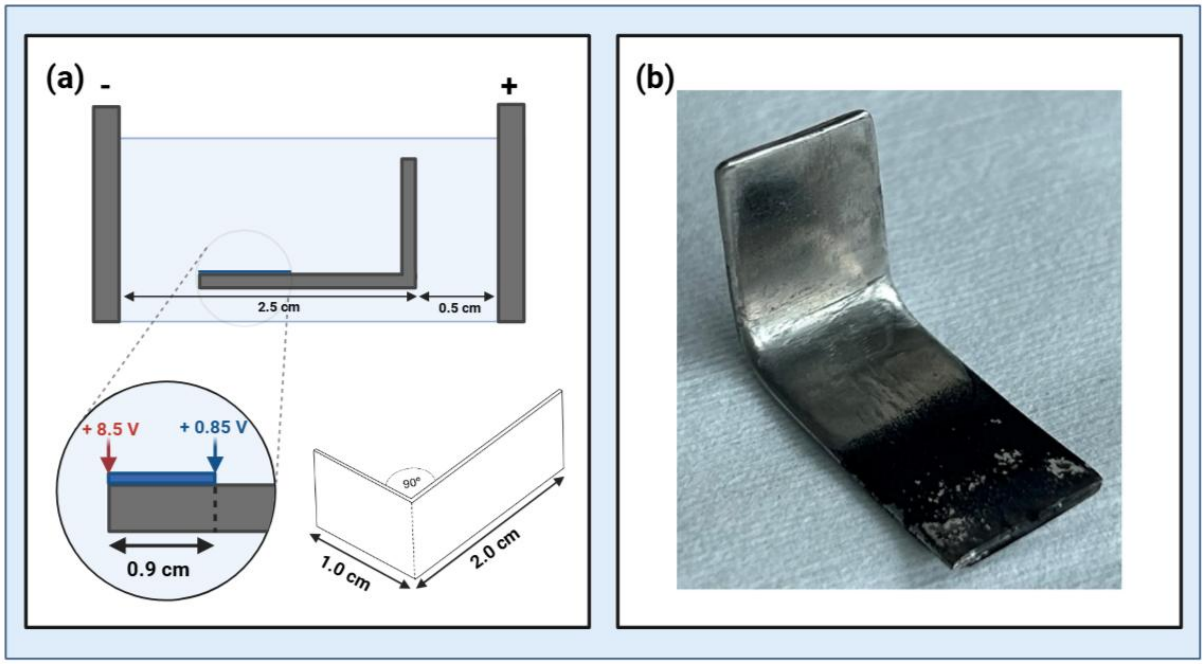


Figure 4 (a) Schematic illustration of L-Shaped bipolar electrode consisting of a 2cm x 1cm horizontal base and 1cm x 1cm vertical flag bent at 90°. PEDOT deposition occurs exclusively on the horizontal base and progressed approx. 0.9 cm from the anodic terminal. **(b)** Image of the PEDOT distribution.

Figure 4 above shows a single-piece L-shaped BPE that includes a 2.0 x 1.0 x 0.1 cm horizontal base with a 1.0 x 1.0 x 0.1 cm vertical flag. This architecture reflects vertical and horizontal BPEs that are *electrically connected* into a single L-shaped BPE. Here, PEDOT formed exclusively on the horizontal base, extending ~ 0.9 cm from the anodic tip with relatively uniform thickness (600 nm). In contrast to experiments with the vertical BPE alone or with an electrically disconnected horizontal BPE present, no PEDOT deposition was observed on the upright portion of the BPE.

The absence of PEDOT on the upright arm indicates that, in the single L-shaped conductor, the solution-potential gradient is preferentially focused along the horizontal base, effectively suppressing bipolar activation of the vertical segment, i.e., at no point along the vertical component does the solution-BPE potential difference become sufficiently positive to oxidise EDOT. This highlights how electrical continuity alone is insufficient to guarantee activity across all parts of a 3D BPE architecture; the decisive factor is how electrode geometry shapes the local BPE-solution potential difference.

Compared with isolated 2 cm horizontal BPEs, which produced PEDOT over only ~ 0.46 cm from the anodic tip, the continuous L-shaped BPE supports a much longer deposition zone (~ 0.9 cm) along its horizontal segment. This indicates that the electronically connected vertical arm changes the local solution-potential difference profile so that EDOT oxidation is sustained over a larger fraction of the horizontal electrode. This contrasts with the split-L configuration, where the small gap creates two adjacent floating conductors rather than one continuous electrode, enabling more localised field partitioning and a segmented deposition profile on the horizontal element. The intact L-shape, therefore, appears to promote a broadened, anodic growth region. When normalised to the actual area of PEDOT deposition, the isolated horizontal BPE exhibits a capacitance of 8.7×10^{-4} F cm^{-2} (4.0×10^{-4} F cm^{-2} over 0.46 cm^2), whereas the horizontal segment of the L-shaped BPE shows a capacitance of 4.8×10^{-4} F cm^{-2} (4.32×10^{-4} F cm^{-2} over 0.9 cm^2). This lower surface coverage further indicates that the vertical flag does not significantly increase the potential difference between the BPE and the solution, i.e., the maximum driving force achieved is lower for the L-shaped BPE, but the threshold value is achieved over a greater area.

Conclusion

This study demonstrates that the behaviour of floating BPEs can be controlled through their three-dimensional geometry and spatial proximity to localise and maximise the interfacial potential difference in ways that are not possible simply by changing the overall electric field strength using 2D BPEs. Across four configurations, i.e., isolated horizontal, isolated vertical, electrically disconnected split-L and electrically continuous L-shaped BPEs, we demonstrate that the BPEs themselves can be used to control local BPE-solution potential differences, to direct ionic currents and exploit local ohmic drop to drive redox reactions in areas of the electrode that were previously inaccessible using a wire-free electrochemistry approach.

In contrast to isolated horizontal BPEs oriented perpendicularly to the feeders, vertical BPEs that are relatively close to the side walls of the bipolar cell display striking and unexpected one-sided PEDOT deposition despite the effective BPE length being only one millimetre. This demonstrates that controlling the orientation and ohmic drop through the relative sizes of the cell and BPE can significantly amplify and localise the induced potential beyond predictions from the linear 1D model. Split-L configurations demonstrate a distinct cooperative behaviour between the two electrically disconnected bipolar electrodes, where the vertical and horizontal components interact to produce striking polymerisation on ***both*** faces of the vertical electrode. For the single electronic conductor, L-shaped 3D BPE, PEDOT deposits only on the horizontal portion, but the presence of the vertical aspect approximately doubles the area over which PEDOT is formed.

Collectively, these observations establish that geometric modifications, orientation, topology and proximity of multiple BPEs can be used to control the location and topography of redox reactions in a way that is impossible using single BPEs or indeed, conventional three-electrode cells. These findings provide a framework for spatially programmed wireless electrosynthesis, the design of three-dimensional microdevices with shape-dependent functionality and advanced electrochemical architectures where multiple, 3D BPEs are exploited to localise redox reactions. It also suggests new strategies for designing distributed electrochemical sensors and devices such as self-patterning sensor arrays, anisotropic catalytic surfaces, and shape-programmed actuators.

Acknowledgements

This publication has emanated from research supported in part by a research grant from Taighde Éireann under the Frontiers for the Future programme Grant Number 21/FFP-P/10255 and 21/RC/10294_P2 co-funded under the European Regional Development Fund and by FutureNeuro industry partners. The European Union under the MSCA Doctoral network Horizon Europe programme Grant Agreement Number 101119951 (ECLectic) is gratefully .

The authors gratefully acknowledge the Nano Research Facility (NRF) at Dublin City University for the provision of facilities and technical assistance.

References

1. A PEDOT-reinforced exfoliated graphite composite as a Pt- and TCO-free flexible counter electrode for polymer electrolyte dye-sensitized solar cells, S. Nagarajan, P. Sudhagar, V. Raman, Woohyung Cho, K. S. Dhathathreyan and Yong Soo Kang J. Mater. Chem. A, 2013,1, 1048-1054 DOI https://doi.org/10.1039/C2TA00091A

2. Enhanced wireless cell stimulation using soft and improved bipolar electroactive conducting polymer templates, C Qin, Z Yue, XF Huang, RJ Forster, GG Wallace, J Chen, Applied Materials Today 2023, 27, 101481

3. C. Qin, Z. Yue, Y. Chao, R.J. Forster, F.Ó. Maolmhuaidh, X.-F. Huang, S. Beirne, G.G. Wallace, J. Chen, Bipolar electroactive conducting polymers for wireless cell stimulation, Applied Materials Today 21 (2020) 100804. https://doi.org/10.1016/j.apmt.2020.100804.
4. PEDOT: PSS conducting eutectogel for enhanced electrical recording and stimulation in implantable neural interfaces. Authors Martin Kasavetov, Ruben Ruiz-Mateos Serrano, Antonio Dominguez-Alfaro, Chaeyeon Lee, Matias L Picchio, David Mecerreyes, George G Malliaras, Viviana Rincón Montes, Amparo Güemes Journal of Materials Chemistry C 2026, 14 (2), 616-629

5. A PEDOT/3D-N-Ti3C2Tx nanoflower hydrophilic regulation molecular imprinting electrochemical sensor for ultrasensitive detection of levofloxacin. Zhigang Wang, Guoliang Zhang, Ruxangul Jamal, Tursun Abdiryim, Feng Xu, Yanqiang Zhou, Kai Song, Lirong Ma, Jing Tan, Luyao Wana and Yiwu Zhu, J. Mater. Chem. A, 2025,13, 31371-31384

6. Cardiac troponin I: ultrasensitive detection using faradaic electrochemical impedance E Spain, S Carrara, K Adamson, H Ma, R O'Kennedy, L De Cola, ...Acs Omega 2018, 3 (12), 17116-17124

7. Advances in biosensors for diagnosis of Alzheimer's and Parkinson's diseases M Negahdary, I Sakthinathan, E Mirsadoughi, FS Ligler, GL Coté, ...Biosensors and Bioelectronics 284, 117535

8. R. K. Perdue, D. R. Laws, D. Hlushkou, U. Tallarek and R. M. Crooks, "Bipolar Electrode Focusing: The Effect of Current and Electric Field on Concentration Enrichment," Anal. Chem., 2009, 81, 10149–10155.

9. M. Wagner, Á. Brady, O.F. Doyle, R.J. Forster, Advancing Bipolar Electrochemistry for Targeted Deposition of Biocompatible Polymers in Electrolyte-Free Solutions via Finite Element Modeling, ChemElectroChem 12 (2025) e202400506. https://doi.org/10.1002/celc.202400506.
10. G. Loget, D. Zigah, L. Bouffier, N. Sojic and A. Kuhn, Bipolar electrochemistry: from materials science to motion and beyond, Accounts of Chemical Research, 2013, 46, 2513–2523.

11. Bipolar Electrochemistry: A Powerful Tool for Electrifying Functional Material SynthesisNaoki ShidaYaqian ZhouShinsuke Inagi* Acc. Chem. Res. 2019, 52, 9, 2598–2608

12. Wirefree electroceuticals: 3D electrical and electrochemical stimulation of biological systems RJ Forster, Current Opinion in Electrochemistry, 2023, 39, 101297

13. Wirefree Electrochemistry for Enhanced Detection and Treatment of Disease OF Doyle, RJ Forster, Electrochemistry Communications 2024, 169, 107832

14. F. A. Bravo-Plascencia, M. P. Flores-Morales, A. Kuhn, G. Salinas, and B. A. Frontana-Uribe, Fundamental concepts of 3,4-alkoxythiophene-based polymeric systems, from synthesis to applications, Journal of Materials Chemistry A, 2025, 13, 27772–27793.

15. Directing the glow: 3D feeder geometries to enhance planar bipolar electrochemiluminescence, OF Doyle, GG Wallace, Z Yue, J Chen, S Beirne, RJ Forster, Chemical Communications 2025, 61 (97), 19221-19224

16. Electric Field Distribution in Bipolar Electrochemical Cells: Effects on the Wirefree Electrodeposition of Conducting Polymer Films, Á Brady, RJ Forster, Analytical Chemistry 2024, 97 (1), 410-418

17. Regio selective deposition of conducting polymers using wireless electropolymerisation Á Brady, M Wagner, RJ Forster, Chemical Communications, 2024, 60 (89), 13000-13003

18. Wireless electrochemiluminescence at functionalised gold microparticles using 3D titanium electrode arrays SF Douman, D Collins, LR Cumba, S Beirne, GG Wallace, Z Yue, E. I Iwuoha, F. Melinato, Y. Pellegrin, R. J. Forster, Chemical Communications 2021, 57 (38), 4642-4645

19. S.E. Fosdick, K.N. Knust, K. Scida, R.M. Crooks, Bipolar electrochemistry, Angew Chem Int Ed Engl 52 (2013) 10438–10456. https://doi.org/10.1002/anie.201300947.

20. Principles of Bipolar Electrochemistry - Crooks - 2016 - ChemElectroChem - Wiley OnlineLibrary,(n.d.).https://chemistryeurope.onlinelibrary.wiley.com/doi/10.1002/celc.201500549 (accessed April 8, 2026).

21. Experimental Methods for Measuring Potential and Current Density Distributions at Bipolar Electrodes Elena Villani*Shinsuke Inagi, *Anal. Chem.* 2025, 97, 11, 5837–5846

22. G. Loget, S. So, R. Hahn and P. Schmuki, Bipolar anodization enables the fabrication of controlled arrays of TiO_2 nanotube gradients, Journal of Materials Chemistry A, 2014, 2, 17740–17745.

23. 3D Printing of Conducting Polymer Hydrogels for Electrostimulation-Assisted Tissue Engineering, CM Tran, Z Yue, C Qin, KBC Imani, M Dottori, RJ Forster, GG Wallace Advanced Materials 37 (36), 2025, 2507779

24. On demand, wireless electrochemical release of brain derived neurotrophic factor C Qin, Z Yue, RJ Forster, J Chen, GG Wallace Electrochemistry Communications, 2023, 157, 107626

25. Shaping and exploring the micro- and nanoworld using bipolar electrochemistry | Analytical and Bioanalytical Chemistry | Springer Nature Link, (n.d.). https://link.springer.com/article/10.1007/s00216-011-4862-1 (accessed April 21, 2026).

26. M. Li, S. Liu, Y. Jiang, W. Wang, Visualizing the Zero-Potential Line of Bipolar Electrodes with Arbitrary Geometry, Anal. Chem. 90 (2018) 6390–6396. https://doi.org/10.1021/acs.analchem.7b04881.
27. L. Koefoed, S. U. Pedersen and K. Daasbjerg, “Bipolar electrochemistry—A wireless approach for electrode reactions,” Curr. Opin. Electrochem., 2017, 2, 13–17.

28. L. R. Arias-Aranda, G. Salinas, A. Kuhn, G. Xu, F. Kanoufi, L. Bouffier and N. Sojic, Complex electrochemiluminescence patterns shaped by hydrodynamics at a rotating bipolar electrode, Chemical Science, 2024, 15, 8723–8730.

29. Ismail, S. Voci, P. Pham, L. Leroy, A. Maziz, L. Descamps, A. Kuhn, P. Mailley, T. Livache, A. Buhot, T. Leïchlé, A. Bouchet-Spinelli and N. Sojic, Enhanced bipolar electrochemistry at solid-state micropores: demonstration by wireless electrochemiluminescence imaging, Analytical Chemistry, 2019, 91, 8900–8907.

30. Mapping the Distribution of Potential Gradient in Bipolar Electrochemical Systems through Luminol Electrochemiluminescence Elena VillaniShinsuke Inagi, Anal. Chem. 2021, 93, 23, 8152–8160

31. PEDOT-Based Eutectogel Electrode Arrays for Enhanced High-Resolution Electrogastrography: Fabrication, Stability, and Wearable Performance ,C Slaughter, L Gatecliff, X Tao, R Ruiz-Mateos Serrano, Amy T Jin, Matias L Picchio, Daniele Mantione,

Antonio Dominguez-Alfaro, George G Malliaras Advanced Functional Materials, 2026, e19081

32. S. Anantharaj and S. Noda, iR drop correction in electrocatalysis: everything one needs to know!, J. Mater. Chem. A, 2022, 10, 9348–9354.

33. G. Lang, M. Ujvari, S. Vesztergom, V. Kondratiev, J. Gubicza, K. Szekeres, The Electrochemical Degradation of Poly(3,4-ethylenedioxythiophene) Films Electrodeposited from Aqueous Solutions, Zeitschrift Für Physikalische Chemie 230 (2016). https://doi.org/10.1515/zpch-2016-0752.

34. A.J. Bard, L.R. Faulkner, H.S. White, Electrochemical Methods: Fundamentals and Applications, John Wiley & Sons, 2022.
35. György Inzelt, Conducting polymers. A new era in electrochemistry | Journal of Solid State Electrochemistry Springer Nature Link,(n.d.). https://link.springer.com/article/10.1007/s10008-009-0857-7 (accessed April 8, 2026).
36. B.D. Paulsen, K. Tybrandt, E. Stavrinidou, J. Rivnay, Organic mixed ionic-electronic conductors, Nat Mater 19 (2020) 13–26. https://doi.org/10.1038/s41563-019-0435-z.
37. Capacitive studies of electrodeposited PEDOT-maleimide Yuhang Wu, Samadhan S. Nagane, Peter Sitarik, Shrirang Chhatre, Junghyun Lee and David C. Martin J. Mater. Chem. A, 2022,10, 8440-8458

38. Proctor, C.M., Rivnay, J. and Malliaras, G.G. (2016), Understanding volumetric capacitance in conducting polymers. J. Polym. Sci. Part B: Polym. Phys., 54: 1433-1436. https://doi.org/10.1002/polb.24038

39. L. Pigani, A. Heras, Á. Colina, R. Seeber, J. López-Palacios, Electropolymerisation of 3,4-ethylenedioxythiophene in aqueous solutions, Electrochemistry Communications 6 (2004) 1192–1198. https://doi.org/10.1016/j.elecom.2004.09.021.

40. Zhao, J., Liu, W., Azari, R. et al. Electrophoretic deposition. Nat Rev Methods Primers 6, 12 (2026). https://doi.org/10.1038/s43586-025-00462-3

41. Bipolar electrochemistry—A wireless approach for electrode reactions Line Koefoed 1, Steen U. Pedersen 1, Kim Daasbjerg, Current Opinion in Electrochemistry Volume 2, Issue 1, April 2017, Pages 13-17

42. X. Fan, N. E. Stott, J. Zeng, Y. Li, J. Ouyang, L. Chu, and W. Song, PEDOT:PSS materials for optoelectronics, thermoelectrics, and flexible and stretchable electronics, J. Mater. Chem. A, 2023, 11, 18561–18591.

Thesis Conclusion

Conclusion

(i) From Wireless Electrochemistry to Spatially Programmable Systems

The work presented throughout this thesis has explored how bipolar electrochemistry can be transformed from a largely phenomenological wireless electrochemical effect into a predictive and architecturally programmable framework for controlling electrochemical function. Rather than treating bipolar systems simply as floating conductors polarised by an externally applied field, the studies presented here demonstrate that electrochemical behaviour emerges through coupled interactions between spatial confinement, ionic current redistribution, interfacial polarisation, and electrode architecture. By integrating electrochemical modelling, materials synthesis, electrochemiluminescence (ECL) mapping, and three-dimensional electrode design, the thesis establishes that electrochemical activity in wireless systems can be engineered through spatial control of polarisation rather than direct electrical input.

At the heart of this thesis lies a broader challenge extending across electrochemistry and bioelectronics alike, i.e., how can electrochemical activity be localised, controlled, and scaled within complex environments without relying on increasingly intricate wiring conditions? Conventional electrochemical systems depend on direct electrical connection between electrodes and external instrumentation. While this provides precise electrical control, it also imposes significant limitations in applications where miniaturisation, scalability, and spatial flexibility are required. In biological systems, these limitations become particularly pronounced. Implantable bioelectronic devices such as deep brain stimulators, neural interfaces, and electrochemical sensing arrays require physical leads, external circuitry, and power delivery systems that increase device complexity, restrict spatial resolution, and introduce long-term failure modes associated with mechanical damage, electrode migration, and tissue response.

These limitations are not simply engineering inconveniences but reflect a deeper architectural restriction within conventional electrochemistry itself. Spatial electrochemical control is typically achieved through direct electrode-to-electrode wiring. As the number of functional

electrochemical elements increases, system complexity scales accordingly. This becomes particularly problematic in the translation to biologically relevant environments, where future electroceutical technologies will likely require distributed sensing, localised stimulation, and adaptive electrochemical communication across highly heterogenous tissue structures.

Bipolar electrochemistry offers a fundamentally different strategy. By exploiting electric fields to remotely polarise electrically floating conductors, electrochemical reactions can be induced without direct electrical connection. Importantly, the significance of bipolar electrochemistry extends beyond simple wire removal. Because electrochemical behaviour is governed by local field gradients and interfacial polarisation, bipolar systems provide a means of spatially directing electrochemical activity through architecture itself. Across the studies presented throughout this thesis, electrode design emerges not simply as a structural consideration, but as a determinant of how electric fields, ionic currents, and electrochemical reactions evolve throughout open bipolar systems.

Chapter 2 positioned bipolar electrochemistry within the emerging field of wire-free electroceuticals and bioelectronic systems. Through critical evaluation of the existing literature, it became clear that bipolar electrochemistry possesses several intrinsic characteristics uniquely suited to future biomedical technologies. The ability to remotely induce electrochemical activity without direct electrical wiring creates opportunities for minimally invasive sensing and stimulation systems capable of operating in a targeted and spatially distinct manner within in complex biological environments. Moreover, because multiple BPEs can be simultaneously polarised using a single externally applied field, bipolar electrochemistry provides a route towards scalable electrochemical architectures that avoid many of the spatial and mechanical limitations associated with conventional implanted systems.

Importantly, the review also established that bipolar electrochemistry should not be interpreted merely as a wireless analogue of conventional electrochemical analysis. Instead, it represents a distinct mode of electrochemical control in which spatial field distribution, rather than direct electrode connection, governs reactivity and localisation of redox events. This distinction is especially significant in the context of electroceuticals, where localised

stimulation, distributed sensing, and spatially selective therapeutic modulation will likely be central design requirements. Conducting polymers and electroactive nanomaterials were identified as particularly important in this regard because they provide interfaces capable of simultaneously supporting ionic transport, electronic conduction, and biocompatibility, thereby forming a functional bridge between electric fields and biological response.

However, despite the considerable promise of bipolar electrochemistry for bioelectronic integration, a mechanistic limitation remained. Existing descriptions of bipolar systems predominantly rely on simplified one-dimensional models that assume uniform conductivity, approximate linear decay in potential, and planar electrode geometries. While these assumptions may adequately describe idealised systems containing highly conductive electrolytes, they become increasingly inadequate in low-conductivity environments or systems containing complex three-dimensional structures. Since many biologically relevant environments often exhibit heterogenous ionic composition and spatially diverse conductivity, understanding how bipolar electrochemistry behaves beyond classical electrolyte-rich systems is essential if wireless electrochemical technologies are to progress toward realistic applications.

(ii) Electric Field Redistribution in Low-Conductivity Bipolar Systems

Addressing this challenge formed the basis of Chapter 3, which investigated the electropolymerisation of PEDOT in ultrapure water using bipolar electrochemistry. The successful formation of conducting polymer films under these conditions is itself highly significant because conventional three-electrode electrochemistry typically requires deliberately added supporting electrolyte to minimise solution resistance and enable efficient charge transfer. Demonstrating that conducting polymer deposition can occur in ultrapure water therefore extends the operational landscape of bipolar electrochemistry into regimes traditionally considered inaccessible for electrochemical synthesis.

More importantly, however, the resulting deposition profiles revealed behaviour that could not be adequately explained using conventional linear field approximations. Polymer growth was highly non-uniform and strongly dependent on local geometry and spatial position along

the bipolar electrode surface, despite the externally applied field remaining constant across the system. In classical bipolar electrochemistry, deposition behaviour is often interpreted through simplified 1D descriptions whereby the solution potential decays approximately linearly between feeder electrodes, resulting in correspondingly predictable polarisation along the BPE surface. The experimentally observed PEDOT profiles clearly deviated from this behaviour, indicating that local field perturbation, confinement effects, and variations in ionic transport were exerting a dominant influence over where electrochemical reactions could occur.

This observation is particularly important as it demonstrates that redox activity under low-conductivity environments becomes exceptionally sensitive to local distortions in field distribution. Under such conditions, even relatively subtle geometric features or changes in confinement can substantially alter local interfacial polarisation and redirect ionic current pathways throughout the system. Electrochemical activity therefore cannot be interpreted solely as a function of externally applied voltage but instead emerges through coupled interactions between local solution resistance, field redistribution, mass transport, and interfacial kinetics.

To investigate these effects, FEM was combined with electrochemical characterisation of wirelessly deposited PEDOT-functionalised BPEs to map potential distributions, local interfacial polarisation behaviour, and diffusive transport processes within open bipolar cells. This modelling framework provided detailed insight into the local BPE-solution potential differences governing electrochemical activity, while also identifying regions of preferential deposition and quantifying solution volumes available for polymer growth. Importantly, the model successfully reproduced experimentally observed film capacitance profiles, establishing a strong correlation between predicted electric field distributions and measured electrochemical responses.

This work therefore represents a significant conceptual advance because it demonstrates that bipolar electrochemistry in low ionic solutions cannot be adequality described using simplified linear approximations alone. Rather than behaving as uniformly polarised conductors, BPEs exhibit highly localised electrochemical behaviour arising from complex

coupling between field redistribution, interfacial kinetics, ionic transport, and geometric confinement. More broadly, the integration of FEM into bipolar electrochemistry represents an important transition from descriptive to predictive wireless electrochemistry. Rather than relying solely on empirical observation, local electrochemical behaviour can instead be rationalised and engineered through quantitative spatial analysis of field distributions.

It is worth noting that while the present model successfully captures the influence of electric field redistribution on local bipolar behaviour and reproduces experimentally observed deposition trends, it necessarily represents a simplified description of the overall electrochemical system. Processes including coupled diffusion-migration mass transport, complex activation controlled heterogenous electron transfer kinetics, electrical double-layer structure or lack thereof in low ionic strength media alongside other interfacial phenomena were not explicitly incorporated within the present framework. Incorporating these processes into next-generation Multiphysics models would provide a more complete description of bipolar electrochemical behaviour, enabling increasingly accurate prediction of reaction localisation, polymer growth dynamics, and wireless electrochemical performance under complex operating conditions e.g. 3D bipolar systems.

(iii) Geometric Confinement as a Strategy for Localised Bipolar Activation

Having established the importance of local field distribution in governing electrochemical behaviour, the thesis next examined whether electrochemical activity could be deliberately localised through control of feeder electrode geometry. Feeder electrodes are typically regarded as relatively passive components whose primary role is simply to establish the externally applied electric field necessary for bipolar polarisation. Consequently, comparatively little attention has been given to whether feeder architecture itself can actively shape local electrochemical behaviour.

A persistent limitation in bipolar electrochemistry is that miniaturisation progressively reduces the induced potential difference across the BPE, necessitating increasingly large fields to sustain effective electrochemical activation. This voltage-scaling issue becomes especially restrictive in biologically relevant systems whereby excessive fields complicate device

integration and operation. Developing alternative strategies capable of enhancing local electrochemical activation without simply increasing voltage therefore represents a significant challenge within the field.

To investigate this possibility, bipolar electrochemiluminescence (BP-ECL) was employed as a spatial probe of electrochemical activity. BP-ECL provided means of visualising regions of local activation but moreover, the intensity of the generated light can be used as a proxy of reaction efficiency (total photon output) thereby providing extensive real-time mapping of the evolving field distribution on BPE surfaces.

The results demonstrated that feeder electrode geometry exerts a profound influence on both the localisation and intensity of ECL emission, despite a constant field strength across all systems. Planar feeder electrodes generated relatively broad and uniform emission across the BPE surface, behaviour consistent with more homogenous electric field distributions. In striking contrast, compact three-dimensional feeder geometries such as single wire and pin array pairs produced highly localised and intensified emission patterns.

Most noticeably, single-wire feeder pairs generated focused ECL hotspots directly opposite the feeder tip, accompanied by secondary edge emissions associated with fringing electric fields and confined current pathways. Critically, these results demonstrate that electrochemical activation can be intensified locally without increasing the acting field strength. Rather than relying on voltage escalation to compensate for reduced bipolar dimensions, geometric confinement itself can be exploited to focus field intensity into highly localised reactive domains.

Additionally, 3D-printed pin-array feeders distributed electrochemical activation via superposition of electric fields generated by multiple pins, producing enhanced ECL propagation and greater photon output compared to the planar feeder controls. Importantly, both single-wire and pin-array feeders occupied only a fraction of the active BPE footprint, demonstrating that highly localised and efficient bipolar activation can be achieved using compact feeder architectures substantially smaller than the electrode surface being

addressed. This has major implications for miniaturised electrochemical systems whereby reducing physical footprint while maintaining local electrochemical control is essential.

The significance of these findings extends beyond ECL emission patterns alone. Feeder electrodes emerge not as passive field-generating components, but as active tools for sculpting where electrochemical activity occurs within open bipolar cells. More fundamentally, the work demonstrates that geometric confinement provides an alternative route towards enhancing planar redox performance that does not rely exclusively on progressively increasing field strengths. This distinction is particularly important for the future development of miniaturised bipolar systems where maintaining sufficient local polarisation becomes increasingly challenging as dimensions decrease.

(iv) Topology-driven Electrochemical Coupling in Three-dimensional BPE Architectures

The final component of the thesis extended these concepts further by investigating whether three-dimensional BPE architectures could themselves be used to spatially programme electrochemical behaviour. While traditional bipolar electrochemistry predominantly uses planar electrode geometries, relatively little is understood about how vertical elements, geometric asymmetry, or electronically coupled structures influences local polarisation behaviour.

This represents a major limitation because classical bipolar electrochemical models generally assume linear potential decay and uniform field distribution along a single electrode axis. Although such approximations have proven useful for describing idealised planar systems, they become increasingly inadequate once geometric confinement, insulating boundaries, or couple three-dimensional structures perturb local field distributions. Consequently, the possibility of deliberately exploiting topology itself to direct electrochemical behaviour has remained comparatively underdeveloped within bipolar electrochemistry.

Using modular three-dimensional architectures including, planar, vertical, split-L and L-shaped configurations, it was demonstrated that topology profoundly influences local

electrochemical behaviour in ways inaccessible using conventional planar systems. Vertical BPEs positioned near insulating boundaries i.e. cell walls, generated unexpectedly amplified and highly localised one-sided PEDOT deposition across an effective length of 1 mm. This observation is particularly significant because it demonstrates that local interfacial polarisation can be substantially amplified through orientation and confinement effects rather than increasing the overall applied field.

The work therefore demonstrates that the relative dimensions of the BPE and electrochemical cell can be deliberately exploited to manipulate local ohmic drop, redistribute ionic current pathways, and amplify interfacial polarisation in highly specific regions of the BPE surface. Importantly, these effects emerge without altering field strength, indicating that spatial confinement itself can function as a practical electrochemical design strategy rather than merely a geometric constraint.

Strikingly, cooperative electrochemical behaviour emerged in systems containing multiple spatially coupled BPE structures. Electrically disconnected split -L systems consisting of both vertical and planar BPE elements exhibited spatially redistributed polymer growth compared to isolated configurations, while electronically continuous L-shaped architectures demonstrated that vertical elements could amplify and extend electrochemical activity across connected planar surfaces on the same single BPE structure.

Perhaps most significantly, the work demonstrates that BPEs occupying different spatial planes cannot necessarily be treated as electrochemically independent, even under identical applied fields. Whereas multiplexed *planar* BPE systems often behave quasi-independently because neighbouring electrodes experience relatively comparable field environments, the introduction of vertically oriented structures fundamentally perturbs local electric field distributions. The resulting anisotropic field focusing and ionic current redistribution generate cooperative electrochemical behaviour that cannot be predicted using conventional planar or one-dimensional approximations.

Consequently, spacing, and relative orientation emerge as critical electrochemical design parameters in three-dimensional bipolar systems. BPEs possessing different normal axes relative to the imposed electric field can interact cooperatively through the surrounding

solution, redistributing electrochemical activity to regions that would otherwise remain electrochemically inaccessible. In this sense, vertically oriented structures behave analogously to field-focusing elements capable of reshaping local redox landscapes within open bipolar cells.

Collectively, these findings demonstrate that electrochemical behaviour within three-dimensional BPE structures emerges through dynamic coupling between topology, confinement, and local ionic current redistribution rather than through linear polarisation of isolated BPEs. More fundamentally, the work suggests that electrochemical functionality can be encoded structurally rather than electronically. This represents a conceptual shift away from conventional electrochemical systems in which functionality is predetermined primarily through wiring architecture and external stimulation.

Outlook for Wireless Electroceutical Systems

This thesis helps to establish that bipolar electrochemistry cannot be interpreted solely through simplified linear models or treated merely as a wireless adaptation of conventional electrochemistry. Instead, electrochemical behaviour emerges through coupled interactions between spatial confinement, ionic current redistribution, interfacial polarisation, and electrode architecture. Quantifying these interactions is essential for rational design of wireless electrochemical systems capable of precise and localised function.

The broader significance of this thesis therefore lies not simply in the individual experimental observations, but in establishing a coherent electrochemical framework linking electrode architecture directly to local electrochemical behaviour. Through the integration of FEM, conducting polymer deposition, ECL-mapping, and modular three-dimensional electrode design, the work demonstrates that electrochemical activity within open bipolar cells can be deliberately directed through spatial manipulation of field distributions.

Importantly, this control is achieved not through increasingly complex wiring strategies or progressively high applied voltages, but through deliberate manipulation of confinement, orientation, topology, and field focusing effects. Collectively, the work establishes bipolar

electrochemistry as an electrochemical design framework in which functionality can emerge through engineered spatial interactions rather than direct electrical addressing alone.

With the context of bioelectronics and electroceuticals, these findings are especially significant because future systems will require precise spatial control while simultaneously reducing device complexity and physical footprint. The ability to localise and amplify electrochemical activity through geometry-driven field manipulation alone offers a potential route towards reliable distributed sensing and stimulation platforms that avoid, many of the limitations associated with traditional wired structures.

A broader conceptual transition within electrochemistry itself is also highlighted. Conventional electrochemical systems derive functionality primarily through direct electrical connections and externally imposed circuitry. In contrast, the studies presented here demonstrate that electrochemical behaviour can emerge through deliberate manipulation of spatial interactions within architecturally engineered environments. Electrode topology, orientation, confinement, and field redistribution therefore become active determinants of electrochemical function rather than passive structural parameters.

Future Work

Current Work in Progress :

1. Fully 3D Bipolar Configurations (Array BPE + Array Feeders)

Employing three-dimensional highly organised pin arrays ad feeder electrodes has shown to not only increase the activation area of a planar BPE, to also enhance the emission intensity. Therefore, the logical next step could be to investigate three-dimensional structures as both feeders and BPEs.

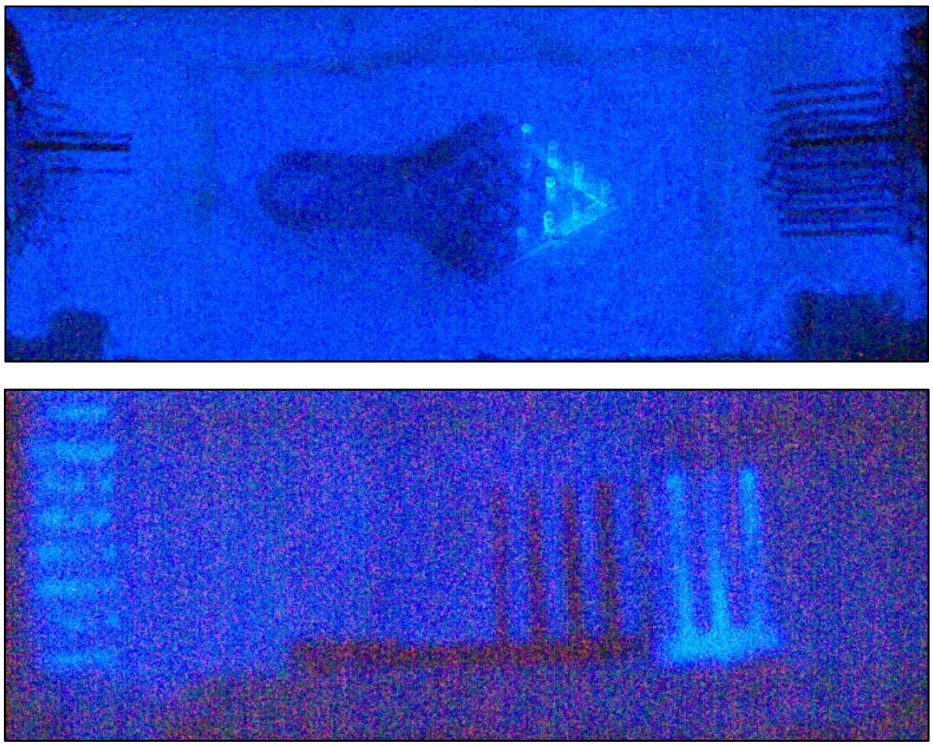


Figure 1 Top – Fully three-dimensional bipolar system, employing pin array as feeder pairs and BPE. An applied field of 3 V cm^{-1} was applied to the system containing 3 mL of 10mM Luminol with 3 µL H_2O_2 in 0.1M NaOH. Light generation spans across 3 pin rows with areas of high curvature and edges such as pin heads and underlying grid base edges showcasing localised light intensity as expected via the lightning rod effect. **Bottom** – Side view of the 3D system showcasing relatively uniformly distributed light generation along the z-direction i.e. pin walls.

2. Reconfigurable BP Activation via Confined Feeders

Preliminary studies currently underway further extend the principles of geometric field confinement explored throughout this thesis by investigating three-dimensional feeder architectures capable of sustaining highlight localised BP-ECL within interconnected electrode arrays. Early experiments using non-insulated wire feeder pairs (Figure 2) already demonstrate that compact feeder geometries can generate intense and spatially confined electrochemical activation despite possessing footprints substantially small than the underlying BPE network. In these systems, local electric field amplification at the wire tips and underlying grid edges, consistent with lightning-rod effects, concentrates ionic current pathways and promotes highlight localised BP-ECL while simultaneously enabling activation to propagate laterally across electrically connected regions of the array.

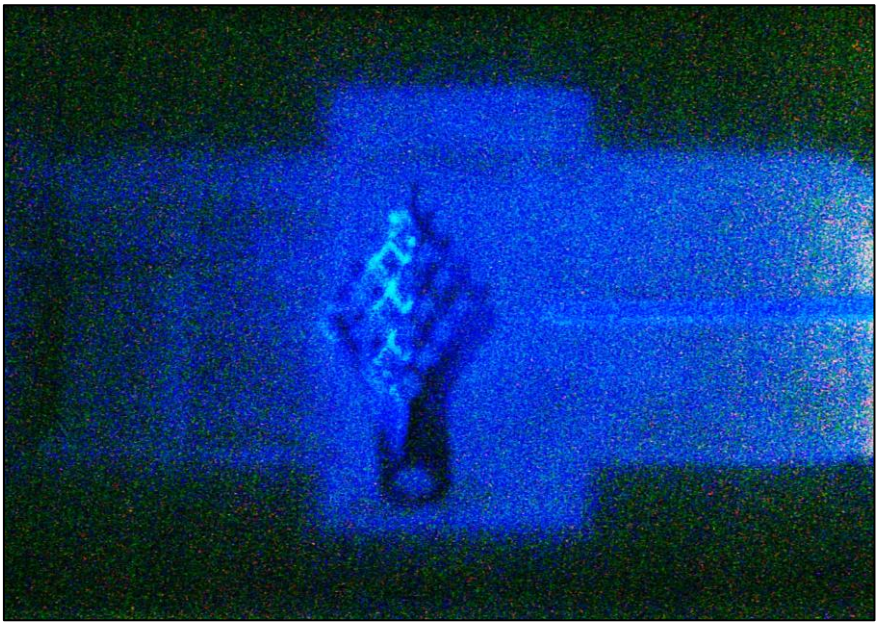


Figure 2 – BP-ECL generated from a 3D-printed array BPE coupled with a pair of wire feeder electrodes. Despite the comparatively small feeder dimensions relative to the interconnected BPE network, intense and spatially confined BP-ECL is observed across selective regions (bisecting the BPE surface) of the array under a fixed field strength of 3 V cm^{-1}.

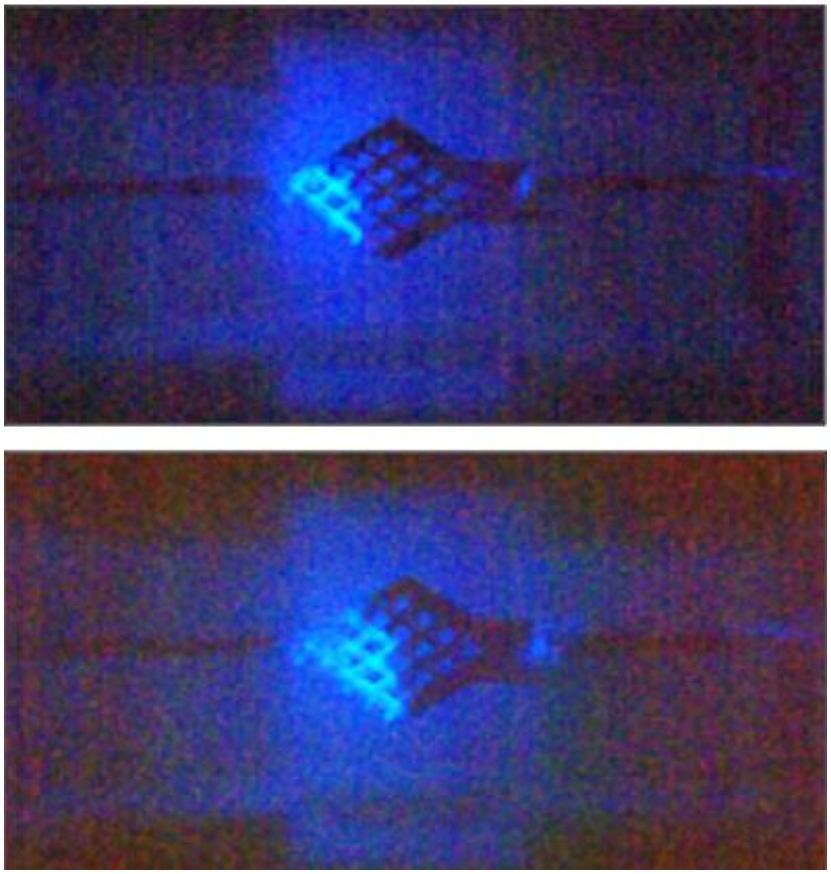


Figure 3 – BP-ECL generated from a 3D pin-array BPE coupled with partially insulated wire feeder pairs, where only the 0.8 mm^2 flat wire tip remained exposed to the supporting solution. **Top:** An applied field strength of 3 V cm^{-1} produces a highly localised activation zone spanning approximately three rows of pins. **Bottom:** Increasing field strength to 4.5 Vcm^{-1} enhances approximately four pin rows. These results demonstrate that geometric confinement of the feeder-electrolyte interface enables spatially selective and progressive wireless electrochemical activation within interconnected three-dimensional BPE architectures.

Building upon these observations, selective insulation of the feeder shaft walls has been introduced to further confine the effective feeder interface to a flat exposed wire tip of approx. 1mm diameter, corresponding to an electrochemically active area of only ~ 0.8 mm^2. Under constant applied field conditions, these partially insulated feeder geometries produced sustained and highly selective bipolar activation across individual pins and localised regions of the interconnected underlying grid base. Importantly, these results demonstrate that

electrochemical activation can be directed not only through overall electrode topology, but also through deliberate confinement of the feeder-electrolyte interface itself. By spatially restricting where the field couples to the supporting solution, the feeder effectively behaves as a field focusing element capable of selectively redistributing electrochemical activity across complex bipolar architectures without direct electrical addressing of each individual electroactive site.

Interestingly, the resulting BP-ECL profiles exhibit a distinct cone-like activation profile, suggesting that spatial confinement of the feeder-electrolyte interface generates a non-uniform radial field distribution rather than a simple one-dimensional potential gradient. In this regime, local fringing and divergent ionic current pathways originating from the exposed feeder tip likely redistribute interfacial polarisation laterally across the array, producing progressive spatial expansion of electrochemical activation under increasing field strengths.

Future Work & Next Steps

(i) Spatially Programmable Wireless Therapeutic Systems

One immediate opportunity arising from this work is the development of wireless and spatially selective therapeutic delivery platforms. Conducting polymers such as PEDOT can simultaneously function as electroactive interfaces, ionic reservoirs, and electrically responsive release matrices. Therapeutic agents including anti-inflammatory compounds, neurotransmitter analogues, chemotherapeutics, or immunosuppressive drugs such as methotrexate could potentially be incorporated within the deposited film via electrochemical doping/de-doping regimes and subsequently released using electric fields. This may be especially valuable for therapeutics possessing narrow therapeutic windows or significant systemic toxicity, where localised delivery remains a major clinical challenge.

Importantly, the findings of this thesis suggest that release behaviour need not be governed solely by the magnitude of applied voltage, but instead be spatially programmed through feeder geometry, electrode topology, and local field confinement. The ability to localise electrochemical activation using compact feeder architectures or 3D BPEs creates

opportunities for selectively triggering therapeutic release only within targeted regions of a distributed bipolar system without requiring individually addressable electrodes.

Beyond localisation alone, bipolar geometry may provide a means of controlling drug loading and release kinetics through spatially directed polymer growth itself. For example, vertically oriented BPEs were shown to produce highly confined, ultra-thin and comparatively uniform film deposition profiles, whereas planar configurations generated more pronounced deposition gradients across the electrode surface. Since polymer thickness, morphology, conductivity, and electroactive surface distribution directly influence drug incorporation and subsequent electrochemical release behaviour, controlling BPE architecture may provide a route towards tailoring not only where therapeutics are released, but also the rate and duration of release.

This introduces the possibility of engineering conducting polymer systems with deliberately heterogeneous loading profiles, where difference regions of the same wireless electrochemical architecture exhibit distinct release characteristics under identical external fields. Such control could prove especially important for future electroceutical systems requiring standard local release, sequential delivery profile, or spatially differentiated therapeutic responses within complex biological environments.

(ii) Temporal and Frequency-dependent Electrochemical Programmability

A major future direction arising from this work is the introduction of temporal programmability into bipolar electrochemical systems through dynamic controlled electrical inputs. The collection of works described throughout the thesis have utilised direct current (DC) field generation. However, building on this foundation, an important next step is to extend control from purely spatial tuning to systems in which electrochemical response can be modulated in both space and time. In this context, programmable electrical inputs, such as alternating current (AC) waveforms, pulsed potentials, frequency modulation, and time-varying field gradients, offer a route to BP electrochemical platforms whose response is intrinsically dynamic rather than steady state. Such approaches would enable real-time modulation of interfacial potential distributions, redox kinetics, ionic transport, and double-

layer charging processes, introducing a temporal degree of freedom that is currently underexplored in BP electrochemistry.

The temporal dimension is particularly relevant when considering biological systems, where electrical signalling is inherently dynamic and spans multiple time scales, from slow circadian cycles to rapid neuronal and cardiac excitation. Pathological electrical activity, such as that associated with epilepsy, Parkinson's tremor, and cardiac arrhythmias, is likewise characterised by distinct frequencies and amplitude-dependent signatures. In contrast, most electrochemical systems are operated under steady-state or slowly varying conditions that do not reflect this complexity.

Future BP electrochemical platforms could therefore be used to investigate how time-varying electrical inputs influence interfacial electron-transfer processes, ionic fluxes, and the switching behaviour of electroactive materials, including conducting polymers and stimulus-responsive films. In particular, waveform dependent effects on charging dynamics, faradaic processes, and mass transport may provide insight into how bipolar systems respond under non-equilibrium, biologically relevant driving conditions.

Within this framework, BP-ECL provides a particularly sensitive and informative reporting modality. Because ECL emission is directly coupled to local redox reactions and reactive intermediate generation, it is highly responsive to changes in potential distribution, mas transport, and reaction kinetics. Temporally structured excitation therefore has the potential to generate characteristic time-resolved emission profiles that reflect both the applied waveform and the evolving electrochemical state of the system. More speculatively, but within a physically grounded framework, such time-resolved BP-ECL responses could be explored as a form of electrochemical "signature mapping," where distinct waveform inputs produce reproducible emission-time profiles that encode information about system dynamics, material state, or environmental conditions. While not a diagnostic tool at this stage, this concept aligns with broader trends in electrochemical sensing towards multidimensional, time-resolved data acquisition rather than single point intensity measurements.

More broadly, aligning electrical waveforms with physiologically relevant frequency regimes offers a route to systematically probing electrochemical systems under conditions that more closely resemble biological electrical environments. In this way, future BP platforms may evolve from static stimulation into dynamic information rich interfaces for interrogating and controlling coupled electrochemical biological processes.

Declaration of Authorship for PhD by Publication

Section 1: Candidate's Details	
Candidate's Name	Oisín Foley Doyle
DCU Student Number	23271697
School	School of Chemical Sciences, Dublin City University
Principal Supervisor	Prof Robert J Forster
Title of PhD by Publication Thesis	Wireless Electrochemistry: 3D Bipolar Systems for Spatially Controlled Bioelectronic Function
Section 2: Paper Details	
Title of co-authored paper included in the thesis under examination	Wirefree Electrochemistry for Enhanced Detection and Treatment of Disease
List of authors as in order given on accepted/published version	Oisín Foley Doyle, Robert J Forster
Publication Details (e.g. Year of Publication, Journal Name, Issue Number, Page Numbers, Place of Publication, DOI, ISSN, URL etc.)	Electrochemistry Communications 169 (2024) 107832 31st October 2024 doi.org/10.1016/j.elecom.2024.10782
Publication Status (e.g. Published, Accepted)	Published
Provide a brief statement here on the disciplinary ranking of this publication and the peer-review process involved (e.g. how many reviewers, single blinded or other, initial decision, revision timeline etc and any other details that	Electrochemistry Communications is a well-established peer-reviewed journal specialising in the rapid dissemination of significant advances in electrochemistry. The manuscript underwent independent single-blinded external peer-review (2 reviewers) following an initial acceptance from a designated editor, the manuscript was revised in

speak to the rigour of the peer review process)	response to the reviewer comments prior to full acceptance and final publication.

This paper (Chapter 2) is one of 4 co-authored papers to be submitted as part of the PhD by publication thesis submitted for examination.

Section 3: Candidate's Contribution to the Paper

Provide details below of the **nature** and **extent of your contribution** to the paper (include both your intellectual and practical contributions) and your overall contribution in **percentage terms**. Note that these categories can be customised according to disciplinary norms

Briefly outline your contribution to the **conception** of the work described in this paper:

Contributed to the development of the review topic, scope, and overall structure of the manuscript.

Briefly outline your contribution to the **literature review** in this paper:

Conducted the literature search, evaluated relevant publications, and identified key themes, developments, and knowledge gaps within the field.

Briefly outline your contribution to the **methodological design**:

Contributed to the design of the review framework, including the selection, organisation, and thematic categorisation of relevant literature.

Briefly outline your contribution to **data collection**:

Collected and compiled the published literature and supporting sources discussed throughout the review.

Briefly outline your contribution to **data analysis**:

Critically evaluated and compared findings from the published literature, identifying emerging trends, challenges, and opportunities within the field.

Briefly outline your contribution to the **synthesis and summary of findings**:

Synthesised the findings from the literature into a coherent narrative and contributed to the development of the conclusions and future perspectives presented in the review.

Finally, outline your contribution to the **writing** and **revision** of the paper:

Prepared original manuscript draft and contributed to subsequent revisions, editing, and refinement of the manuscript prior to publication

Overall Contribution : 60 %

Section 4: Signature and Validation

I confirm that the following statements are true:

(a) the information I have provided in this form is correct
(b) this paper is based on research undertaken during my candidature at DCU

Signature of PhD Candidate: Oisín Foley Doyle **Date:**_03/05/2026_

I confirm that the information provided by the candidate is correct:

Signature of Principal Supervisor: Robert Forster **Date:**_03/05/2026_

Section 1: Candidate's Details	
Candidate's Name	Oisín Foley Doyle
DCU Student Number	23271697
School	School of Chemical Sciences, Dublin City University
Principal Supervisor	Prof Robert J Forster
Title of PhD by Publication Thesis	Wireless Electrochemistry: 3D Bipolar Systems for Spatially Controlled Bioelectronic Function
Section 2: Paper Details	
Title of co-authored paper included in the thesis under examination	Advancing Bipolar Electrochemistry for Targeted Deposition of Biocompatible Polymers in Electrolyte-Free Solutions via Finite Element Modeling
List of authors as in order given on accepted/published version	M.Wagner, Á.Brady, O.F.Doyle, R. J. Forster
Publication Details (e.g. Year of Publication, Journal Name, Issue Number, Page Numbers, Place of Publication, DOI, ISSN, URL etc.)	ChemElectroChem, 2025, 12, e202400506 doi.org/10.1002/celc.202400506
Publication Status (e.g. Published, Accepted)	Published
Provide a brief statement here on the disciplinary ranking of this publication and the peer-review process involved (e.g. how many reviewers, single blinded or other, initial decision, revision timeline etc and any other details that speak to the rigour of the peer review process)	ChemElectroChem is an international peer-reviewed journal specialising in fundamental and applied electrochemistry by Chemistry Europe and Wiley. Journal is recognised within the electrochemistry community and maintains a rigorous peer-reviewed process involving assessment by independent expert reviewers (x3) (single-blinded), with the manuscript undergoing external peer review and revision before acceptance, with reviewer comments addressed through the revision process.

This paper (Chapter 3) is one of 4 co-authored papers to be submitted as part of the PhD by publication thesis submitted for examination.

Section 3: Candidate's Contribution to the Paper

Provide details below of the **nature** and **extent of your contribution** to the paper (include both your intellectual and practical contributions) and your overall contribution in **percentage terms**. Note that these categories can be customised according to disciplinary norms

Briefly outline your contribution to the **conception** of the work described in this paper:

Contributed to the conceptualisation of the study, including the development of the research objectives and application of finite element modelling in conjunction with comparative experimental analysis.

Briefly outline your contribution to the **literature review** in this paper:

Reviewed the relevant literature on bipolar electrochemistry, conductive polymer deposition, finite element modelling, and low-conductivity electrochemical systems to establish the scientific context and rationale for the study.

Briefly outline your contribution to the **methodological design**:

Contributed to the design of the experimental and modelling methodology, including development of the finite element modelling framework and optimisation of experimental conditions for polymer deposition studies.

Briefly outline your contribution to **data collection**:

Conducted all experimental work associated with polymer deposition via bipolar electropolymerisation, conventional cyclic voltammetry and impedance analysis presented in the manuscript.

Briefly outline your contribution to **data analysis**:

Analysed and interpreted both modelling and experimental results, evaluated correlations between simulation and experimental observations.

Briefly outline your contribution to the **synthesis and summary of findings**:

Synthesised the modelling and experimental findings to establish the relationship between electric field distributions and targeted polymer deposition behaviour in electrolyte-free solutions.

Finally, outline your contribution to the **writing** and **revision** of the paper:

Contributed to preparation of the manuscript, including drafting sections of the paper, preparation of some figures and critical review of the text alongside revisions in response to co-author and reviewer feedback.

Overall Contribution : 60 %

Section 4: Signature and Validation

I confirm that the following statements are true:

(a) the information I have provided in this form is correct
(b) this paper is based on research undertaken during my candidature at DCU

Signature of PhD Candidate: Oisín Foley Doyle **Date:**_03/05/2026_

I confirm that the information provided by the candidate is correct:

Signature of Principal Supervisor: Robert Forster **Date:**_03/05/2026_

Section 1: Candidate's Details	
Candidate's Name	Oisín Foley Doyle
DCU Student Number	23271697
School	School of Chemical Sciences, Dublin City University
Principal Supervisor	Prof Robert J Forster
Title of PhD by Publication Thesis	Wireless Electrochemistry: 3D Bipolar Systems for Spatially Controlled Bioelectronic Function
Section 2: Paper Details	
Title of co-authored paper included in the thesis under examination	Directing the glow : 3D feeder geometries to enhance planar bipolar electrochemiluminescence
List of authors as in order given on accepted/published version	Oisin Foley Doyle, Gordon G Wallace, Zhilian Yue, Jun Chen, Stephen Beirne and Robert J. Forster
Publication Details (e.g. Year of Publication, Journal Name, Issue Number, Page Numbers, Place of Publication, DOI, ISSN, URL etc.)	ChemComm, Volume 61, Issue 97 18th December 2025, pages 19135-19322 doi.org/10.1039/D5CC04706D
Publication Status (e.g. Published, Accepted)	Published
Provide a brief statement here on the disciplinary ranking of this publication and the peer-review process involved (e.g. how many reviewers, single blinded or other, initial decision, revision timeline etc and any other details that speak to the rigour of the peer review process)	Chemical Communication is a leading international journal of the Royal Society of Chemistry that publishes high-impact communications across all areas of chemistry. The journal is widely recognised as a top-tier chemistry journal and employs a rigorous peer-review process involving independent expert reviewers (single-blinded) and editorial assessment. The manuscript underwent external peer review and revision prior to acceptance.

This paper (Chapter 4) is one of 4 co-authored papers to be submitted as part of the PhD by publication thesis submitted for examination.

Section 3: Candidate's Contribution to the Paper

Provide details below of the **nature** and **extent of your contribution** to the paper (include both your intellectual and practical contributions) and your overall contribution in **percentage terms**. Note that these categories can be customised according to disciplinary norms

Briefly outline your contribution to the **conception** of the work described in this paper:

Led the conceptualisation of the study, including the development of the research hypothesis and investigation of how three-dimensional feeder geometries influence bipolar electrochemiluminescence behaviour.

Briefly outline your contribution to the **literature review** in this paper:

Conducted the literature review and identified the key knowledge gaps relating to feeder electrode design, bipolar electrochemistry, and electrochemiluminescence that informed the study objectives.

Briefly outline your contribution to the **methodological design**:

Designed the experimental methodology, including bipolar electrochemical cell configuration, feeder electrode geometries, electrochemiluminescence measurements and image-based analysis procedures.

Briefly outline your contribution to **data collection**:

Performed the experimental work and collected all electrochemiluminescence imaging and electrochemical data presented in the manuscript.

Briefly outline your contribution to **data analysis**:

Analysed and interpreted the experimental results , quantified electrochemiluminescence intensity profiles, performed data fitting and statistical analysis, and prepared the figures prepared in the manuscript.

Briefly outline your contribution to the **synthesis and summary of findings**:

Synthesised the experimental findings and developed the mechanistic interpretation linking feeder geometry, electric field distribution and spatially resolved bipolar electrochemiluminescence behaviour.

Finally, outline your contribution to the **writing** and **revision** of the paper:

Prepared the original manuscript draft, including preparation of figures and graphical content. Contributed substantially to manuscript revision, editing, and response to reviewer comments throughout the publication process.

Overall Contribution : 80 %

Section 4: Signature and Validation

I confirm that the following statements are true:

(a) the information I have provided in this form is correct
(b) this paper is based on research undertaken during my candidature at DCU

Signature of PhD Candidate: Oisín Foley Doyle **Date:**_03/05/2026_

I confirm that the information provided by the candidate is correct:

Signature of Principal Supervisor: Robert Forster **Date:**_03/05/2026_

Section 1: Candidate's Details	
Candidate's Name	Oisín Foley Doyle
DCU Student Number	23271697
School	School of Chemical Sciences, Dublin City University
Principal Supervisor	Prof Robert J Forster
Title of PhD by Publication Thesis	Wireless Electrochemistry: 3D Bipolar Systems for Spatially Controlled Bioelectronic Function
Section 2: Paper Details	
Title of co-authored paper included in the thesis under examination	Spatially Controlled Wireless Electrochemistry via 3D Bipolar Electrodes
List of authors as in order given on accepted/published version	Oisín Foley Doyle, Áine Brady, Robert J. Forster
Publication Details (e.g. Year of Publication, Journal Name, Issue Number, Page Numbers, Place of Publication, DOI, ISSN, URL etc.)	Electrochimica Acta, Volume 576, 2026,149658. doi.org/10.1016/j.electacta.2026.149658
Publication Status (e.g. Published, Accepted)	Published
Provide a brief statement here on the disciplinary ranking of this publication and the peer-review process involved (e.g. how many reviewers, single blinded or other, initial decision, revision timeline etc and any other details that speak to the rigour of the peer review process)	Electrochimica Acta is a leading international journal in electrochemistry published by Elsevier. The journal is recognised as a high-quality, peer-reviewed outlet for fundamental and applied electrochemical research and employs a rigorous review process involving independent expert reviewers (x3) (single-blinded) and editorial assessment. Publication is contingent upon successful completion of external peer review and revision in response to reviewer comments.

This paper (Chapter 5) is one of 4 co-authored papers to be submitted as part of the PhD by publication thesis submitted for examination.

Section 3: Candidate's Contribution to the Paper

Provide details below of the **nature** and **extent of your contribution** to the paper (include both your intellectual and practical contributions) and your overall contribution in **percentage terms**. Note that these categories can be customised according to disciplinary norms

Briefly outline your contribution to the **conception** of the work described in this paper:

Led the conceptualisation of the study, including the development of the central hypothesis that three-dimensional bipolar electrode topology can be exploited to direct electric field distributions and spatially programme electroactive material synthesis.

Briefly outline your contribution to the **literature review** in this paper:

Conducted the literature review and identified the key knowledge gaps relating to bipolar electrochemistry, electric field manipulation, conductive polymer deposition, and programmable electrochemical material synthesis that informed the study design and interpretation.

Briefly outline your contribution to the **methodological design**:

Designed the experimental methodology, including the development of the bipolar electrochemical cell, design and fabrication of the three-0dimenionsal electrode architectures, electropolymerisation procedures, electrochemical characterisation protocols, and image analysis methodologies.

Briefly outline your contribution to **data collection**:

Performed all experimental work, including electrode preparation, wireless PEDOT electropolymerisation, electrochemical measurements, image analysis, and collection of all data presented in the manuscript.

Briefly outline your contribution to **data analysis**:

Analysed and interpreted the experimental results, quantified deposition behaviour across the different bipolar electrode geometries, calculated electrochemical parameters, developed the mechanistic framework describing topology dependent field effects and prepared all figure and data presentations.

Briefly outline your contribution to the **synthesis and summary of findings**:

Led the synthesis of the findings and developed the overall scientific narrative demonstrating how electrode geometry, topology, and spatial arrangement influence local electric field distributions and enable programmable electrochemical materials synthesis.

Finally, outline your contribution to the **writing** and **revision** of the paper:

Prepared the original manuscript draft, including the introduction, experimental sections, results and discussion, conclusions, figures, and graphical content. Led manuscript revision and editing, incorporating feedback from co-authors throughout the preparation of the submission.

Overall Contribution : 80 %

Section 4: Signature and Validation

I confirm that the following statements are true:

(a) the information I have provided in this form is correct
(b) this paper is based on research undertaken during my candidature at DCU

Signature of PhD Candidate: Oisín Foley Doyle **Date:**_03/05/2026_

I confirm that the information provided by the candidate is correct:

Signature of Principal Supervisor: Robert Forster **Date:**_03/05/2026_